

University of Naples “FEDERICO II”



PhD PROGRAM IN NEUROSCIENCE
XXXII CYCLE

PhD Thesis:

***Exploring the role of Kv7.3 in excitability control:
novel insights from human mutations and a mice model***

Coordinator

Prof. Maurizio Tagliatela

Tutor

Prof. Maurizio Tagliatela

Candidate

Anna Lauritano

Academic Year 2018/2019

Abstract

The *KCNQ3* gene encodes for voltage-gated potassium channel subunits known as Kv7.3 which, together with subunits encoded by other members of the KCNQ gene subfamily, provide a critical contribution to the M-current. This current is a major controller of neuronal excitability at distinct brain areas and neuronal subtypes, as also revealed by the fact that variants in Kv7.3 cause mostly neonatal-onset epilepsies with wide phenotypic heterogeneity. However, despite these genetic evidences, several questions regarding the role of Kv7.3 subunits in controlling the excitability of specific brain regions and neuronal subtypes are still unmeasured the molecular pathophysiology of the human phenotypes associated to Kv7.3 variants is yet poorly understood.

In the present study, I have addressed some of these pressing issues in *KCNQ3* neurobiology using tools and models ranging from *kcnq3* KO mice to individuals/families carrying Kv7.3 mutations. In particular, using electrophysiological recordings in brain slices from *kcnq3* KO mice, I have evaluated the differential role of Kv7.3 channel subunits in controlling the excitability of neurons located in the subiculum, the main output of the hippocampal circuit, and in the hippocampal CA1 area; notably, both the subiculum and the hippocampal formation are two cortical brain regions critically involved in seizure onset and propagation. In addition, I reported the functional consequences of mutations in Kv7.3 found associated with distinct clinical phenotypes in humans. In particular, I have investigated *ex vivo* and *in vitro* consequences of a new Kv7.3 variant (Kv7.3 F534Ifs*15), found in homozygous configuration in a 9-year-old girl with pharmacodependent neonatal-onset epilepsy and non-syndromic intellectual disability. This specific variant represents a unique opportunity to investigate the consequence of a complete deletion of Kv7.3 in humans given that all previously-found Kv7.3 mutations, except one, are found in heterozygosity. Finally, I have carried out electrophysiological and modeling studies to evaluate the functional consequences on channel properties determined by four *de novo* variants (Kv7.3-R227Q, -R230C, -R230S, and -R230C) found in patients with global neurodevelopmental disability (NDD), autism spectrum disorder (ASD), and Sleep-Activated Near-Continuous Multifocal Spikes.

These pathogenic variants have been of great relevance given that they were responsible of a unique phenotype, not associated to neonatal-onset seizure, thus allowing a further expansion of the phenotypic spectrum of diseases associated to Kv7.3 gene variants.

Index

Abbreviations	4
1. A brief introduction to ion channels	6
1.1 Potassium channels	8
1.2 The Kv7 family members	9
1.3 The KCNQ3 gene	11
1.4 Structure and regulation of Kv7.3 channel subunits	12
1.4.1 The Voltage Sensing Domain (VSD)	13
1.4.2 The Pore Domain	13
1.4.3 The regulation of Kv7.3 channels	14
1.5 Neuronal distribution of Kv7.2/7.3 channels	17
1.6 Kv7.2 and Kv7.3 ontogenesis	19
1.7 The M-Current	21
1.8 Biophysical properties of Kv7.2 and Kv7.3 channels	24
1.9 Kv7.3 Channelopathies: from Neonatal and Infantile Epilepsies to Developmental Disability	25
1.10 Pharmacological features of Kv7.2/7.3 channels	27
1.11 The Kcnq3 transgenic mice	30
2. Aim of work	34
3. Materials and methods	
3.1 Site-Directed Mutagenesis of Kv7.3 cDNA	37
3.2 Bacterial transformation and plasmidic DNA preparation	38
3.3 Cell cultures	40
3.3.1 Chinese Hamster Ovary cells	40
3.3.2 Human fibroblasts	40
3.4 Animals and genotyping	40
3.5 Whole-cell electrophysiology	41
3.5.1 CHO cells preparation and electrophysiology	41
3.5.2 Slices preparation and electrophysiology	43
3.6 Western Blotting	45

3.7	Real-Time PCR	46
3.8	Homology modeling	47
3.9	Immunofluorescence	47
3.10	Statistics	47

4. Results

4.1	Role of Kv7.3 in neuronal excitability of subiculum and CA1 pyramidal neurons	48
4.2	Clinical, molecular and functional properties of Kv7.3 F534Ifs*15 variant	60
4.2.1	Clinical features of the proband	60
4.2.2	Genetic data	62
4.2.3	Kv7.3 F534Ifs*15 mRNA is expressed at lower levels in proband's fibroblasts when compared to unaffected noncarrier brother fibroblasts	63
4.2.4	In-vitro (in CHO cells) and ex-vivo (in primary fibroblasts) biochemical studies on Kv7.3 mutant subunits	65
4.2.5	Electrophysiological and pharmacological characterization of Kv7.2, Kv7.3 or Kv7.2/Kv7.3 currents in CHO cells	67
4.2.6	Kv7.3 F534Ifs*15 mutation induces loss-of-function effects on Kv7.3 currents	69
4.3	Clinical, functional and structural properties of Kv7.3 R227Q and R230C/S/H variants	74
4.3.1	Clinical features of the patients	74
4.3.2	R227Q and R230C/S/H mutations induce gain-of-function effects on Kv7.3 currents	76
4.3.3	The gain-of-function effects induced by the Kv7.3 mutations are due to destabilization of the resting state of Kv7.3 channels	81

5. Discussion

5.1	Kv7.3 subunits contribute to M-current heterogeneity	84
5.2	Role of Kv7.3 in control of neuronal excitability	84

5.3	Kv7.3 pathogenic variants revealed novel features of Kv7.3-related disorders	86
5.3.1	A novel homozygous Kv7.3 F534Ifs*15 frameshift variant	87
	<i>Clinical and ex vivo results</i>	
	<i>Functional consequences of the homozygous Kv7.3 F534Ifs*15 variant</i>	
	<i>Clinical spectrum and genetic mechanisms of Kv7.3-related diseases</i>	
5.3.2	Gain-of-function Kv7.3 variants responsible of a non-epileptic phenotypes	89
5.4	Kv7.2 and Kv7.3 Genotypes and Phenotypes	90
5.5	Pharmacological rescue in Kv7.3-related disorders	92

References	93
-------------------	----

Appendix: Published papers	110
-----------------------------------	-----

- *A novel homozygous KCNQ3 loss-of-function variant causes non-syndromic intellectual disability and neonatal-onset pharmacodependent epilepsy*
- *Autism and developmental disability caused by KCNQ3 gain-of-function variants*

Abbreviations

Ab: antibody

ankG: ankyrin G

AHP: afterhyperpolarization

AIS: axon initial segment

AP: action potential

ASD: autism spectrum disorder

BFNE: Benign Familial Neonatal Epilepsy

BFIE: Benign Familial Infantile Epilepsy

CA1: cornu ammonis 1

CaM: Calmodulin

CHO: Chinese Hamster Ovary

CNS: central nervous system

CTL: control

DAG: diacylglycerol

DC: direct current

DD: developmental disability

DG: dentate gyrus

DN: dominant-negative

EOEE: Early Onset Epileptic Encephalopathy

EC: entorhinal cortex

EC50: half maximal effective concentration

EEG: electroencephalogram

GoF: gain-of-function

IC50: half maximal inhibitory concentration

ID: intellectual disability

I_{KM} : M-current

IP3: inositol triphosphate

Kcnq3 cKO: conditional Kcnq3 knockout mice

LoF: loss-of-function

MRI: magnetic resonance imaging
MW: molecular weight
NDD: neurodevelopmental delay
NMD: non-sense mediated mRNA decay
PKC: protein kinase C
PIP2: Phosphatidylinositol 4,5-bisphosphate
PLC: phospholipase C
Po: maximal probability of opening
PTC: premature termination codon
RIKEE: Rational Intervention for KCNQ2/3 Epileptic Encephalopathy
RT: room temperature
RTG: retigabine
SID: subunit interaction domain
SUB: subiculum
TEA: tetraethylammonium
Vrest: resting membrane potential
VSD: Voltage Sensing Domain
 $V_{1/2}$: half-activation potential

1. A brief Introduction to ion channels

The physiological function of numerous cells is due to the movement of ions across their hydrophobic plasma membranes, guaranteed by the presence of ionic transporters. For decades, the study of ionic transporters has sought to unravel the simple question of how ions translocate from one side of the non-conducting membrane to the other. As the list of discovered ion channels grew, patterns behind their properties emerged. Currently, these ion channels are grouped on common properties which typically translate to comparable cellular function, such as the ionic specie(s) they conduct. Many channels restrict their availability to a single ion, whether it is Na^+ , K^+ , Ca^{2+} , Cl^- , H^+ , or some other. This creates subsets of ion channels whose functions directly stem from the role their permeant ion plays in physiologic cellular processes. Another property is their mode of gating, or the method that drives their activation and deactivation (if they possess one at all). In ion channel gating, passage of a channel's permeant ion is obstructed unless specific conditions are met. For some channels, ligand-binding lifts the obstruction and activates the channel to continue conducting ionic flow. In other channels, transmembrane potential must become sufficiently positive or negative to activate the channel. Gating and ion specificity are not mutually exclusive, and often combine to create ion channels with highly specialized functions. The ion flow between the intracellular and the extracellular compartment is determined by the *conductance* (γ) of the channel, which is a measure of how many ions enter or exit the cell through the channel in a given time. Conductance, in turn, is influenced by two different forces driving the ions across the plasma membrane: a *chemical driving force*, depending on the concentration gradient across the membrane, and an *electrical driving force*, determined by the potential difference between the intracellular and the extracellular compartments. After a while, the ion flux through the channel reaches a point where the chemical force and the electrical force counterbalance each other and so, as result, the outward movement of an ion is equal to its inward movement. That is the *equilibrium potential* specific for that specific ion. Homeostatic regulation of these ionic gradients is critical for most functions, in particular for excitable cells, such as neurons, in which ion channel activity leads to brief electrical impulses (Dubyak, 2004). This

brief electrical phenomenon is crucial to certain cellular events, driving cell-to-cell communication as well as triggering intracellular processes.

A brief change in the voltage across the membrane due to the flow of certain ions into and out of the neuron is known as *action potential*. The roles of ions in shaping the action potential were built on the hypothesis established by Julius Bernstein in 1902 wherein he predicted that the resting membrane potential was established by K⁺ ions, and that the action potential was a result of sudden membrane permeability of other ions (Seyfarth, 2006). Afterwards, Hodgkin and Huxley, by studying the squid giant axon, identified that the action potential is driven first by an increased permeability to sodium, followed by an increased permeability to potassium, and established the non-linear mathematical principles that underlie their relationship (Schwiening, 2012).

Among the different ion species, potassium (K⁺) ion seems to play a primary role in the regulation of neuronal excitability. The equilibrium potential can be calculated with the Nernst's equation, and in the case of K⁺ Nernst's equation will be:

$$E_{K^+} = \frac{RT}{F} \cdot \ln \frac{[K^+]_o}{[K^+]_i}$$

where R is the gas constant, T the temperature (in Kelvin degrees), F the Faraday constant, and [K⁺]_o and [K⁺]_i are respectively the concentrations of K⁺ outside and inside the cell. So, when the channel opens, it will generate a current that will bring the membrane potential (V_M) to the value of the equilibrium potential specific for K⁺ (E_{K⁺}). This current can be described with a modified version of the *Ohm's law*:

$$I = \gamma (V_M - E_{K^+})$$

where γ is the conductance, V_M is the membrane potential and E_{K⁺} is the equilibrium potential of K⁺.

1.1 Potassium channels

The ability of the central nervous system (CNS) to receive, integrate and process information is dependent on the operation of receptors and ion channels that reside at the surface of excitable cells. Among these, many types of K^+ channels act together to control some of the most fundamental parameters of excitable activity, such as the frequency and the duration of the action potentials, and the resting membrane potential (V_{rest}). Changes in the value of V_{rest} can indicate either *depolarisation*, due to the inward movement of cations and the outward movement of anions, or *hyperpolarisation*, due to the outward movement of cations and the inward movement of anions.

Based on peculiar structure and biophysical properties, K^+ channels fall into three main families: those which possess six transmembrane segments, those which are formed from two and four transmembrane segments, and those with seven transmembrane segments (Fig. 1):

- *Voltage-dependent K^+ channels containing six transmembrane segments (6TM)*. This group comprises K^+ channels activated by membrane depolarization, divided in subfamilies with a homology sequence of about 25-30%. Functionally, this group is characterized by several channels, like Kv1-4 channels, KCNQ (or Kv7) channels, Eag (or Kv10) channels, Erg (or Kv11) channels, Elk (or Kv12) channels, SK channels.
- *Voltage-independent K^+ channels containing two (2TM) or four transmembrane segments (4TM)*. They include all the families of inward-rectifying K^+ channels with 2TM (Kir channels) and 4TM, the latter characterized by the tandem repetition of two pore domains. These channels are insensitive to changes of the membrane potential and they are ubiquitously expressed with several functions, as V_{rest} regulation, maintenance of K^+ homeostasis, control of heart rate, and hormone secretion.
- *K^+ channels containing seven transmembrane segments (7TM)*. Slo (or BK) channels are large-conductance potassium channels activated by both membrane depolarisation or increase in cytosolic Ca^{2+} that mediate export of K^+ . Its activation dampens the excitatory events that elevate the cytosolic Ca^{2+} concentration and/or depolarize the cell membrane.

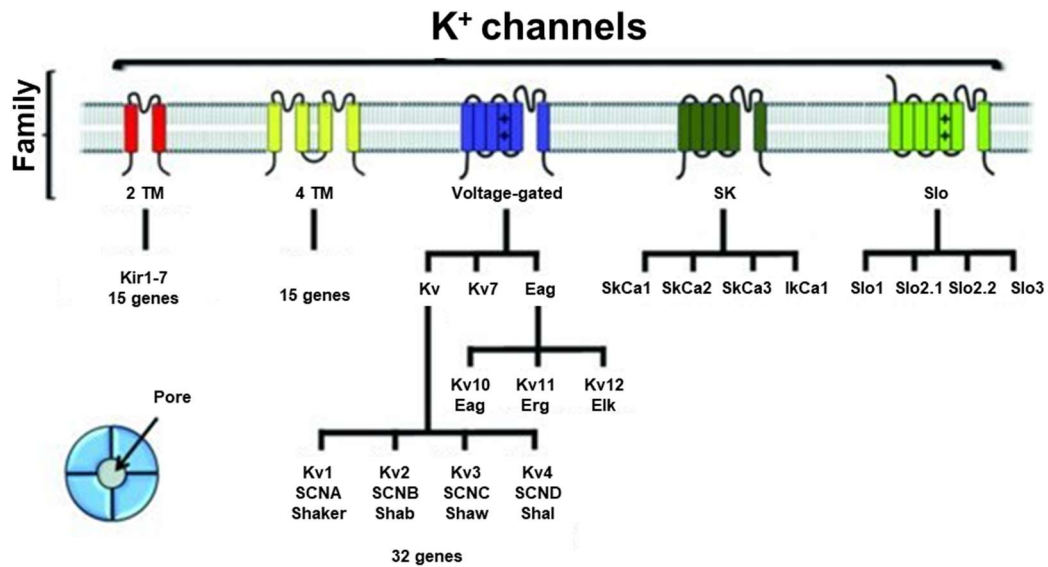


Fig. 1. Potassium channel families arranged according to their subunit structure.

Potassium channel families can be grouped in those having two transmembrane segments (2TM; Kir), 4TM (2-pore domain), 6TM (voltage gated and SK), and 7TM (Slo). Subdivisions of the voltage-gated Kv channels into four subfamilies and Eag into three subfamilies are also named according to the *Drosophila melanogaster* genes (adapted from Zhong et al., 2013).

1.2 The Kv7 family members

Among K⁺ channels, there is a Kv7 voltage-gated potassium channel family, first called KCNQ (acronym for *K* potassium, *CN* channel, *Q* long QT syndrome) since the first KCNQ gene to be identified was KCNQ1. The Kv7 channels family are characterized by five members, namely Kv7.1-Kv7.5, each showing a distinct tissue distribution (Soldovieri et al., 2011).

As stated before, KCNQ1 was the first gene identified. This encodes for **Kv7.1** subunits that assemble into tetramers, forming heterologous channels together with auxiliary KCNE1 β -subunits to create channels that generate the slow delayed rectifier K⁺ current, *I_{KS}*, which plays a key role in cardiac late-phase action potential repolarization (Sanguinetti et al., 1996). Kv7.1/KCNE1 channels are mainly localized in the heart but also in the inner ear, thyroid gland, lung, gastrointestinal tract, small intestine, pancreas, forebrain neuronal networks and brainstem nuclei and in the ovaries. Mutations in the KCNQ1 gene are associated to Long QT Syndrome (LQTS), an arrhythmic disorders characterized by the lengthening of the QT interval

of the electrocardiogram, indicative of a delayed cardiac action potential repolarization, which predisposes affected individuals to ventricular torsade de pointes and cardiac sudden death. Mutations in Kv7.1 and KCNE1 have also been linked to familial atrial fibrillation or to short QT syndrome. In LQTS syndrome, the disease pathogenetic mechanism is an impairment of I_{Ks} function (loss-of-function mutations) while gain-of-function mutations in both Kv7.1 and KCNE1 have been linked to familial atrial fibrillation or to short QT syndrome.

By contrast to Kv7.1 channel, the Kv7.2- Kv7.5 subunits are most known for their roles in the nervous system, as essential regulators of neuronal excitability (Brown et Passmore, 2009). In particular, **Kv7.2** and **Kv7.3** are co-expressed in many areas of the brain, including the cerebral cortex, hippocampus, cerebellum, and thalamus, suggesting the formation of heteromeric Kv7.2/7.3 channels (Schroeder et al., 1998; Tinel et al., 1998) which underline a voltage-dependent K^+

current, M-current (I_{KM}). Mutations in KCNQ2 or KCNQ3 genes, encoding for Kv7.2 or Kv7.3 subunits respectively, have been associated to Benign Familial Neonatal Epilepsy (BFNE), an autosomal dominant idiopathic epilepsy of newborns (Plouin, 1994), and more recently mutations in KCNQ3 gene have also been associated in rare families with epileptic encephalopathy (Miceli et al, 2015b), nonsyndromic sporadic intellectual disability (Rauch et al., 2012; McRae et al., 2017), and intellectual disability with seizures and cortical visual impairment (Bosch et al., 2016).

The **Kv7.4** subunit plays an important role in hearing (Kubisch et al., 1999), and its expression in the central nervous system is restricted to some areas of the brainstem, including nuclei and tracts of the auditory pathway (Maljevic et al., 2010). Mutations in the KCNQ4 gene cosegregated with an inherited, autosomal-dominant form of nonsyndromic progressive hearing loss (DFNA2). Functional studies have shown that DFNA2 mutations in KCNQ4 induce a loss-of-function of Kv7.4 channels either by haploinsufficiency mechanism or by dominant-negative effects (Maljevic et al., 2010). It has been proposed that mutations causing dominant-negative effects are preferentially found in patients showing hearing loss with younger onset, while mutations associated to a haploinsufficiency mechanism have been

identified in patients affected by a late onset hearing impairment (Topsakal et al., 2005).

KCNQ5 gene encodes for **Kv7.5** channel subunit, the last member of Kv7 family to be identified. Kv7.5 transcripts (splice variant I) are broadly expressed in the brain and show an overlapping cellular pattern expression with Kv7.2 and Kv7.3 subunits. Unlike Kv7.3, Kv7.5 is highly expressed in CA3 area of hippocampus (Tzingounis et al., 2010). In addition, Kv7.5 transcripts (splice variant II and III) are found also in non neuronal tissue, such as skeletal and smooth muscle cells (Lerche et al., 2000; Schroeder et al., 2000). Only recently, four variants in Kv7.5 responsible of epileptic encephalopathy have been identified (Lehman et al., 2017).

1.3 The KCNQ3 gene

The KCNQ3 gene is located on the long arm of chromosome 8 at the position 24.22 (8q24.22) and, as stated before, encodes for Kv7.3 channel, a protein of 872-amino acids with a predicted molecular weight of 100 kDa (Fig.2).

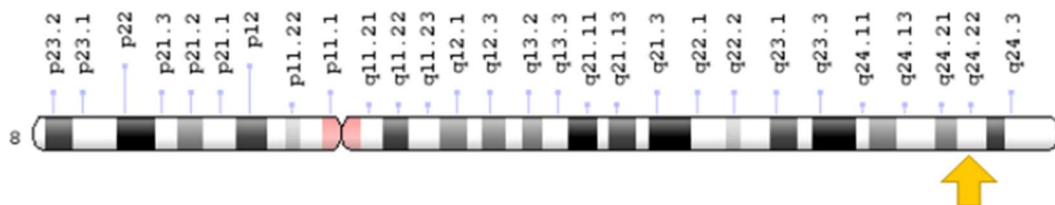


Fig.2. KCNQ3 chromosomal location (8q24.22).

This gene can produce multiple differentially spliced transcripts: to date, 2 isoforms (isoform 1 and 2) have been described and 5 potential isoforms have been computationally mapped (UniProtKB - O43525). The variant 1 represents the longer transcript and encodes the longer isoform 1; whereas the variant 2 contains an alternate 5' terminal exon, resulting in a distinct N-terminus and a shorter isoform (Fig.3).

KCNQ3iso1	MGLKARRAAGAGGGGDDGGGGGGGAANPAGGDAAAAGDEERKVGGLAPGDVEQVTLALGAG	60
KCNQ3iso2	-----	0
KCNQ3iso1	ADKDGTLLLEGGGRDEGQRRTPOGIGLLAKTPLSRPVKRNNAKYRRIQTLIYDALERPRG	120
KCNQ3iso2	-----	0
KCNQ3iso1	WALLYHALVFLIVLGLILAVLTTFKYEYTVSGDWLLLLLETFAIFIFGAEFALRIWAAGC	180
KCNQ3iso2	MKPAEHATMFLIVLGLILAVLTTFKYEYTVSGDWLLLLLETFAIFIFGAEFALRIWAAGC	60
	* * : *****	
KCNQ3iso1	CCRYKGWRGRLKFARKPLCMLDIFVLIASVPVAVGNQGNVLATSLRSLRFLQILRMLRM	240
KCNQ3iso2	CCRYKGWRGRLKFARKPLCMLDIFVLIASVPVAVGNQGNVLATSLRSLRFLQILRMLRM	120

KCNQ3iso1	DRRGGTWKLLGSAICAHSKELITAWYIGFLTILSSFLVYLVEKDVPEVDAQGEEMKEEF	300
KCNQ3iso2	DRRGGTWKLLGSAICAHSKELITAWYIGFLTILSSFLVYLVEKDVPEVDAQGEEMKEEF	180

Fig.3. Partial alignment of two KCNQ3 gene isoforms.

1.4 Structure and regulation of Kv7.3 channel subunits

Like all Kv7 channels, Kv7.3 channel subunit contains six transmembrane segments, denoted S1-S6, characterized by two functional modules of the channel: the Voltage Sensing Domain, VSD, (S1-S4) and the Pore Domain, (S5-S6) (MacKinnon, 2003; Doyle et al., 1998) (Fig 4A). Kv7.3 subunits are assembled homomerically or heteromerically with homologous Kv7.2 subunits, forming tetrameric channels that underlie the M-current (Fig. 4B).

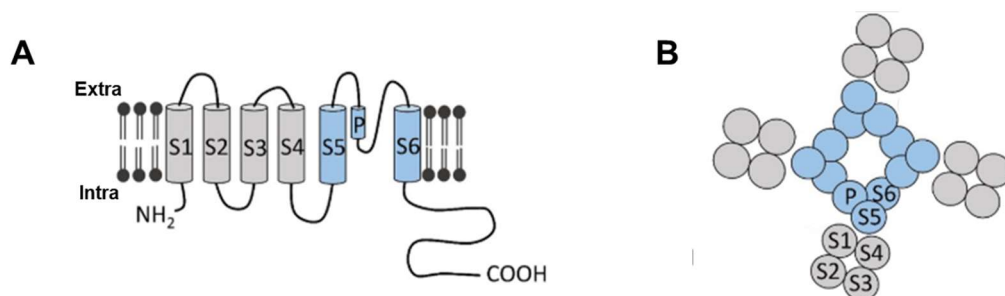


Fig. 4. Kv7.3 channel subunit.

A) The architecture of a Kv7.3 channel subunit. Cylinders are helical segments. The pore domain is shown in blue, the voltage-sensing domain (VSD) in violet. B) The Kv7.3 tetramer, top view.

1.4.1 The Voltage Sensing Domain (VSD)

Changes in transmembrane electrical potential are sensed by the S4 transmembrane helix, as it is packed with multiple positively charged residues (arginines and lysines) positioned every three amino acids and surrounded by hydrophobic residues. A vertical translation of S4, caused by the charge transfer in S2 and S3, leads to the opening of the pore (Long et al., 2005; Jiang et al., 2003; Aggarwal et MacKinnon, 1996). These positive charges in S4 are stabilized by electrostatic bonds with residues connecting the negatively charged S1, S2, S3 or by interactions with the polar heads of the phospholipid bilayer, necessary for activating/deactivating process (Fedida et al., 2001; Miceli et al., 2011). The VSD of each subunit interacts with the pore module of the adjacent subunit: this phenomenon is called *domain swapped architecture*, which is typical of many families of Kv7 channels. In particular, opening of the channel is a result of the S4-S5 linker, a thread of residues connecting the positively charged S4 to the S5 transmembrane helix, one of the helices lining the pore.

As noted in the recently solved crystal structure of Kv1, the S4-S5 linker of Kv7.3 channel subunit is excessively long, effectively separating the S4 transmembrane from the pore's gate in the absence of Phosphatidylinositol-(4,5)-Bisphosphate (Sun et MacKinnon, 2017).

1.4.2 The Pore Domain

Each Kv7.3 subunits are characterized by four individual alpha subunits that converge at the subunit interacting domain (Sid) on the C-terminal region to form the functional channel with central pore, by the S5-S6 segments and interconnecting P-loop of each subunit (Tombola et al., 2006; Börjesson et Elinder, 2008). Pore domain allows the flow of K⁺ ions across the plasma membrane and, as well as for other Kv7 channels, Kv7.3 channel selectivity is established by a motif of residues, **GYGD** (glycine-tyrosine-glycine-aspartate), (MacKinnon, 2003; Doyle et al., 1998). Moreover, each alpha Kv7.3 subunit shows a sequence of residues, **PAG** (proline-adenine-glycine) motif, that assembles with each other to form a four-helix bundle in the lower

part of the pore. This structure is extremely flexible: these helices are arranged peripherally during pore opening, but they recompact during closure, interrupting the flow of K⁺ ions (Bezanilla, 2000; Long et al., 2005).

1.4.3 The regulation of Kv7.3 channels

While the transmembrane region plays an important role in selective flow of K⁺ ions across the membrane upon changes in transmembrane potential, the long C-terminal segment is responsible of Kv7.3 channel function and regulation (Fig.5).

The long (>500 amino acids in Kv7.2 and Kv7.3) C-terminal segment contains multiple important sites for regulation, subunit interaction, and surface trafficking; four α -helical domains, called A-D, are particularly crucial (Etxeberria et al., 2004; Yus-Nájera et al., 2002). Among them, a handful of interacting molecules that can be recognize as follow:

- *Calmodulin (calcium-modulated protein, CaM)*. CaM is a small protein that binds calcium ions and plays an important role in surface trafficking and channel function (Wen et Levitan, 2002; Etxeberria A et al., 2008). Helices A and B act as binding sites for CaM due to the presence of CaM-binding motifs: an IQ CaM-binding motif in helix A and two overlapping consensus 1-5-10 CaM-binding motifs in helix B (Etxeberria et al., 2008). CaM also imparts some [Ca²⁺]_i sensitivity to Kv7 channels: recent evidence outlines a model for CaM regulation of Kv7.2/7.3 where binding of Ca²⁺-CaM (or apo-CaM), particularly to Kv7.2, increases PIP2 efficiency; in contrast, increasing [Ca²⁺]_i has been shown to decrease Kv7 channel activity (Gomis-Perez et al., 2015; Alberdi et al., 2015).
- *Phosphatidylinositol-(4,5)-Bisphosphate (PIP2)*. Under physiological conditions, activation of Gq/11-coupled receptors, such as M1 muscarinic acetylcholine receptors, leads to depletion of PIP2 into membrane-bound diacylglycerol (DAG) and inositol triphosphate (IP3) by hydrolysis via phospholipase C (PLC) (Putney et Tomita, 2012). PIP2 promotes Kv7 channel activity, increasing the opening probability of homomeric and heteromeric channels, thus stabilizing their open state. Among Kv7

subunits, Kv7.3 subunits seem to have the greatest affinity. Recently, four different Kv7.3 interacting domains have been identified: 1) the A–B helix linker, important for both Kv7.2 and Kv7.3 (Hernandez et al., 2008), 2) the junction between S6 and the A helix, 3) the S2–S3 linker, and 4) the S4–S5 linker (Choveau et al., 2018).

- *Protein Kinase C (PKC) and A-Kinase Anchoring Protein 79/150 (AKAP79/150)*. It has been shown the ability of PKC to phosphorylate Kv7 channels when coordinated by A-Kinase Anchoring Protein 79/150 (AKAP79/150) (Higashida et al., 2005; Hoshi et al., 2003; Bal et al., 2010). Phosphorylation mediated by PKC leads to an increased sensitivity to suppression by PIP2 depletion, and decreasing AKAP79/150 either through RNAi or transgenic deletion leads to a decrease in muscarinic suppression of the M current (Hoshi et al., 2005; Zhang et al., 2011). Importantly, the analogous residues for Kv7.3 to the S558 phosphorylation site on Kv7.2 is threonine, making Kv7.3 a potential target for PKC phosphorylation. Furthermore, this site resides in the B helix of the C-terminal domain, clearly a critical region for regulating PIP2 interactions with Kv7 subunits.
- *Ankyrin G (ankG)*. In Kv7.2 and Kv7.3 subunits, but not in other Kv7 subunits, a binding-site for ankG has been identified. The function of this adaptor protein is to anchor Kv7.2 and Kv7.3 subunits at the axon initial segment and at the nodes of Ranvier, sites important for the generation and propagation of action potentials, respectively (Devaux et al., 2004; Pan et al., 2006).
- *Syntaxin-1A (syx-1A)*. The SNARE protein syntaxin-1A is located on the presynaptic membrane and acts as an anchoring site for synaptic vesicles. In fact, the N-terminal of syx-1A interacts with the neuronal protein Sec1 (STXBP1) constituting a complex necessary for the fusion of the vesicles with the membrane and the subsequent release of neurotransmitters. The interaction among the syx-1A with helix A of the C-terminal domain of the Kv7.2 or Kv7.3 subunits gives a different effect: it reduces the current elicited by the Kv7.2 channel by at least 50%, while it does not affect the current mediated by Kv7.3. This could be due to the presence of additional binding sites for syx-1A in the Kv7.2 channel (in particular, in the N-terminal domain) which may not be present in Kv7.3 (Regev et al., 2009).

- *Nedd4-2*. The plasma membrane expression of Kv7.2/7.3, Kv7.3/7.5 and Kv7.1/KCNE channels is regulated by the ubiquitin-protein ligase Nedd4-2. This protein reduces the current elicited by these channels, probably by promoting the ubiquitination, internalization and degradation of these channels: a PY domain, localized at the C-terminal domain of Kv7.1, is crucial for this process, whereas the role of the same region in Kv7.2/7.3 subunits is less defined.

The functional significance of the N-terminus is less well understood. Studies have shown that the N-terminal may play roles in surface trafficking and influencing the probability of opening (Fig. 5); however, the mechanism underlying these roles has yet to be determined (Choveau et Shapiro, 2012; Etxeberria et al., 2004; Dahimene et al., 2006).

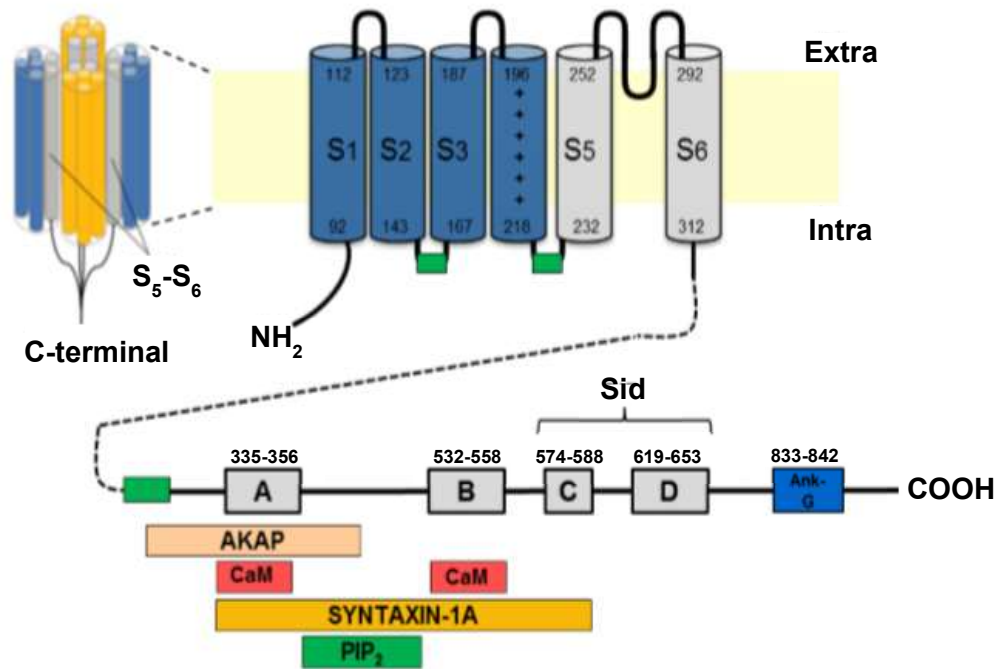


Fig. 5. Topological representation of Kv7.3 subunit.

Left, tetrameric structure of a Kv7 channel formed by co-assembly of Kv7.2 (in yellow) and Kv7.3 (in blue) subunits. Right, schematic topology of a Kv7.3 subunit formed by six transmembrane segments (S1-S6), and intracellular NH₂- and COOH-terminal. The region encompassing S1-S4 segments forms the VSD (in blue), whereas the S5-S6 region (in gray) and the intervening linker forms the ion-selective pore. The S4 segment is characterized by the presence of six arginine residues (+). A long C-terminal region is characterized by 4 α -helix domains (boxes from A to D) and is an important platform for interaction with regulatory molecules, as indicated by colored rectangles in the figure. The C and D helices form the *Subunit interaction domain* (Sid), which is involved in multimerization and subunit-specific heteromerization (adapted from Soldovieri et al., 2011).

1.5 Neuronal distribution of Kv7.2/7.3 channels

Kv7.2 and Kv7.3 channel subunits are co-expressed in the neurons of the central and peripheral nervous system (Fig. 6), in several regions including the dentate gyrus and CA1-3 regions of the hippocampus, the subiculum, within all layers of the neocortex, and in the reticular nucleus of the thalamus (Cooper et al., 2001; Tzingounis et al., 2010; Weber et al., 2006; Geiger et al., 2006).

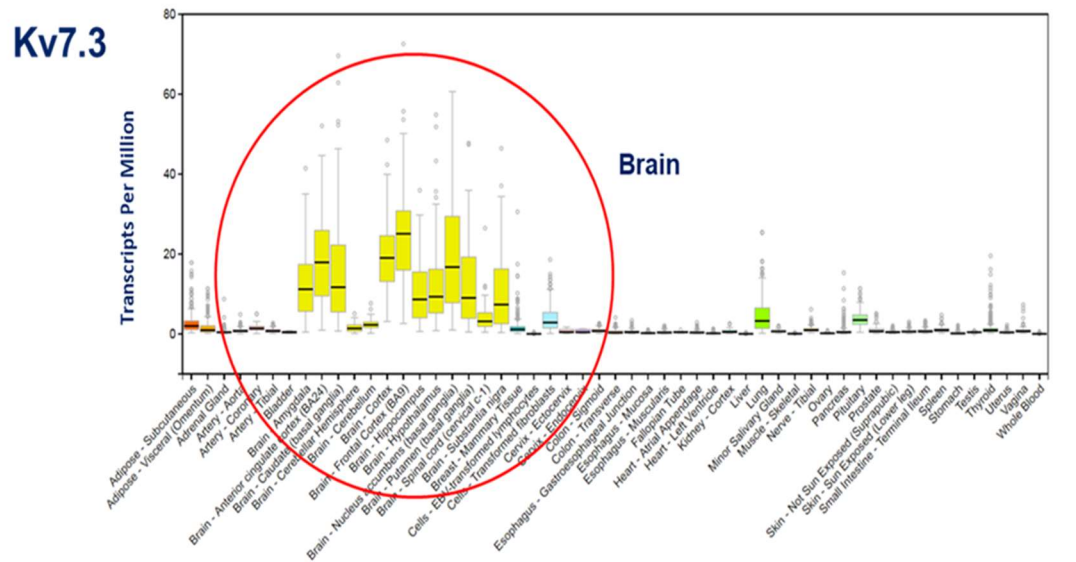
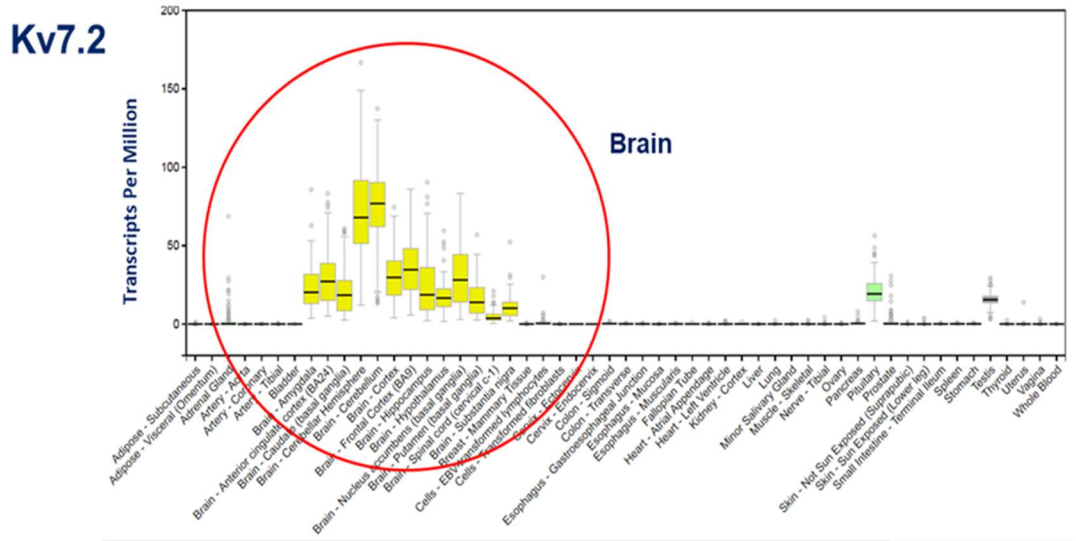


Fig. 6. Kv7.2 and Kv7.3 expression levels in the brain. Data obtained from GTEx Portal.

At the subcellular level, Kv7.2 and Kv7.3 are most abundantly found in the distal end of the axon initial segment (AIS) and the nodes of Ranvier (Fig. 7), as evidenced by immunohistochemical and electrophysiological experiments (Chung et al., 2006; Pan et al., 2006; Schwarz et al., 2006), and expressed at lower densities at the soma and dendrites and synaptic terminals (Martire et al., 2004).

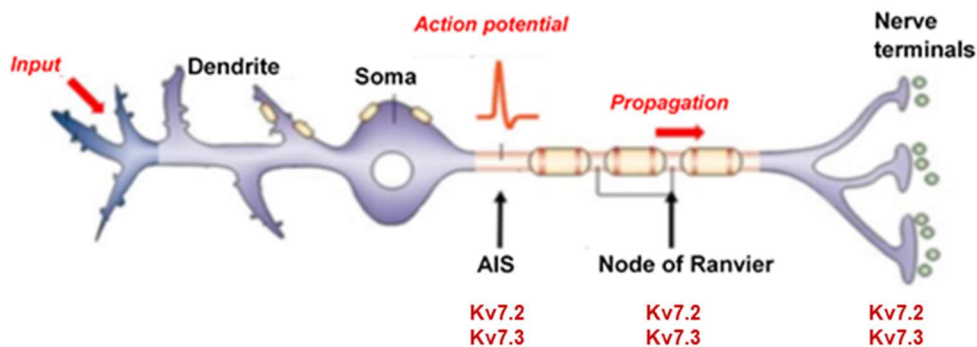


Fig. 7. Neuronal distribution of Kv7.2 and Kv7.3.

The Kv7 channel is found at the AIS, nodes of Ranvier and presynaptic terminals (adapted from Lai et al., 2006).

1.6 Kv7.2 and Kv7.3 ontogenesis

Different studies underlined the different Kv7.2 and Kv7.3 age-dependent expression in several brain areas, both in pre- and post-natal period (Tinel et al., 1998; Kanaumi et al., 2007). In particular, in 1998, Tinel and coworkers demonstrated that, in mice brain, Kv7.2 was already expressed 3 days after birth, differently from Kv7.3: in fact, its expression is very low during the first week of life, but it increases continuously until the adult age (30 days after birth) where no significant differences are shown between both Kv7.2 and Kv7.3 mRNA expression levels.

About ten years later, Kanaumi and colleagues have investigated the developmental changes in the density of Kv7.2 and Kv7.3 in human brain, during the gestation weeks and the post-natal period. They have demonstrated how, unlike Kv7.2, the Kv7.3 expression levels increased during the post-

natal period in the hippocampus, the temporal lobe and the cerebellum area (Fig. 8).

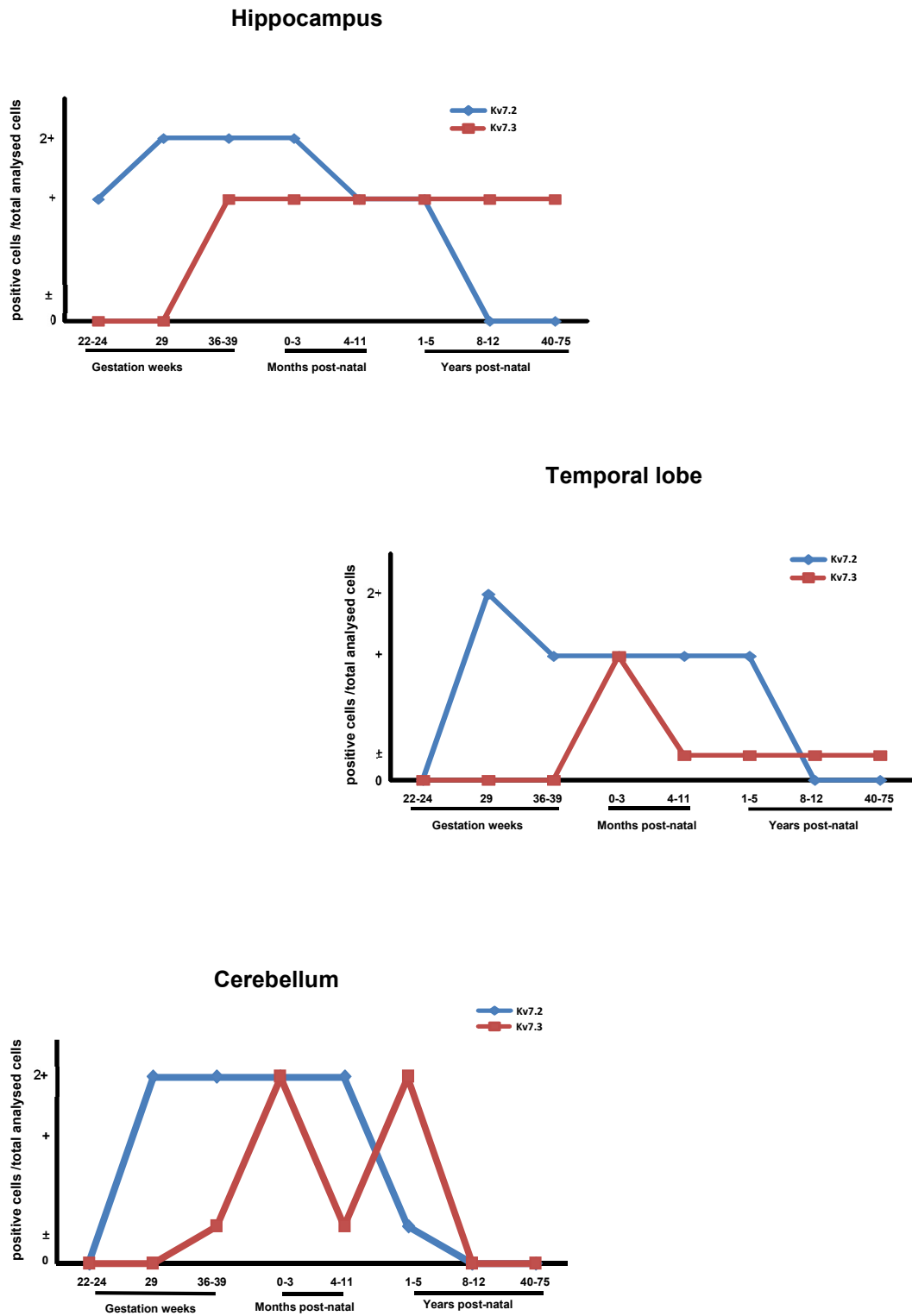


Fig. 8. Developmental changes in the density of Kv7.2- and Kv7.3-positively stained neurons in the human brain. (±): positively stained neurons <10% of all neurons; (+): positively stained neurons <50% of all neurons; (2+): positively stained neurons ≥50% all neurons (revised from Kanaumi et al., 2008).

1.7 The M-Current

During the early years of ion channel identification, multiple labs sought to determine the mechanism behind a muscarine-induced slow excitatory postsynaptic potential, as the addition of muscarinic agonists appeared to increase neuronal activity. While the phenomenon was noted by multiple groups, David Brown and colleagues ultimately uncovered the mechanism in 1980 using two-electrode voltage-clamp in bullfrog sympathetic neurons (Brown et Adams, 1980; Adams et Brown, 1980). It was then that they discovered that muscarine blocked a slowly-deactivating, non-inactivating delayed rectifier current, and thus excitation of neurons by the activation of muscarinic receptors was shown to be a result of impaired delayed rectification (Adams et Brown, 1982; Adams et al., 1982; Brown DA et al., 1982).

A line of electrophysiological experimentations using heterologous cell lines identified Kv7.2/7.3 heteromers as having properties matching the neuronal M-current though the mechanism behind this was not elucidated until later (Wang et al., 1998; Schwake et al., 2000; Shapiro et al., 2000). These muscarinic acetylcholine receptors are coupled to G-proteins (principally Gq and/or G11 subtypes), which stimulate PLC with the subsequent depletion of PIP2 into membrane-bound DAG and IP3. This depletion leads to Kv7.2/7.3 closure state and, in turn, the inhibition of the M-current.

Immunoreactivity for Kv7.2, but not Kv7.3, was also prominent in some terminal fields, suggesting a presynaptic role for a distinct subgroup of M-channels in the regulation of action potential propagation and neurotransmitter release (Cooper et al., 2000). Cooper et al. (2000) suggested that these studies provided a view of a signaling complex that may be important for cognitive function as well as epilepsy, and that analysis of this complex may shed light on the transduction pathway linking muscarinic acetylcholine receptor activation to M-channel inhibition.

As stated before, heteromeric Kv7.2/7.3 channels underlie the M-current which allows to regulate several aspects of neuronal excitability: control of membrane potential and spike afterdepolarization, modulation of interspike intervals and release of neurotransmitters from presynaptic terminals.

- *Control of membrane potential and spike afterdepolarization.* The Kv7 channels are implicated in the control of V_{rest} , necessary to increase the recovery of inactivated channels, as Na^+ channels and K^+ channels A-type (Battefeld et al., 2014). The depolarization upstroke of the action potential spike is mediated by an increase in Na^+ conductance and, instead, the repolarization downstroke is mediated by the inactivation of some of those voltage-gated Na^+ channels and an increase of K^+ efflux (Fig 9A). The repolarization phase is followed by a brief afterhyperpolarization (AHP) before the membrane potential reaches again the resting potential level; this latter phase is a result of K^+ channels remaining open (Fig 9A). AHP is characterized by three phases: a fast one (fAHP, lasting 1-5 ms), a medium one (mAHP, typically lasting 50-200 ms) and slow one (sAHP, lasting from about 0.5 s to several seconds). These three phases are due to distinct K^+ channels: the fAHP is largely mediated by Ca^{2+} and voltage-dependent BK channels, mAHP is mediated by SK and Kv7 channels, and sAHP by Kv7 and SK channels as well (Tzingounis et Nicoll, 2008; Andrade et al., 2012; Kim KS et al., 2012). When Kv7/M channels are blocked (by channel blockers such as linopirdine and XE991), the neuron remains depolarized for a long period during which it may generate multiple spikes (Yue et Yaari, 2004) (Fig 9B). Thus, the functional consequence of M-current is to clamp the membrane at more negative potentials than resting membrane potential, preventing repetitive action potential firing (Yue et Yaari, 2004).

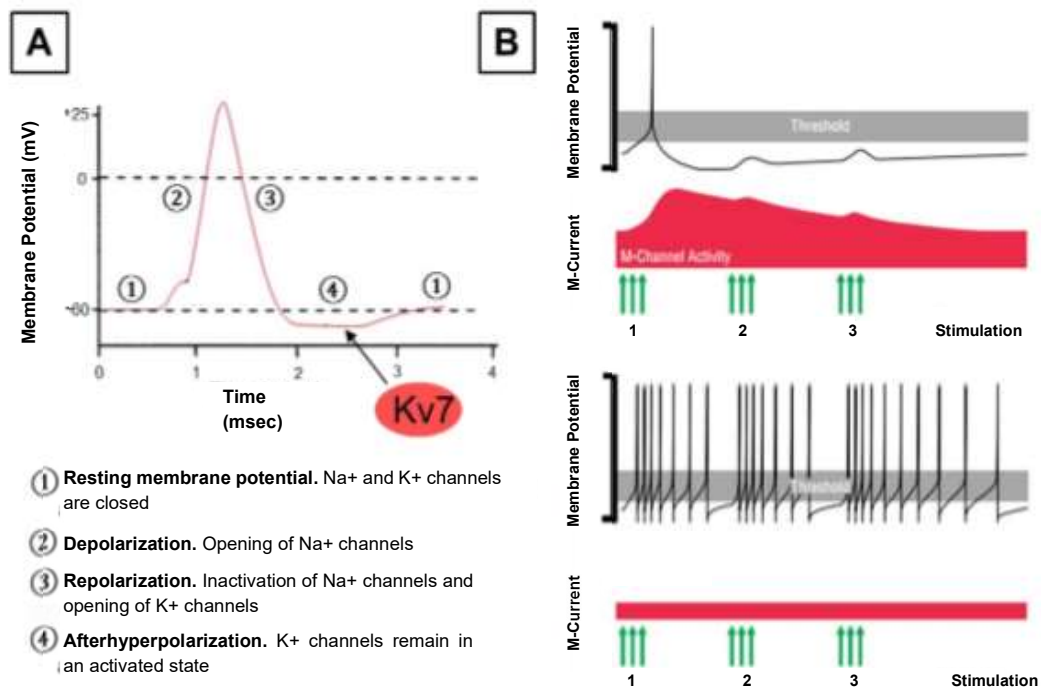


Fig. 9. Role of neuronal M-current in controlling excitability. A) Representation of an action potential. B) Top: excitatory inputs (green arrows, 1) cause membrane depolarization and a single action potential. Afterward, increased activation of M-channels hyperpolarizes the membrane potential, preventing spiking in response to recurrent excitation (green arrows, 2,3). Bottom, when M-channel activity is reduced (for example in the presence of mutations), excitatory inputs lead to multiple action potentials (adapted from Cooper and Jan, 2003).

- **Modulation of interspike intervals.** High frequency bursts of action potentials leads to Kv7.3 channel activation: that, in turn, increases spike interval (Suh et Hille, 2002). The M-current contributes to certain functional differences of cholinergic and GABAergic neurons, as spike frequency adaptation, action potential firing frequency or the amplitude difference of medium afterhyperpolarizations (mAHPs) (Aiken et al., 1995), and thus playing an prominent role in the modulation of interspike intervals.
- **Release of neurotransmitters from presynaptic terminals.** As Hille demonstrated in 1992, the inhibition of the M-current is due by the release of neurotransmitters, like acetylcholine, or peptides, such as gonadotropin-releasing hormone, angiotensin, substance P, bradykinin. Cooper and

colleagues, in 2000, demonstrated the distribution of Kv7.2 subunits in presynaptic terminals of rodents brain, suggesting its role in neurotransmitters release: in fact, the activation of presynaptic M-current may hyperpolarize hippocampal nerve endings, thus reducing Ca^{2+} influx through voltage-gated Ca^{2+} channels. These decrease in $[\text{Ca}^{2+}]$ reduces the release of neurotransmitters, such as norepineprine, GABA and D-aspartate (Martire et al., 2004). Involvement of Kv7.2 subunits have been described also in dopamine release from rat striatal synaptosome: $[3\text{H}]$ dopamine release is inhibited by the IKM activator retigabine while M-current blockers TEA and XE991 enhanced K^{+} -evoked $[3\text{H}]$ dopamine release and prevented retigabine-induced inhibition of depolarization-evoked $[3\text{H}]$ dopamine release (Martire et al., 2007). A class of drugs known as “cognition enhancers” (such as linopiridine or XE991) increases neurotransmitter release by suppressing M-current and this affect seems to mediate an increase in animal performance of memory tests (Zaczek et al., 1998).

1.8 Biophysical properties of Kv7.2 and Kv7.3 channels

The biophysical properties of Kv7 channels depend on their subunit composition. In particular, Kv7.2 homomers and Kv7.3 homomers have differences in their biophysical properties (Table 1): Kv7.2 homomers exhibit a half-activation potential ($V_{1/2}$) at -20/-30 mV, with an activation time constant (τ_{act}) of 130 ms at +40 mV and a deactivation time constant (τ_{deact}) of 150-200 ms at -60 mV (Wang et al., 1998; Miceli et al., 2009; Gamper et al., 2003). Single channel measurements indicate that the maximal probability of opening (P_o) for Kv7.2 channels, measured at voltages where conductance is saturated, is ~ 0.2 (Selyanko, 2001; Li et al., 2005). Kv7.3 homomers, on the other hand, have a more hyperpolarized $V_{1/2}$, -35 to -45 mV, displaying faster kinetics, τ_{act} being 60 ms and τ_{deact} being 100-150 ms, and have a maximal P_o that approaches unity. The decreased $V_{1/2}$, faster kinetics, and high P_o of Kv7.3 are thought to be imparted by a dramatically higher affinity for PIP2.

Kv7.2/7.3 heteromers account for the vast majority of neuronal M-current and they yield currents that are at the least 10-fold larger than those of Kv7.2 homomers, with mostly intermediate properties between Kv7.2 and Kv7.3 homomers: $V_{1/2}$ of -20 to -27 mV, τ act of 130-170 ms, maximal $P_o \sim 0.3$, yet faster deactivation, τ deact of 75-100 ms.

Table 1. Biophysical properties of Kv7.2 and Kv7.3 channels

	Biophysical properties				
	$V_{1/2}$ (mV)	k (mV/e-fold)	τ act (ms at +40 mV)	τ deact (ms at -60 mV)	P_o
Kv7.2	$\sim -30^a$	$\sim 8^a$	$\sim 130^b$	$\sim 150^b$	Low ^c
Kv7.3	$\sim -40^a$	$\sim 7^a$	$\sim 60^b$	$\sim 100^b$	High ^c

^aMiceli et al., Channels 2009; ^bGamper et al., J Neurosci 2003; ^cLi et al., J Neurosci 2005.

Low = $p_o < 20\%$; High = $p_o > 80\%$.

1.9 Kv7.3 Channelopathies: from Neonatal and Infantile Epilepsies to Developmental Disability

Information about KCNQ3 pathogenic variants are given by the Rational Intervention for KCNQ2/3 Epileptic Encephalopathy (RIKEE) database which collects features about patients where genetic tests show KCNQ3 (and KCNQ2) sequence variants, their phenotypes, and related lab studies (website: www.rikee.org). Among these, several mutations of KCNQ3 gene have been described as a cause of epileptogenic channelopathies with significant phenotype heterogeneity, ranging from more benign forms, like *Benign Familial Neonatal Epilepsy (BFNE)* and *Benign Familial Infantile Epilepsy (BFIE)*, to a more severe form.

Based on the age of seizures onset, benign familial epilepsies are divided in:

- **BFNE**, described for the first time in 1964 by the austrian neurologist Andreas Rett, in which multifocal seizures starting around the third day of life and disappearing within few weeks or months;

- **BFIE**, described in 1992, characterized by focal and generalized seizures which occur in the first year of life, beyond the neonatal period, and spontaneously disappear after age 1-2 years.

BFNE and BFIE are autosomal dominant epilepsies of newborns and infants, respectively, who have structurally normal brain, normal interictal neurologic examination and normal neuropsychological development (Miceli et al., 2017). Though a subset of patients, as 15% of those, experience additional seizures later in life with also developmental or intellectual disorders (Plouin, 1994), the vast majority do not.

Several hypotheses have been made to explain the disappearance of seizures within few weeks or months. In particular, this effect could be due to the excitatory, and not inhibitory, action of GABA-ergic system in immature brain due to the higher intracellular concentration of Cl⁻ ions in neurons. Infact, in the early postnatal period the intracellular concentration of Cl⁻ is elevated with subsequent outward Cl⁻ currents, leading to membrane depolarization, contrarily to the hyperpolarizing effect due to GABA-induced inward Cl⁻ currents in the mature brain. Hence, with GABA acting as a depolarizing signal during the early postnatal period, the M-current might have an even more important role in the inhibition of an excessive neuronal firing (Okada et al., 2003). Infact, it is generally believed that a reduction of about 25% of the M-current is required for the disease's manifestation (Schroeder et al., 1998). Kv7.3-BFNE/BFIE mutations are only missense, randomly localized throughout the protein and responsible of loss-of-function (LoF) effect of channel activity.

Despite the common "benign" phenotype associated to mutations in Kv7.3, recently, the identification of new phenotypic features associated with Kv7.3 pathogenic variants has allowed to widen the phenotypic spectrum of Kv7.3, defining Kv7.3-related disorders as Kv7.3-developmental disability disorders (**Kv7.3-DD**). In fact, *de novo* variants have been identified in rare families with EOEE (Allen et al., 2013; Miceli et al., 2015), nonsyndromic sporadic intellectual disability (Rauch et al., 2012; McRae et al., 2017), and intellectual disability with seizures and cortical visual impairment (Bosch et al., 2016). Additionally, a recent clinical case of EOEE has been described in a patient

affected carrying two Kv7.3 *missense* mutations in compound heterozygosis (Ambrosino et al., 2018).

Notably, all pathogenic variants in Kv7.3 occur in heterozygosity, except one (Kothur et al., 2018). In this work, Kothur and colleagues have identified a homozygous frameshift variant, Kv7.3 S407Ffs*27, in three siblings. Clinical analyses revealed that these patients are affected with neonatal-onset seizures (reported as pharmacosensitive in one of them) and intellectual disability of variable severity (Kothur et al., 2018). Nevertheless, functional studies were not performed. Unlike Kv7.3, no homozygous frameshift variant in Kv7.2 has ever been described in humans (gnomAD), underlining that a minimal Kv7.2 residual activity probably is necessary, under penalty of potential lethality.

The molecular basis of the phenotypic heterogeneity of epileptic disease associated to Kv7.3 mutations is not clearly understood. Infact, since few families carrying Kv7.3 variants have been reported to date (RIKEE), genotype-phenotype correlations are difficult to establish. However, the phenotypic manifestation (BFNE and DD phenotypes) appears to be directly dependent on the underlying genetic mutation: it has been observed as a same Kv7.3 R230C pathogenic variant is responsible of developmental disability phenotype, allowing a probably genotype-phenotype correlation in Kv7.3.

The different clinical phenotypes could be a consequence of different functional alterations induced by mutations. Infact, while Kv7.3 variants in BFNE are LoF, *de novo* variant (R230C) recently identified showed a gain-of-function (GoF) effect. The identification of functional consequences prompted by Kv7.3 mutations could influence the choice of activators or blockers that enhance Kv7.3 channel function, leading to consider these channels and its modulators as important pharmacological targets.

1.10 Pharmacological features of Kv7.2/7.3 channels

The identification of activators and blockers on Kv7.2/7.3 channel function has been critical to elucidate their role in neuronal activity through a reduction or increase of the amplitude of the M-current, respectively.

Most effective Kv7 channel inhibitors includes the compound **linopirdine** and its derivate compound **XE991**, which potently block all Kv7 channels at low micromolar concentrations (Zaczek et al. 1998; Rockwood et al., 1997; Aiken et al., 1995). It is important to note that XE991 and linopirdine have recently been shown to be state-dependent blockers of these channels, only blocking channels that are in the open state (Greene et al., 2015). In addition, another blocker of Kv7 channels is Tetraethylammonium (**TEA**). TEA-sensitivity differs between Kv7.2 and Kv7.3 channel subunits: indeed, while Kv7.2 is highly sensitive to TEA (IC₅₀=0.3 mM), Kv7.3 is TEA-insensitive (IC₅₀=30 mM). This is a result of a tyrosine residue Y284, which is present in other known TEA-sensitive delayed rectifier potassium channels and is absent in Kv7.3 (Hadley et al., 2000). Moreover, Kv7.1 and Kv7.4 show an intermediate sensitivity: IC₅₀ are 5 and 3 mM, respectively (Hadley et al., 2000). Another inhibitor, 3-(triphenylmethylaminomethyl) pyridine (**UCL-2077**), inhibits Kv7 channels in a subtype-selective manner, acting mainly on Kv7.2 homomers, though has complex interactions with Kv7.3 (enhancing activity at hyperpolarized potentials, and inhibiting activity at depolarized potentials). Four additional compounds have been identified as potent inhibitors of Kv7.2, **ML213**, **ML252** (Yu et al., 2010; Cheung et al., 2012), the retigabine analogue **HN38** (Hu et al., 2013), and **NH17** (Kornilov et al., 2014), although the specificity of these compounds for Kv7.2 has not yet been established. Finally, the centipede toxin Ssm Spooky Toxin (**SsTx**) has recently been identified as a potent and specific inhibitor for all five Kv7 family members (Luo et al., 2018).

In addition to blockers, several activators of Kv7 channels have been identified. Most notably, **flupirtine** has been shown to activate Kv7.2 homomers (Wua et Dworetzky, 2005; Boscia F et al., 2006), but with several negative side-effects associated with flupirtine, including severe liver injury, have limited its clinical use (Michel et al., 2012; Klein et al., 2011). Another anticonvulsant, and flupirtine derivative, **retigabine** (ezogabine) is also a potent activator of neuronal Kv7 channels (Boscia et al., 2006; Wuttke et al., 2005; Tatulian et al., 2001). Retigabine acts by accelerating activation and decelerating deactivation kinetics, hyperpolarizing the V_{1/2} (Wuttke et al., 2005; Tatulian et Brown, 2003), stabilizing the open conformation of Kv7

channels. The effect of retigabine is slightly different depending on the subtype of Kv7 channels: the cardiac Kv7.1 channel, for instance, is completely insensitive to retigabine, while in the Kv7.3 homomers the effect on voltage sensitivity reaches its maximal extent. Despite the growing interest in anticonvulsant properties of retigabine and its use to treat various conditions resulting from neuronal hyperexcitability, multiple side-effects, including urinary retention, bluegray skin discoloration, poor brain penetration, chemical instability, and fast clearance rate, have been identified (Tang et al., 2016; Clark et al., 2015), limiting the clinical use of the retigabine as anti-epileptic drug: in fact, this drug has been withdrawn since June 2017 (https://assets.publishing.service.gov.uk/media/57fe4b6640f0b6713800000c/Trobalt_letter.pdf). Importantly, both flupirtine and retigabine lacked complete specificity for Kv7 channels as they also potentiate GABA-activated currents, particularly through GABA_A receptors (Treven et al., 2015). These limitations led to the development of flupirtine/retigabine analogues in attempt to improve the short comings of retigabine without compromising its anticonvulsant effectiveness. These include **SF0034** (Kalappa et al., 2015) and **RL648_81** (Kumar et al., 2016), both of which are more potent for Kv7.2, as well as **NS15370** (Dalby-Brown et al., 2013), which enhances Kv7.2-7.5 channels. In particular, preclinical studies performed in animal models revealed that SF0034 exhibits a more potent anticonvulsant activity and less toxicity than retigabine. Furthermore, SF0034 was significantly less active on Kv7.4 and Kv7.5 channels, suggesting that side effects observed for retigabine because of the activation of these channels could be reduced. SF0034 seems to be more chemically stable than retigabine and does not produce blue metabolites (Kalappa et al., 2015).

Multiple activators of Kv7.2/7.3 channels beyond flupirtine and its derivatives have also been identified. Three major classes of compounds, acrylamides, benzamides, and fenamates activate Kv7.2 or Kv7.2/7.3 channels.

- *Acrylamide family*. The derivative named **(S)-2** and its analogue compounds **(S)-3** through **(S)-6** all potently activate Kv7.2 channels, though their selectivity among Kv7 members has not been established (Wu et al., 2004; Wu et al., 2004). These compounds have proven effective at reducing neuronal activity, as shown by the ability of (S)-2 to reduce spontaneous

neuronal discharges measured in rat hippocampal slices, and the efficacy of (S)-6 when used to treat pain in two neuropathic models and in a formalin-induced pain test (Wu et al., 2013).

- *Benzamide family*. **ICA-27243** has been shown to activate Kv7.2/7.3 heteromeric channels at low concentrations ($EC_{50} = 0.4 \mu\text{M}$) and other Kv7 channels at much higher concentrations (Blom et al., 2010; Padilla et al., 2009; Roeloffs et al., 2008). Its clinical use has been restricted due to issues with toxicity, though a series of analogue alternatives have been analyzed including **ICA-069673**, an orally active compound with good pharmacokinetic properties, and **ICA-110381** (Provence et al., 2015; Boehlen et al., 2013).
- *Fenamates family*. They are most notably a class of nonsteroidal anti-inflammatory drugs (NSAIDs) known to inhibit cyclooxygenases COX-1 and COX-2; however, they also activate Kv7.2/7.3 channels, showing a surprising *in vivo* antiepileptic activity. In particular, meclofenamic acid and diclofenac activate Kv7.2/7.3 channels ($EC_{50} \approx 3 \mu\text{M}$) by hyperpolarizing the voltage-dependence of activation and slowing deactivation (Peretz et al., 2005), without activity on cardiac Kv7.1 channels.

Finally, a handful of other compounds has been shown to activate Kv7.2 or Kv7.2/7.3 channels, including Zinc Pyrithione (**ZnPy**; Kv7.2) (Xiong et al., 2007), **ML213** (Kv7.2) (Yu et al., 2010), **NS1643** (Kv7.2 and Kv7.2/3) (Li et al., 2014), and the urate transporter inhibitor **Benzbromarone** (Zheng et al., 2015).

1.11 The Kcnq3 transgenic mice

It is important to note that, to date, no available compound specifically inhibits Kv7.2 or Kv7.3 channels, and only one activator that shows specificity for Kv7.2 and Kv7.2/7.3 over Kv7.4 and Kv7.3/7.5 is ICA-27243 (Bloom et al., 2010). For this reason, multiple lines of transgenic mice have been generated to study the involvement of Kv7.3 in the control of neuronal excitability since its identification as a gene associated with several neurological diseases.

Among these mice lines, an animal model for BFNE has been obtained by the introduction in Kv7.3 genes of human BFNE-causing mutation in mice-strain, to better understand also the possible interference of genetic

background (Singh et al., 2008). The mutation G311V in Kv7.3 affected pore-region, thus causing a dramatic decrease of channel activity, has been characterized using a homozygous mice for Kv7.3 G311V. The Kv7.3 mutant mice has been obtained using the ACN self-excision cassette that is made up of Cre-recombinase gene driven by the testes-specific promoter from the angiotensin-converting enzyme gene (tACE) and a selectable marker driven by the mouse RNA polymerase II (polII) (Bunting et al., 1999). Within the ACN cassette, the neomycin (Neo^R) gene driven by the mice RNA polII promoter confers positive selection of embryo-derived stem (ES) cells, and the entire cassette is flanked by loxP sites. Instead a thymidine kinase (TK) gene is used for the negative selection (Thomas et Capecchi, 1987). The Kv7.3 mutant mice showed early onset spontaneous generalized tonic-clonic seizures, with electro-encephalographic alteration suggesting a limbic origin of convulsions. Moreover, adult homozygous mice had recurrent seizures that triggered molecular plasticity including ectopic neuropeptide Y (NPY) expression; in addition, overall mortality was increased when compared to control littermate, with differences depending on mutation and murine strain. Interestingly, despite the severe phenotype, no significant morphological alteration, such as hippocampal mossy fibers sprouting or neuronal loss, was found in homozygous mice, thus paralleling the normal neurodevelopmental cognitive profile exhibited by most BFNE patients (Singh et al., 2008).

In 2008, Tzingounis and Nicoll reported studies on a constitutive Kcnq3 knockout mouse line. In this case, unlike for constitutive Kcnq2 deletion, Kcnq3 deletion yielded viable mice (Tzingounis et Nicoll, 2008). Kcnq3 knockout mice has a deletion from base 1803 to 1824 by insertion of LacZ-Neo cassette construct. In these mice, electrophysiological experiments were carried out to determine the contribution of Kv7.3 in mediating the apamin-insensitive medium afterhyperpolarization current (ImAHP) in the hippocampus. In particular, Tzingounis and colleagues identified that while in CA1 pyramidal neurons deletion of Kcnq3 did not reduce the ImAHP, recordings in dentate gyrus cells of Kcnq3 KO revealed a decrease of this current of about 50%. The lack of effect of Kcnq3 deletion was later recapitulated by Soh using a conditional knockout line for Kcnq3 utilizing the Cre/LoxP deletion system (Soh et al., 2014). Emx-cre Kcnq3^{flox} mouse line

has been obtained by the crossing between $Kcnq3^{fl/+}$ mice, absent from the neomycin cassette in all somatic and germline cells by FRT/FLP system, and $Emx1$ -ires-cre recombinase strain, a transgenic mice that expressed Cre recombinase only in CA1 pyramidal neurons. Indeed, $Kcnq3$ cKO mice showed a cerebral CA1- specific deletion of Kv7.3 channels. Soh et al. (2014) identified a reduction in the M-current, but, unlike $Kcnq2$ deletion, $Kcnq3$ cKO mice did not show increased excitability in CA1 pyramidal neurons. One major difference between Tzingounis and Soh studies (Tzingounis et al., 2008, and Soh et al., 2014) is the use of conditional versus constitutive $Kcnq3$ knock-out mice. In constitutive $Kcnq3$ knockout mice, $Kcnq3$ deletion occurs throughout the nervous system and development, unlike the conditional knockout mice used in the current study, in which $Kcnq3$ deletion is restricted to hippocampal CA1 area. Consequently, global versus conditional $Kcnq3$ deletion may engage different compensatory programs at the network level, leading to different effects on the M current: it is hypothesized that the loss of $Kcnq3$ gene is compensated for in certain cell types such as CA1 pyramidal neurons, possibly by other members of the Kv7 family.

In 2016, Kim and colleagues generated a $Kcnq3$ KO mice by crossing $Kcnq3^{fl/fl}$ mice to $Hprt$ -cre cassette to evaluate whether changes in PIP2 levels could shift the voltage-activation in genetically ablating $Kcnq3$ (Kim et al., 2016). Recording from CA3 pyramidal neurons in $Kcnq3$ KO mice revealed the critical role of $Kcnq3$ gene for the sAHP under conditions of low or depleted PIP2 levels, underlined by a higher affinity of Kv7.3 channels for PIP2.

In 2018, Soh investigated the role of $Kcnq3$ on firing properties in parvalbumin-positive (PV+) and somatostatin-positive (SST+) interneurons, cell types known to express Kv7.2/7.3 channels (Cooper et al., 2001) using a conditional $Kcnq2/3$ KO (Soh et al., 2018). In particular, $Kcnq2$ or $Kcnq3$ floxed mice ($Kcnq2^{fl/fl}$ or $Kcnq3^{fl/fl}$, respectively) have been crossed to $Nkx2-1^{cre}$ mice, in which Cre recombinase is expressed starting early in development in SST+ and PV+ interneurons, allowing to study the impact of Kv7.2/7.3 channel ablation in young and juvenile neurons. The mice obtained were subsequently crossed with a reporter line (Ai9), a fluorescent protein, allowing to identify Cre-expressing PV+ and SST+ interneurons. The data

obtained demonstrated that ablation of Kcnq2/3 changed PV+ interneurons firing properties, but not effects of this deletion have been shown in SST+ interneurons. In particular, Kcnq2/3 knock-out mice in PV+ interneurons led to elevated homeostatic potentiation of fast excitatory transmission in pyramidal neurons (Soh et al., 2018).

All Kcnq3 transgenic mice are summarized in the follow Table 2:

Table 2. Overview of Kcnq3 transgenic mice.

Kcnq3 transgenic mice	Strategy	Phenotype	Effects	References
Knock-in (G311V, pore domain)	Homologous recombination Kcnq3 G311V mice obtained using an ACN self-excision cassette	Kcnq3 ^{mut/mut} . died prematurely (within P0-P30). Mice showed spontaneous seizures. Kcnq3 ^{wt/mut} . Increased susceptibility to seizures in older mice (P140-P180).	Model of BNFE No significant morphological alteration, such as hippocampal mossy fibers sprouting or neuronal loss	Singh et al., J. Physiol 2008
Constitutive KO	Kcnq3 KO mice obtained breeding Kcnq3 ^{-/-} mice. Deletion from 1803 to 1824 by insertion of a LacZ-Neo cassette	Unlike Kcnq2 KO mice, Kcnq3 deletion yield a viable mice	mAHP current and the M-current were not reduced in CA1 pyramidal neurons, but were significantly smaller in dentate gyrus granule cells	Tzingounis et Nicoll, PNAS 2008
Conditional KO (cerebral cortical pyramidal neurons)	Emx-cre Kcnq3 ^{fllox} mouse line has been obtained by crossing between Kcnq3 ^{fl/+} mice and Emx1-ires-cre mice Deletion of exons 2-4	Kcnq3 ^{fl/fl} : alive at birth	Reduction in the M-current, without changes in CA1 pyramidal neuron activity	Soh et al., J. Neurosc 2014
Constitutive KO	Kcnq3 KO mice generated by crossing Kcnq3 ^{fl/fl} mice to Hprt-cre cassette	Kcnq3 ^{-/-} mice survived to adulthood and showed no evidence of seizures	Role of Kcnq3 in the IsAHP, particularly under conditions of low PIP2 levels	Kim et al., Biophys J 2016
Conditional KO (Interneurons)	Kcnq2/3 ^{fllox} mouse line has been obtained by crossing between Kcnq3 ^{fl/+} mice and Nkx2-1 cre mice	Not reported	Ablation of Kcnq2/3 changed PV+ interneurons firing properties, but not effects of this deletion have been shown in SST+ interneurons	Soh et al., Elife 2018

2 Aim of work

The KCNQ3 gene encodes for neuronal Kv7.3 channel subunits which form heteromeric channels with the homologous Kv7.2 subunits: these channels underline the so-called M-current that inhibits neuronal excitability. However, it is difficult to study the distinct role of neuronal Kv7.3 channel apart from Kv7.2 subunit as no pharmacological compound currently exists that selectively inhibits Kv7.2 or Kv7.3.

Two decades ago, genetic studies have identified Kv7.3 *missense* mutations as a less probable cause compared to Kv7.2 for an autosomal dominant epilepsy, namely Benign Familial Neonatal Epilepsy, characterized by seizures starting during the first week of postnatal life and spontaneously remitting within the first year (Charlier et al., 1998). Only more recently, targeted and whole exome sequencing revealed that some Kv7.3 *de novo* variants are also linked to severe forms of epilepsy including EOEE (Allen et al., 2013), ID (Rauch et al., 2012; McRae et al., 2017), and cortical visual impairment (Bosch et al., 2016). These more recent data highlight that, in close analogy to Kv7.2, also Kv7.3 gene variants in humans are associated to a wide phenotypic variability, ranging from transmittable familial forms on the benign end, to *de novo* mutations occurring in more severe mostly sporadic cases.

On these premises, the aim of the present Doctoral Project has been to elucidate some of the critical aspects of Kv7.3 function in the brain by a combined approach using both an animal model of Kv7.3 disfunction and studies carried out in families/individuals carrying specific Kv7.3 variants. In particular, I have carried out experimental studies aimed at investigating:

1. the role of Kv7.3 channel subunits in controlling the excitability of neurons located in the subiculum and in the CA1 pyramidal neurons, two cortical brain regions critically involved in the seizure onset and propagation. To this aim, conditional *Kcnq3* knockout mice lines have been used to investigate the differential contribution of Kv7.3 subunits to the firing properties of these distinct neuronal populations, as well as the effects on these properties of the pharmacological modulation by retigabine, a neuronal Kv7 activator.
2. the functional consequences of mutations in Kv7.3 found associated with distinct clinical phenotypes in humans. In particular, I have carried out

electrophysiological, biochemical, pharmacological, and modeling studies to assess the consequences on channel properties determined by:

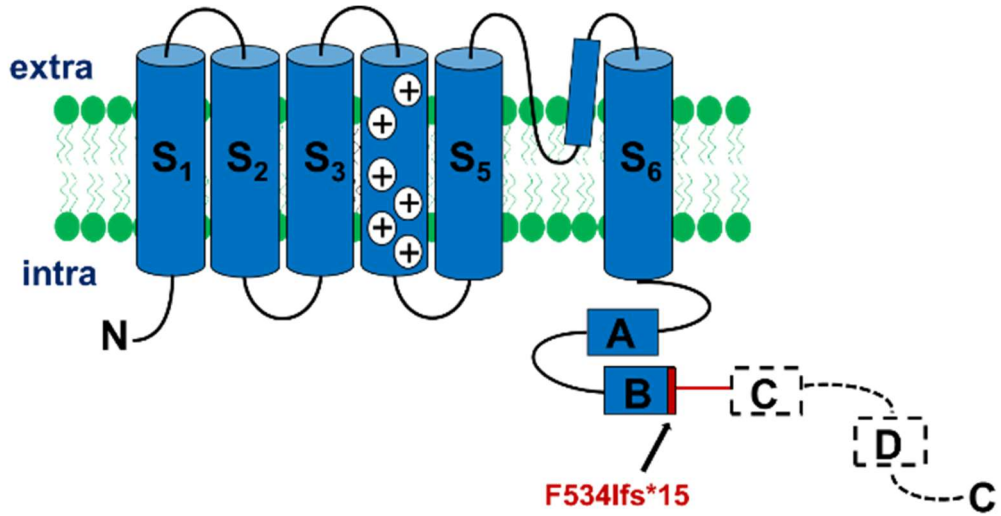
- a. a *frameshift* variant (Kv7.3 F534Ifs*15) found in homozygous configuration in a patient with pharmacodependent neonatal-seizures and non-syndromic ID (Lauritano et al., 2019) (Table 3 and Fig. 10A). This component of my work has been of great relevance given that all (except one, Kothur et al., 2018) previously-found Kv7.3 mutations are found in heterozygosity, and the specific variant represents a unique opportunity to investigate the consequence of a complete deletion of Kv7.3 in humans.
- b. four *de novo* variants (Kv7.3-R227Q, -R230C, -R230S, and -R230C) affecting the first two arginines along the primary sequence of Kv7.3 S4 transmembrane segment of the the voltage-sensing domain found in patients with global neurodevelopmental disability (NDD), autism spectrum disorder (ASD), and Sleep-Activated Near-Continuous Multifocal Spikes (Sands et al., 2019) (Table 3 and Fig. 10B). This newly-described unique phenotype was not associated to neonatal-onset seizure, a distinctive feature which allowed a further expansion of the phenotypic spectrum of diseases associated to Kv7.3 gene variants.

Table 3. List of the naturally-occurring mutations studied in the present work.

Nucleotide substitution	Amino acid substitution	Localization
c.1598_1599ins_A	p.(F534Ifs*15)	C-terminal (helix B)
c.680G>A	p.R227Q	S ₄
c.689C>T c.689G>A (mosaic)	p.R230C	S ₄
c.688C>A	p.R230S	S ₄
c.689G>A	p.R230H	S ₄

“c.” indicates the nucleotide substitutions, “p.” indicates the amino acid mutations.

A



B

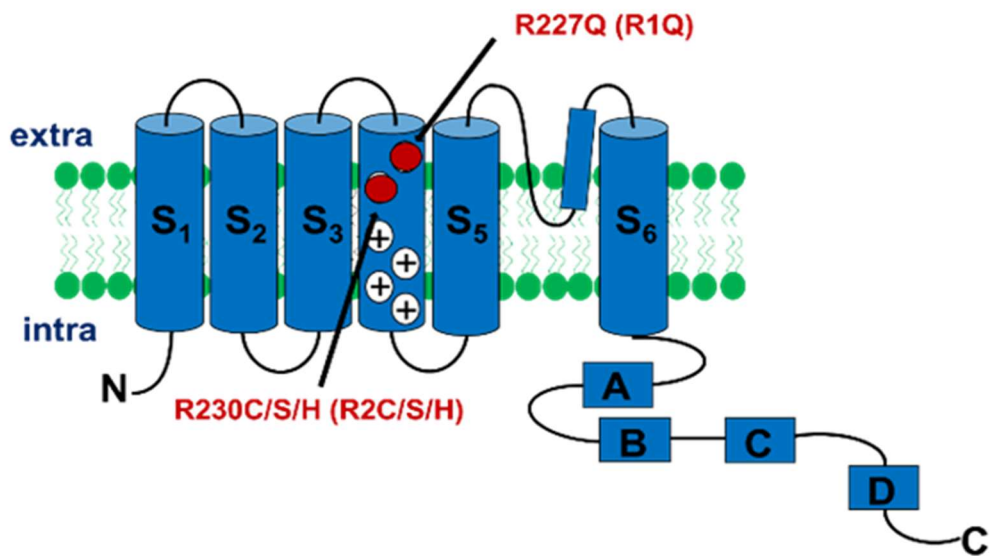


Fig. 10. Schematic drawing of a Kv7.3 subunit and location of the mutations studied in the present work.

A) The red block indicate the location of F534Ifs*15 mutation, located in the helix B of the C-terminal domain; B) the colored circles indicate the location of R230C/S/H variants investigated, located in the S₄ of VSD.

3. Materials and methods

3.1 Site-Directed Mutagenesis of Kv7.3 cDNA

Each mutation was engineered in a pcDNA3.1-Kv7.3 plasmid encoding for the human transcript *variant 1* of Kv7.3 (accession number: NC_004519.3; 872 amino acids) wild-type or incorporating the mutation F534I fs*15 (for electrophysiological and western-blot experiments) and the mutations R227Q and R230C/S/H (for electrophysiological experiments) by Quick-change Site-Directed Mutagenesis (Agilent Technologies). The mutations were engineered in each plasmid by Polymerase Chain Reaction (PCR), using a pair of primers (forward and reverse) (Table 4), incorporating the nucleotide mutation found in the patients.

Mutation	Primers
Kv7.3 F534I fs*15	F 5'-GTCTCTATAAAAAAAAAAATTCAAGGAGACTTTGAG-3' R 5'-CTCAAAGTCTCCTTGAATTTTTTTTTTTATAGAGAC-3'
Kv7.3 R227Q	F 5'-CCTGCGAAGCCTGCACTTCCTGCAGATCC-3' R 5'-GGATCTGCAGGAAGTGCAGGCTTCGCAGG-3'
Kv7.3 R230H	F 5'-CCTGCGAAGCCTGCACTTCCTGCAGATCC-3' R 5'-GGATCTGCAGGAAGTGCAGGCTTCGCAGG-3'
Kv7.3 R230S	F 5'-CCCTGCGAAGCCTGAGCTTCCTGCAGATC-3' R 5'-GATCTGCAGGAAGCTCAGGCTTCGCAGGG-3'
Kv7.3 R230C	F 5'- CCCTGCGAAGCCTGTGCTTCCTGCAGATC -3' R 5'- GATCTGCAGGAAGCACAGGCTTCGCAGGG -3'

Table 4. Experimental conditions used for PCR reaction.

Column 1) Mutations found in patients and engineered in the Kv7.3 templates. Column 2) Nucleotide sequences of primers used for PCR.

The amplification reaction was performed in a final volume of 50 μ L containing the following components: 50 ng of plasmid for Kv7.3-WT, 125 ng primer forward, 125 ng primer reverse, 5% DMSO, 2.5U Pfu DNA Polymerase, 1X buffer Pfu, 1 μ l dNTP mix. The PCR consisted of 12 cycles, with each cycle consisting of three temperature steps, that allow the

denaturation of the DNA Double Helix (95°C for 1'), the annealing of the primers to the single strand of DNA (55°C for 1') and the extension of the primers (68°C for 10') (Fig.11). After the amplification reaction, the volume of the reaction contained both methylated (parental) and unmethylated (neo-synthesized) DNA: therefore, in order to remove the parental DNA, enzymatic digestion was performed with 1 µl DpnI enzyme (10 U/ µl) able to digest only methylated DNA.

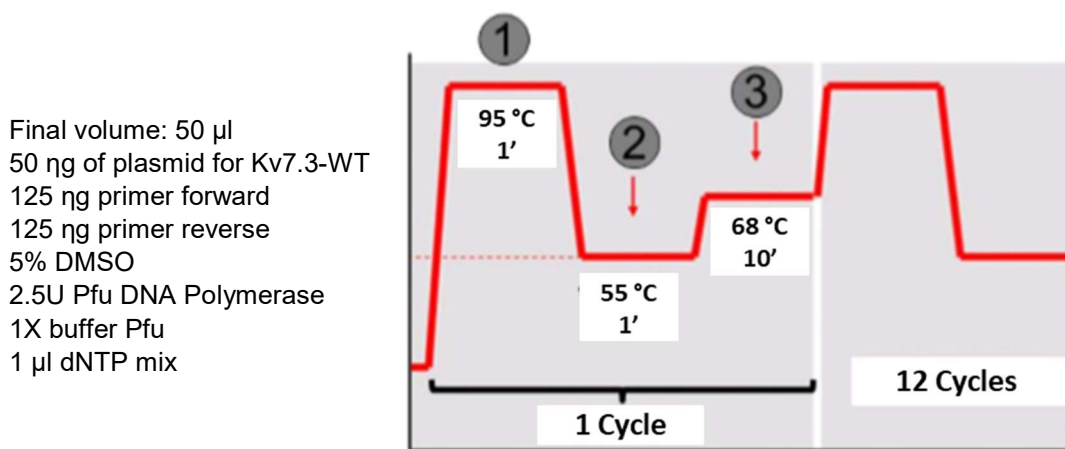


Fig. 11. Schematic representation of the Polymerase Chain Reaction.

Phase 1) Denaturation of the DNA. Phase 2) Annealing of the mutated primers to the specific complementary sequence of the DNA. Phase 3) The Pfu polymerase synthesizes a new DNA strand complementary to the DNA template strand.

3.2 Bacterial transformation and plasmidic DNA preparation

After enzymatic digestion with DpnI, competent *E. coli* DH5α cells were transformed with the PCR product by chemical transformation procedure (30' at 4°C, heat shock step at 42°C for 45'' followed by 3' at 4°C). To help the bacterial cells recover from the heat shock, the cells were incubated with 200 µl SOC medium (2% tryptone, 0.5% yeast extract, 10 mM NaCl, 2.5 mM KCl, 10 mM MgCl₂, 10 mM MgSO₄, 20 mM glucose), for 45' at 37 °C. Finally, the cells were seeded into LB+agar plates (containing 10 g/L tryptone, 5 g/L yeast extract, 5 g/L di NaCl, agar 15 g/L) with the specific antibiotic, to which the plasmids are resistant, such as ampicilin (100 µg/µL) to allow the growth

only of E.coli cells transformed with pcDNA3.1 plasmids (in which Kv7.3 cDNA is present) (Fig. 12).

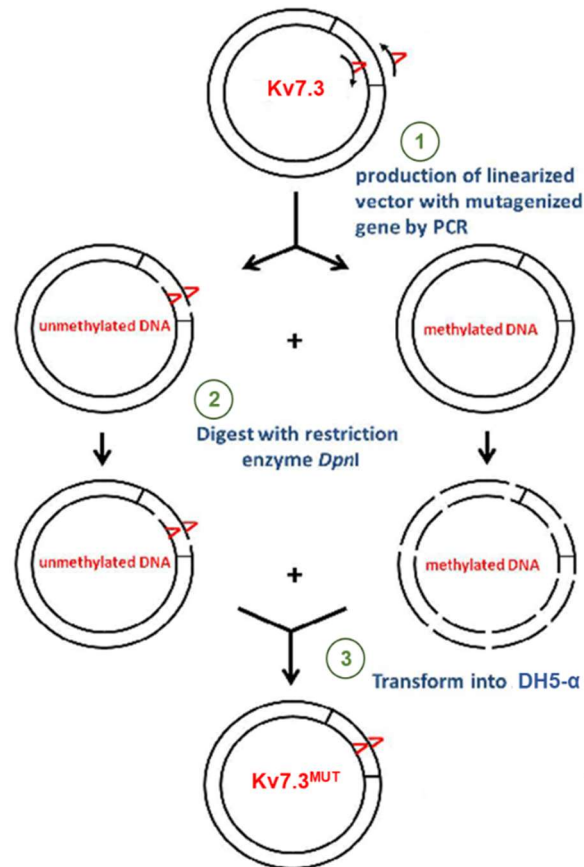


Fig. 12. Overview of the QuickChange Mutagenesis method.

1) PCR amplification. The black arrows indicate the mutagenic primers used for PCR. 2) Methylated and unmethylated DNA, which present the mutation, digested by DpnI enzyme. 3) After transformation, the DH5- α cells repair the nicks in the mutated plasmid.

Plates were then incubated inverted at 37 °C for about 16 h to allow bacterial growth. Each colony grown on the LB medium was inoculated in 5 mL of fresh LB medium with antibiotic selection (Amp/Kan), in agreement with the antibiotic resistance conferred by the plasmids to the E. coli cells, at 37°C/220 rpm overnight. Then, plasmidic DNA was extracted by using a commercially available kit (*QIAprep Spin Miniprep*, QIAGEN). The successful insertion of the desired mutation has been verified by direct sequencing (Eurofins, Milan,

Italy). To obtain DNA in large amount, one of the positive clones was amplified on a large scale (500 mL) and plasmidic DNA was extracted by using a commercially available kit (*Plasmid Plus Maxi*, QIAGEN). The cDNA was sequenced again, to confirm the presence of the mutation of interest and to exclude additional mutations in the entire coding sequence.

3.3 Cell cultures

3.3.1 Chinese Hamster Ovary cells

Chinese Hamster Ovary (CHO) cells were grown in plastic Petri dishes (100 mm, 60 mm or 40 mm, according to the different experimental needs) in DMEM (*Dulbecco's Minimum Eagle Medium*) supplemented with 10% Fetal Bovine Serum (FBS; decompemented at 56°C for 30'), 1% L-glutamine (2 mM in 0.85% NaCl), 1% penicillin (50 U/mL) and 1% streptomycin (50 µg/mL) in a humidified atmosphere at 37°C with 5% CO₂. Everytime cells became confluent within the dishes (about every 2 days), they were split by using 1% trypsin solution and collected in novel dishes with a 1:3 dilution.

3.3.2 Human fibroblasts

Human fibroblasts, samples obtained from the patient's skin, were cultured in plastic Petri dishes (100 mm) in DMEM (*Dulbecco's Minimum Eagle Medium*) supplemented with 10% Fetal Bovine Serum (FBS, decompemented at 56°C for 30'), 1% L-glutamine (2 mM in 0.85% NaCl) in a humidified atmosphere at 37°C with 5% CO₂.

3.4 Animals and genotyping

C57B6/J conditional *Kcnq3* knockout mice lines were generated from Jackson Laboratory. The conditional *kcnq3* KO mice of CA1 pyramidal neurons was obtained by crossing the *Kcnq3^{fl/+}* mice with *Emx1-ires-cre* (*Emx1*) mice, a transgenic mice that expressed Cre only in CA1 pyramidal neurons (Soh et al., 2014); whereas the conditional *kcnq3* KO mice of the subicular neurons was obtained by crossing the *Kcnq3^{fl/+}* mice with *G5-Emx-cre* (*G5*) mice, expressing Cre only in subicular neurons. Both *Kcnq3* cKO mice lines obtained had an exon 2-4 deletion. Genotyping of the *Kcnq3* KO mice consisted of PCR followed by DNA gel electrophoresis. Two primers

were used to amplify the region of interest: a wild-type Kv7.3 forward (5'-CAGCACTCCCATGACAAATG -3') and a wild-type Kv7.3 reverse (5'-TCTCCCATGGCAAGTATTCC -3') primers. The PCR protocol consisted of 0.35 μ L template DNA, 0.38 μ L 10 μ M primer (forward and reverse), 8 μ L Mastermix, and 7.27 μ L ddH₂O for a total volume of 16.0 μ L. The PCR protocol consisted of the following steps: (1) 94°C, 3'; (2) 94°C, 30"; (3) 55°C, 30"; (4) 72°C, 30", steps 2-4 repeated for 34 cycles; (5) 72°C, 5'. PCR product was then loaded into a 2% agarose (MetaPhor) gel and electrophoresis was run at 150 V for 15 minutes in 0.5x TAE buffer. Presence of the Kv7.3 allele produced a 390 bp fragment. Both male and female mice were used for acute slices prepared from mice post-natal day 15-20, as described below (see section 3.5.2 *Slices preparation and electrophysiology*).

3.5 Whole-cell electrophysiology

3.5.1 CHO cells preparation and electrophysiology

For electrophysiological experiments, CHO cells were seeded on glass coverslips, heat-sterilized and pre-coated with poly L-lysine, in 35 mm dishes. After 24h, CHO cells were transfected using Lipofectamine 2000, according to the manufacturer protocol (*Life Technologies*, Milan, Italy). In each transfection mixture, a plasmid encoding for an Enhanced Green Fluorescent Protein (pEGFP; *Clontech*, Palo Alto, CA) was used as transfection marker (3 μ g of plasmids encoding for Kv7.3 cDNA + 1 μ g di pEGFP).

Macroscopic currents were recorded, after 1 day, using patch-clamp technique in the whole-cell configuration with glass micropipettes of 3–5 M Ω resistance. No compensation was performed for pipette resistance and cell capacitance. During patch clamp recordings, cells were perfused with an extracellular solution containing (in mM): 138 NaCl, 5.4 KCl, 2 CaCl₂, 1 MgCl₂, 10 glucose, 10 HEPES, pH 7.4 (adjusted with NaOH). The pipettes used for recordings were filled with an intracellular solution containing (in mM): 140 KCl, 2 MgCl₂, 10 EGTA, 10 HEPES, 5 Mg-ATP, pH 7.4 (adjusted with KOH). The data were acquired and analyzed using a commercially available amplifier (Axopatch 200A, Axon Instruments, Foster City, CA, USA) and pCLAMP10 software (Axon Instruments).

To generate conductance/voltage curves, cells were held at -80 mV, then depolarized for 1.5 s from -80 mV to +40 mV in 10 mV increments, followed by an isopotential pulse at 0 mV (Fig 13). Current values recorded at the beginning of the 0 mV pulse were measured, normalized, and expressed as a function of the preceding voltage. The data obtained were then fit to a Boltzmann distribution of the following form:

$$y = \text{max} / [1 + \exp (V_{1/2} - V)/k]$$

where V is the test potential, $V_{1/2}$ indicate the half-activation potential, and k the slope factor (Fig.13). Current densities (expressed in picoamperes per picofarad, pA/pF) were calculated as peak K^+ currents (pA) measured at 0 mV divided by the capacitance of the same cell (expressed in pF).

The effects of drugs on Kv7.3 currents were tested by using a different protocol, namely by a ramp protocol, in which the voltage was progressively increased from -80 mV to +40 mV (Fig. 14) in a period of 5 sec.

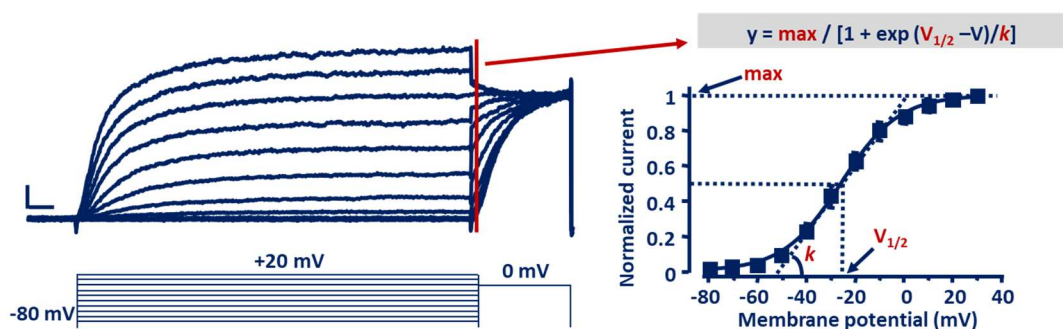


Fig. 13. Whole-cell configuration of patch-clamp technique. On the left, representative trace obtained by application the voltage protocol in the bottom. On the right, conductance/voltage curve obtained fitting to a Boltzman distribution the data.

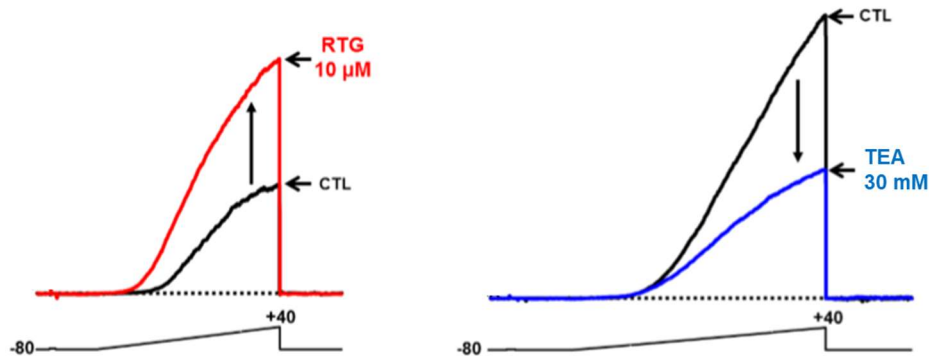


Fig. 14. Functional effects prompted by the Kv7.3 modulators, using ramp protocol. On the left is shown the activator effects of retigabine while on the right is shown the inhibitors effects of TEA.

3.5.2 Slices preparation and electrophysiology

Mice post-natal day 15-20 (P15-P20) were anesthetized using isoflurane (Baxter Healthcare, Deerfield, IL) and euthanized by decapitation. Brains were quickly removed and placed in ice-cold cutting solution consisting of the following: 26 mM NaHCO₃, 210 mM sucrose, 10 mM glucose, 2.5 mM KCl, 1.25 mM NaH₂PO₄, 0.5 mM CaCl₂, and 7 mM MgCl₂. Cerebellum was removed, and 300 μm coronal slices were cut using a vibratome (Microm HM 650 V, Thermo Fisher Scientific, Waltham, MA). Slices were then transferred to a holding chamber containing artificial cerebrospinal fluid (aCSF) consisting of the following: 125 mM NaCl, 26 mM NaHCO₃, 2.5 mM KCl, 1 mM NaH₂PO₄, 1.3 mM MgCl₂, 1.5 mM CaCl₂, and 12 mM D-glucose. Slices were recovered at 35°C for 30 minutes, then left at room temperature (RT; ~22°C) for ≥ 1 h prior to electrophysiological recording. Both cutting and aCSF solutions were saturated with 95% O₂/5% CO₂.

Whole-cell recordings were obtained using electrodes pulled from thin-walled borosilicate glass capillaries (World Precision Instruments, Sarasota, FL) that had resistances of 2-4 MΩ when filled with recording solution, as described below. The internal recording solution for whole-cell recording was different for each area evaluated. For subiculum consisted of the following: 115 mM potassium gluconate, 20 mM KCl, 4 mM Mg·ATP, 0.3 mM Na·GTP, 10 mM HEPES, and 10 mM Na₂-phosphocreatin (osmolarity ~300 mOsm) (Spruston

et al., 2015). For CA1 consisted of the following: 125 mM potassium gluconate, 20 mM KCl, 4 mM Mg·ATP, 0.3 mM Na·GTP, 10 mM HEPES, 0.1 mM EGTA, and 10 mM Tris-phosphocreatine (osmolarity ~278 mOsm). The pH was adjusted to 7.2-7.3 with KOH. All slice recordings were taken from subicular, proximal or distal, or CA1 neurons with an initial resting membrane potential of -65 or -70 mV, respectively. The previously described aCSF was used as the external bathing solution. Resting membrane potential was determined in current clamp as the potential upon break-in, before any current injection. All recordings were performed at 1.5mM Ca²⁺ and high temperature (32°C) using a Multiclamp 700B amplifier (Molecular Devices, Sunnyvale, CA), filtered at 2 kHz and sampled at 50 kHz. To induce firing, we depolarized neurons by injecting currents of variable amplitude for 1 s. As shown in Fig. 15, increasing the magnitude of the injected current from +25 pA to +250 pA in increments of +25 pA led neurons to fire the action potentials (APs) in greater number and frequency (Fig. 15). Data were analyzed offline using Clampfit (Molecular Devices, Sunnyvale, CA), and Prism 7 (GraphPad, La Jolla, CA) software.

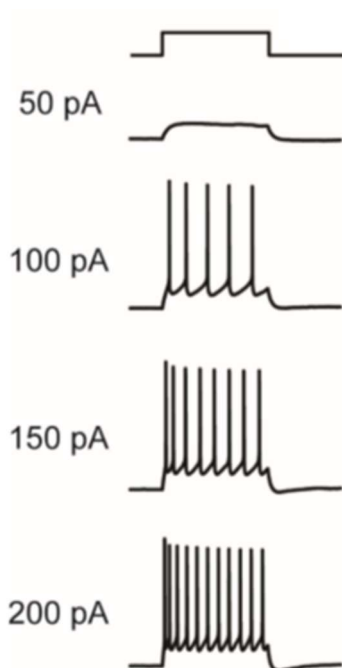


Fig. 15. Representative voltage protocol

This protocol responses to various current injection steps (1 s from +50 pA to +200 pA). Membrane potential was kept at -65 and -70 mV (subiculum and CA1, respectively) by injecting a small direct current (DC) through the recording pipette.

3.6 Western Blotting

CHO cells, obtained 24 hours post-transfection, were homogenized with Laemmly buffer (4% SDS, 20% glycerol, 10% 2 mercaptoethanol, 0.004% bromophenol blue, 0.125 M Tris HCl). Kv7.3 subunits in total protein lysates were then loaded onto 8% SDS-PAGE gels in running buffer (25 mM Tris, 192 mM glycine, 0.1% SDS), subjected to electrophoresis and then transferred onto a nitrocellulose membrane (NC) in transfer buffer (25 mM Tris, 192 mM glycine, 20% methanol). NC blotting papers were then incubated with 5% milk in the blocking solution (5% milk dissolved in PBS-Tween buffer) to block non specific binding sites on the membrane for 1h at RT; then, blots were incubated over night using two primary rabbit antiKv7.3 polyclonal antibodies: (a) the first directed against a C-terminal epitope (rat aa 668-686; accession number O88944; C-Kv7.3) (clone APC-051, dilution 1:1000; Alomone Labs) and (b) the second raised against an N-terminal epitope (rat aa 1-71; N-Kv7.3) (PA1-930; dilution 1:1000; Thermo Scientific). Both antibodies also recognized human Kv7.3 subunits (Fig. 16). Following exposure to primary antibodies, filters were incubated with HRP-conjugated antirabbit secondary antibodies (NA934V; dilution 1:5,000; GE Healthcare) which allows the emission of light in the presence of enhanced chemiluminescence (ECL) solutions (Promega, Madison, WI, USA). Data acquisition and analysis were performed with the Gel Doc Imaging System (Bio-Rad) and ImageLab software (version 4.1; Bio-Rad), respectively.

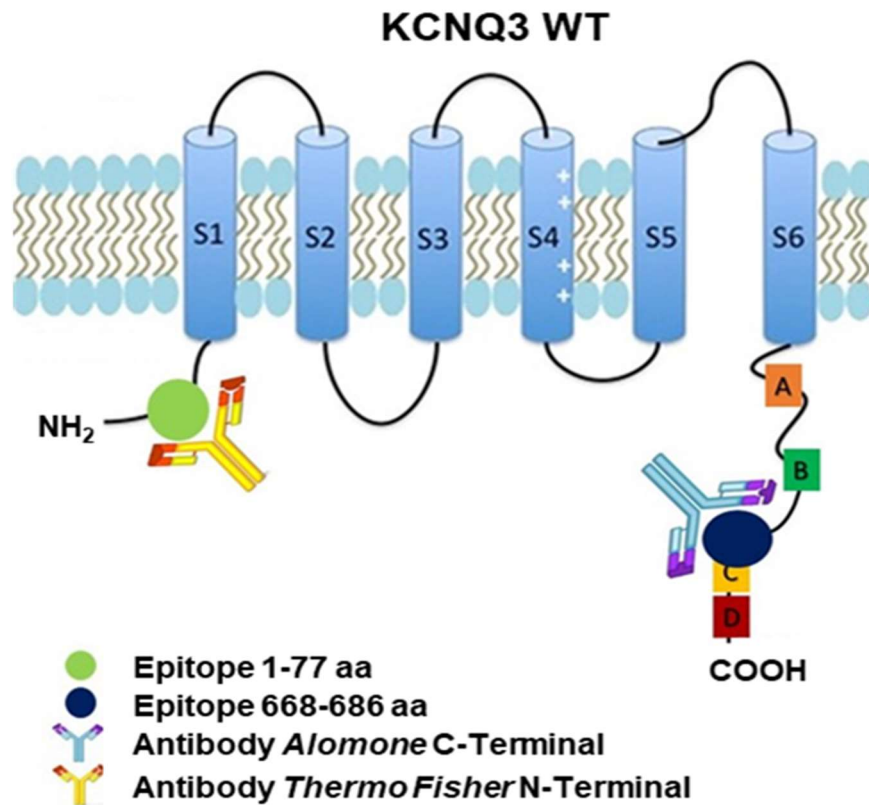


Fig. 16. N- terminal and C-terminal antibodies against Kv7.3 subunit.

3.7 Real-Time PCR

Total RNA was extracted from fibroblasts obtained from the proband (-/-) and the healthy control (+/+) using TriReagent (Sigma).

Isolation and purification of RNA was performed using the TriReagent (Sigma, St. Louis, MO, USA). 1 µg of total RNA was retrotranscribed with the High Capacity cDNA RT Kit (Applied Biosystem, ThermoFisher Scientific, Milan, IT). For quantitative PCR, cDNA was amplified with the TaqMan Gene Expression assay in a 7500 Fast RealTime PCR System thermocycler (Applied Biosystems, ThermoFisher Scientific, Milan, IT). Commercially-available probes were used to amplify Kv7.1, Kv7.2, Kv7.3, Kv7.4 and Kv7.5 mRNAs (Applied Biosystem TaqMan gene expression, codes Kv7.1: hs00923522_m1; Kv7.2: hs01548339_m1; Kv7.3: hs01120412_m1; Kv7.4: hs00542548_m1; Kv7.5: hs01068536_m1). The comparative $\Delta\Delta CT$ method was used to quantify transcript abundance using the Ubiquitin Conjugating

Enzyme (UBC; hs05002522_g1) gene as control (Lanzafame et al., 2015). Three separate experiments, each in triplicate, were performed for each probe.

3.8 Homology modeling

Three-dimensional models of Kv7.3 subunits were generated by using as templates the coordinates of 6 different states of Kv1.2/2.1 paddle chimera obtained in molecular dynamics simulations (Jensen et al., 2012) by SWISS-MODEL (University of Basel, Basel, Switzerland). The models were optimized through all-atom energy minimization by using the GROMOS96 implementation of Swiss-PDBViewer and analyzed using both the DeepView module of Swiss-PDBViewer (v4.0.1; <http://spdbv.vital-it.ch/>) and PyMOL (<http://www.pymol.org/>), as described (Ambrosino et al., 2018; Miceli et al., 2015). Sequence alignment was performed using ClustalOmega (<https://www.ebi.ac.uk/Tools/msa/clustalo/>).

3.9 Immunofluorescence

Fibroblasts were fixed with 4% paraformaldehyde in PBS for 10 minutes at room temperature (RT). After permeabilization with 0.1% Tween-20 for 5 minutes and blocking with 0.5% BSA for 1 hour at RT, cells were incubated overnight at 4°C with the N-KCNQ3 antibody (1:300), followed by a 1 hour incubation with donkey anti-rabbit Cy3-conjugated secondary antibody (Applied Biosystems, Thermo Fisher Scientific) at RT. Nuclei were visualized using Hoechst 33258 (1:5000) in PBS. Coverslips were mounted in Fluoromount G (eBioscience, Hatfield, Hertfordshire, UK). Image acquisition was performed by Zeiss inverted LSM 700 confocal laser scanning microscope (Carl Zeiss) and analyzed with ImageJ (NIH). Slides in which the primary antibody was omitted were used as controls in all experiments.

3.10 Statistics

Data are expressed as the mean \pm standard error of the mean (SEM). Statistically significant differences between the data were evaluated with the Student's t test, with the threshold set at $p < 0.05$.

4.Results

4.1 Role of Kv7.3 in neuronal excitability of subiculum and CA1 pyramidal neurons

The subiculum, a main distal output of the hippocampus, is an anatomical area between the hippocampus and the entorhinal cortex (EC) of the parahippocampal gyrus (Fig. 17).

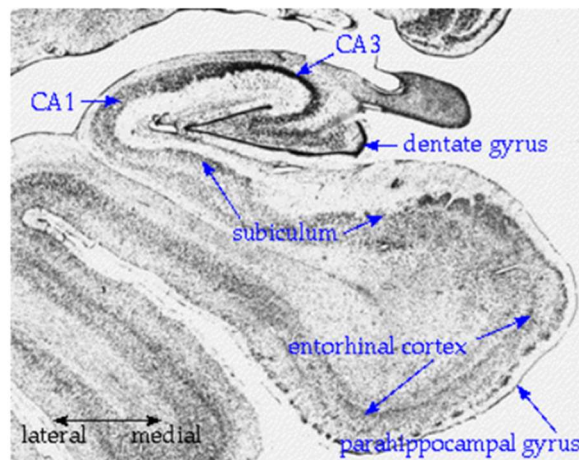


Fig.17. Overview of a coronal section of the hippocampus and parahippocampal region.

The subiculum occupies a central position between hippocampus proper and parahippocampal structures.

CA: cornu ammonis

The hippocampal excitatory pathway consists of EC neuronal projections to the dentate gyrus, projections of the dentate gyrus cells to area CA3 pyramidal neurons, and CA3 projections to area CA1 pyramidal neurons. CA1 neurons transfers excitatory information out of the hippocampus either directly or via a dense projection to the subiculum neurons (Amaral et Witter, 1989, Amaral, 1993, Naber et al., 2001) (Fig. 18).

While the substantial forward projection from hippocampal CA1 to the subiculum has been very well established, accumulating evidence supports the existence of a significant back-projection pathway comprised of both excitatory and inhibitory elements from the subiculum to CA1 (Sun et al.,

2014; Xu et al., 2016) (Fig. 18). The anatomical evidence for subicular projections to area CA1 is supported functionally by several electrophysiological studies. Shao and Dudek (2005), using focal flash photolysis of caged glutamate in adult rat slices, have shown that CA1 pyramidal cells receive excitatory synaptic input originating from the subiculum (Shao et Dudek, 2005).

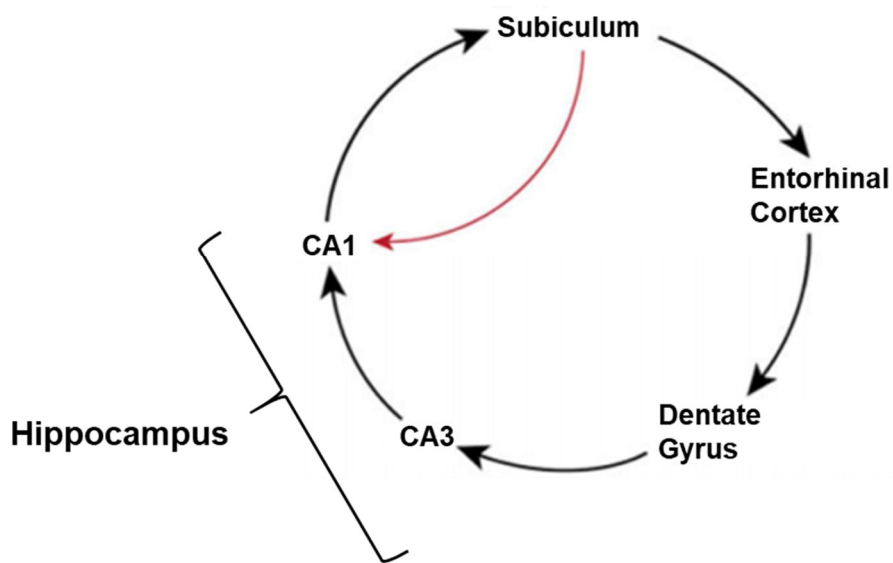


Fig.18. Hippocampal excitatory pathway and subicular back-projection pathway to CA1.

Neurons of the subiculum include a variety of smaller interneurons and pyramidal cells, classified into bursting and spiking neurons (Taube, 1993; Staffet et al., 2000). As shown in Fig. 19, bursting neurons respond with one or more high-frequency bursts (each characterized from two to five APs), usually followed by regular spiking. By contrast, spiking neurons fire a train of action potentials for the duration of the stimulus (Cembroski et al., 2018) (Fig. 19).

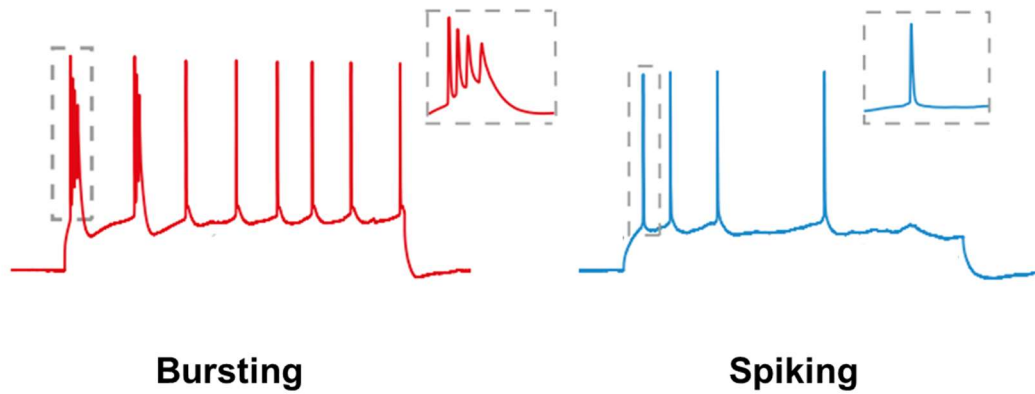


Fig. 19. Representation of bursting and spiking neurons

Firing pattern in response to current pulse in a burst (red) and a spiking cell (blue) (adapted from Böhm et al., 2015).

Bursting and spiking cells are recurrently connected among themselves, but differentially integrated into the local network: in fact, since inhibitory cells are more densely connected to spiking cells, the excitatory pathway of the subiculum is ruled by bursting neurons (Böhm et al., 2015). Previous studies have shown that these two groups of subicular pyramidal neurons, spiking and bursting neurons, are distributed in an organized fashion along the proximal-distal axis, with more spiking neurons close to CA1 (proximal subiculum) and more bursting neurons in the distal subiculum (Jarsky et al., 2008; Staff et al., 2000): it is known that distal CA1 projects to proximal subiculum, and proximal CA1 projects to distal subiculum (Amaral et al., 1991, Amaral, 1993) (Fig. 20).

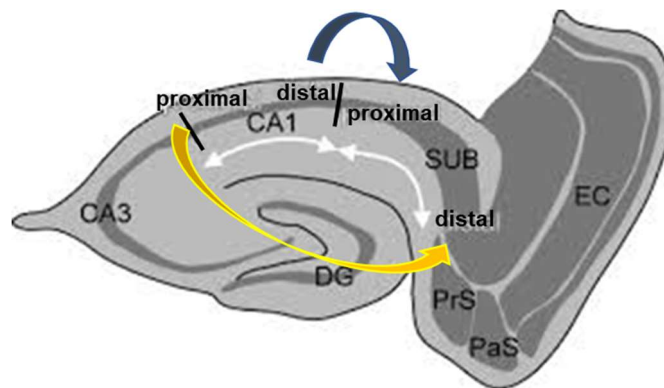


Fig. 20. CA1 projections to the proximal and distal subiculum.

Different brain areas receive inputs from proximal and distal neurons, having different firing properties: neurons projecting to Amygdala, Lateral Entorhinal Cortex (LEC), Orbifrontal Cortex (OfC) and Nucleus Accumbens (NAc) are distributed in the proximal subiculum, whereas those projecting to Medial Entorhinal Cortex (MEC), Presubiculum (Presub), Retrosplenial cortex (RsC), and Ventromedial Hypothalamic Nucleus (VHN) are positioned in the distal subiculum (Kim et Spruston, 2012) (Fig. 21). These different subicular projections suggest the ability to process in parallel several information types and consequently, due to subicular connectivity, it is not surprising that subiculum has been implicated in several disorders, as epilepsy (Stafstrom et al., 2005; de Guzman et al., 2006).

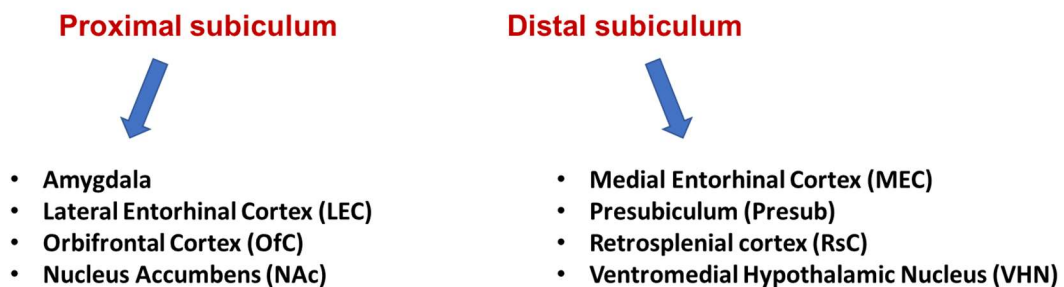


Fig. 21 . Proximal and distal subicular projections

Earlier studies have shown that Kv7.3 channels, and to a lesser extent Kv7.2, are highly expressed in subiculum (Tzingounis et al., 2010; Weber et al., 2006; Geiger et al., 2006), but the role of Kv7.3 channels in setting the excitability of subiculum neurons has yet to be addressed. By contrast, the role of Kv7.2 and Kv7.3 channels on the firing properties in CA1 pyramidal neurons has previously been discussed. In particular, Soh et al. (2014) demonstrated that conditional deletion of Kcnq2 from cerebral CA1 pyramidal neurons resulted in an increased excitability, whereas conditional deletion of

Kcnq3 did not lead to cortical hyperexcitability (Fig. 22). Thus, the data obtained showed the prominent role of Kv7.2 channels in the control of neuronal excitability in CA1, with a minor role instead played by Kv7.3.

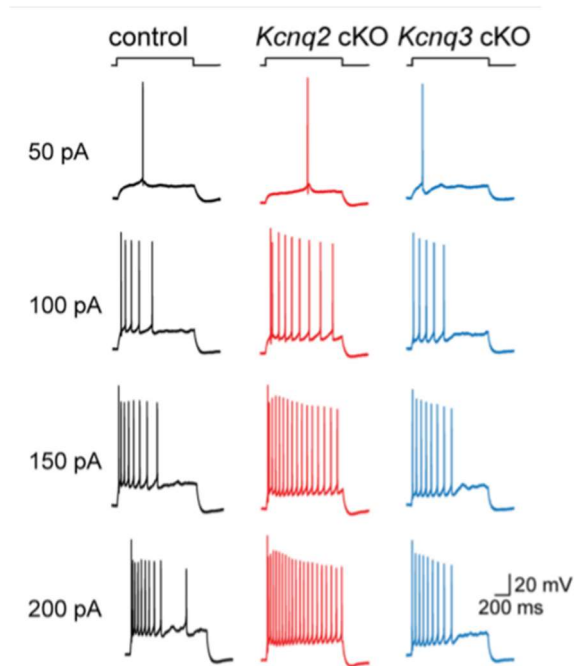


Fig. 22. Neuronal excitability of CA1 pyramidal neurons.

Representative traces showing the effects of deleting either Kcnq2 (red) or Kcnq3 (blue) on pyramidal neuron excitability compared to those in control. Membrane potential was kept at -70 mV by injecting a small direct current (DC) through the recording pipette. (adapted from Soh et al., 2014).

To investigate the role of Kv7.3 in neuronal excitability, I have evaluated the intrinsic membrane properties of neurons carrying a deletion of Kcnq3 in the distal and proximal subicular neurons and in the CA1 pyramidal neurons using two different conditional Kcnq3 knockout mice lines.

The conditional kcnq3 KO mice of CA1 pyramidal neurons was obtained by crossing the Kcnq3^{fl/+} mice with Emx1-ires-cre (Emx1) mice, a transgenic mice that expressed Cre only in CA1 pyramidal neurons (Soh et al., 2014); whereas the conditional kcnq3 KO mice of the subicular neurons was obtained by crossing the Kcnq3^{fl/+} mice with G5-Emx-cre (G5) mice,

expressing Cre only in subicular neurons. Both *Kcnq3* cKO mice lines obtained had an exon 2-4 deletion (Fig. 23).

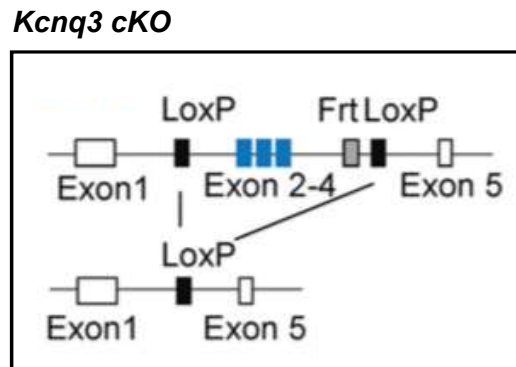


Fig. 23. Targeting strategy for generation of *Kcnq3*^{fl/fl} mice. Targeted axons (blue) were flanked by two loxP sites (adapted from Soh et al., 2014).

These studies were carried out in the laboratory of Dr. Tzingounis, University of Connecticut in Storrs. Current-clamp recordings were first performed to identify cell types, distal and proximal subicular and CA1 pyramidal neurons, according to their responses to intracellular current injection of various amplitudes (1 s, 0 to 250 pA).

Recordings obtained in distal and proximal subicular neurons from wild-type and *Kcnq3* cKO slices showed that the deletion of *Kcnq3* had little impact on the number of the action potentials (APs) when compared to controls (Fig. 24 and 25, top panel). Despite the number of the APs was identical in control and *Kcnq3* cKO mice, a reduction of the initial firing frequency, identified as the frequency measured between the first two APs, was observed only in *Kcnq3* cKO distal neurons (Fig. 24, bottom panel), without any changes in proximal subicular neurons (Fig. 25, bottom panel). Instead, no significant difference was identified in the final firing frequency (measured as the frequency of the last two APs during the depolarizing steps), across a range of depolarizing stimuli in both areas.

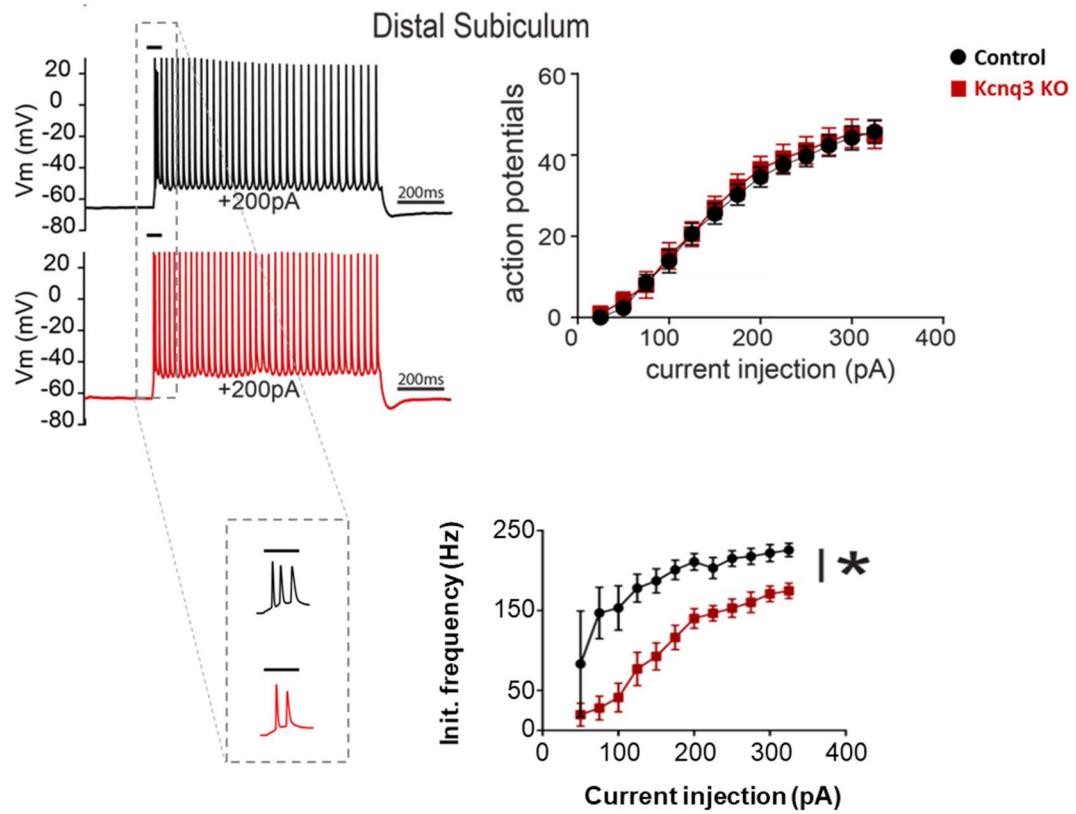


Fig. 24. Firing properties of control and Kcnq3 cKO neurons in the distal subiculum.

Top panel: Left, representative voltage responses to current injection step (+200 pA; 200ms) in distal subiculum neuron from control (n=19) and Kcnq3 cKO (n=20). Membrane potential was kept at -65 mV by injecting a small direct current (DC) through the recording pipette. Right, summary graph showing the effect of deleting Kv7.3 channels on APs number. Bottom panel: Left, representative bursts in control and Kcnq3 cKO neurons. Right, summary graph showing the effect of deleting Kv7.3 channels on initial firing frequency. Asterisk indicates value statistically significant from respective distal control, one-way ANOVA.

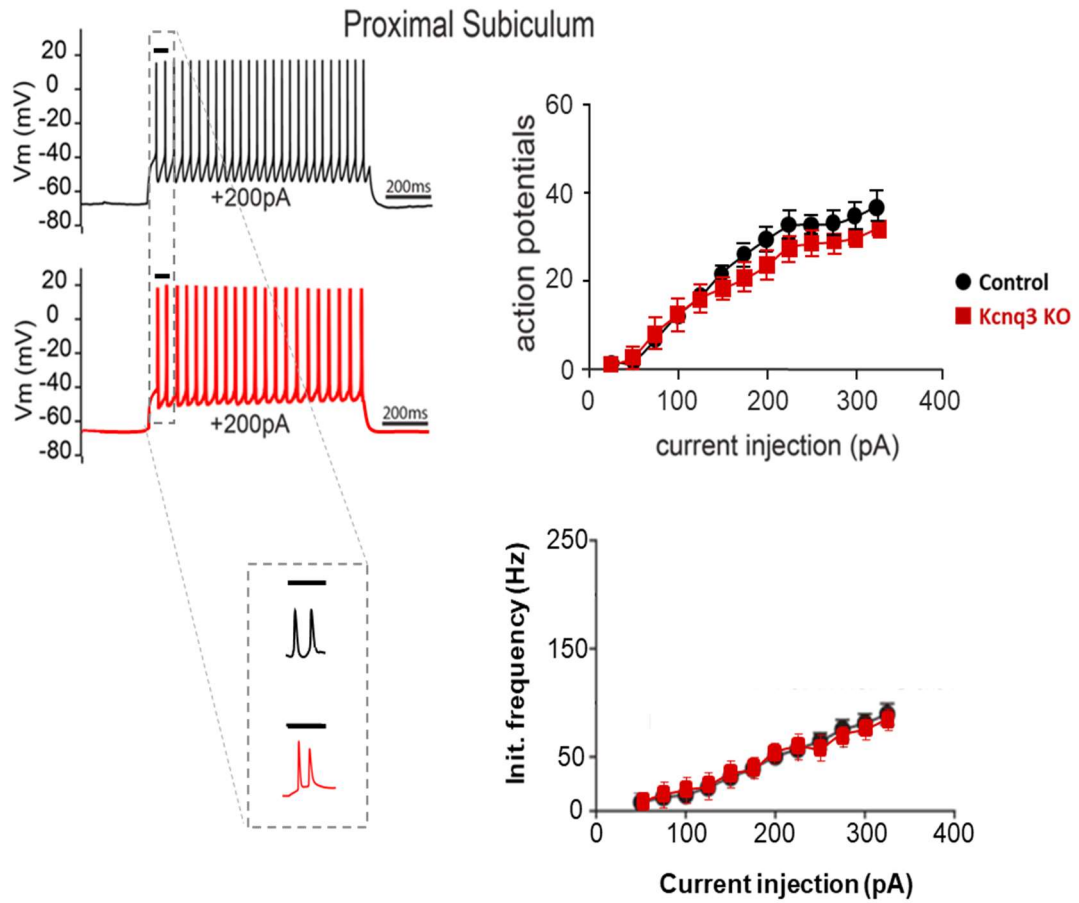


Fig. 25. Firing properties of control and Kcnq3 cKO neurons in the proximal subiculum. Top panel: Left, representative voltage responses to current injection step (+200 pA; 200ms) in proximal subiculum neuron from control (n=20) and Kcnq3 KO (n=20). Membrane potential was kept at -65 mV by injecting a small direct current (DC) through the recording pipette. Right, summary graph showing the effect of deleting Kv7.3 channels on APs number. Bottom panel: summary graph showing the effect of deleting Kv7.3 channels on initial firing frequency.

Differently, recordings obtained from CA1 pyramidal neurons, revealed an increased the neuronal excitability in neurons from *Kcnq3* cKO mice when compared to those in control (Fig. 26). This observation was very surprising given that a previous work from the same lab (Soh et al., 2014) failed to show such difference. Probably, the observed difference in the present experiments could be explained by the different temperature and calcium concentration used when compared to Soh (2014). Indeed, while Soh recordings were carried out at room temperature and high calcium concentration (2.5 mM), in our experiments the temperature was increased to 32°C and the calcium concentration was lowered to 1.5mM. Both experimental conditions were changed to reproduce more closely physiological conditions. Additionally, in contrast to the increase of number of the APs, no significant difference between the initial and final firing frequencies between slices from control and *Kcnq3* cKO mice was observed.

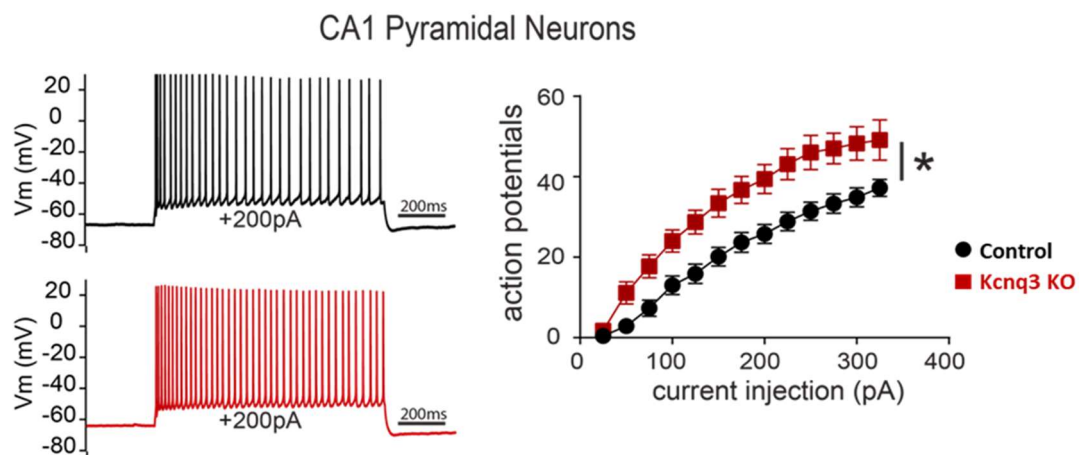


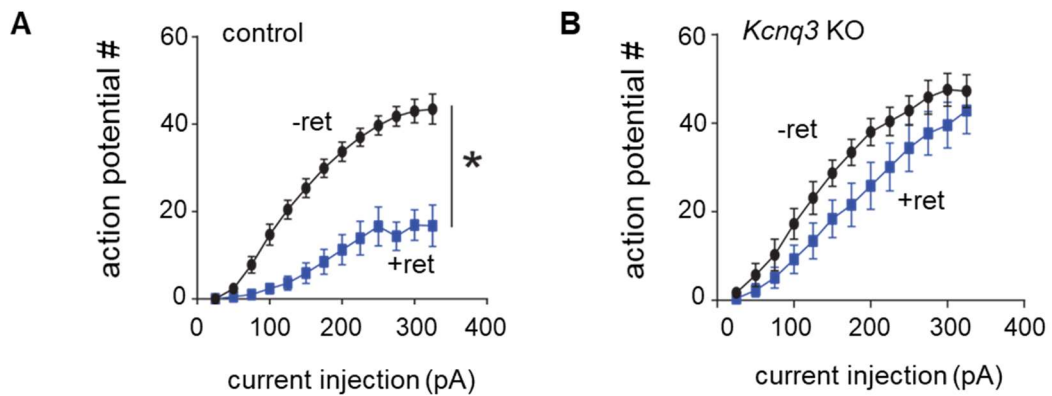
Fig. 26. Firing properties of control and *Kcnq3* cKO neurons in the CA1 pyramidal neurons. Left, representative voltage responses to current injection step (+200 pA; 200ms) in CA1 neurons from control (n=20) and *Kcnq3* cKO (n=21). Membrane potential was kept at -70 mV by injecting a small direct current (DC) through the recording pipette. Right, summary graph showing the effect of deleting *Kv7.3* channels on APs number. Asterisk indicates value statistically significant from respective CA1 control, one-way ANOVA.

I further verified whether the loss of Kcnq3 gene altered the sensitivity to retigabine, a neuronal Kv7 channels activator, either in subiculum and in CA1 pyramidal neurons.

Bath application of 10 μ M retigabine to subicular pyramidal neurons from control mice led a significantly reduction in the number of APs at all current injections tested, as shown in Figure 27A. By contrast, bath application of retigabine to subicular pyramidal neurons from Kcnq3 cKO mice slices caused a little reduction of number of the APs, underling a possible role of Kcnq3 could have in this area to control the firing (Fig. 27B).

Subsequent recordings were carried out to investigate the effect of retigabine in control CA1 pyramidal neurons. As in control subicular neurons, a significantly decrease of number of APs was observed only at lower current injections (from 50 to 150 pA), but, unlike control subicular cells, increasing the amount of injected current, retigabine efficacy became lower (Fig. 27C). Interestingly, bath administration of retigabine in CA1 pyramidal neurons of Kcnq3 cKO mice exhibited a bimodal effect, that is a decrease followed by an increase in firing, without a net inhibition like subicular Kcnq3 cKO neurons (Fig. 27D). This bimodal effect has been mentioned briefly in previous papers. Tatulian et al. (2003) reported that the retigabine-sensitive current plotted against test potential had a distinctive 'bell' shape.

Subiculum



CA1 Pyramidal Neurons

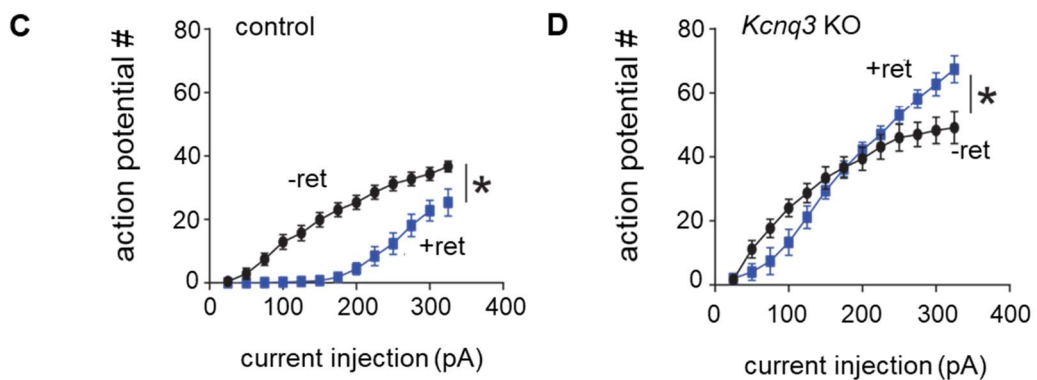


Fig. 27. Effects of Retigabine in subiculum and CA1 pyramidal neurons.

Summary graphs showing the effect of retigabine 10 μ M in control and *Kcnq3* cKO (subiculum and CA1 pyramidal neurons; $n=20$ and $n=19$, respectively). Asterisks indicates value of *Kcnq3* cKO statistically significant from respective each control, one-way ANOVA.

Probably, the different results in the reduction of number of the APs, observed at very low currents injections (50pA), between subiculum and CA1 pyramidal neurons in *Kcnq3* cKO mice could be explained by a CA1-specific upregulation of other retigabine-sensitive Kv7 subunits occurring in the *Kcnq3* cKO mice. In support of this hypothesis is the observation that Kv7.5 plays a relevant role in controlling CA1 excitability, while this subunit does not appears to be expressed in subiculum neurons (Tzingounis et al., 2010).

Altogether, these data provide functional and pharmacological evidence for a differential role played by Kv7.3 subunits in controlling excitability of distinct neuronal subpopulations of cortical neurons, thereby challenging the idea that the M-current is always underlined by Kv7.2 and Kv7.3 assembly in all central and peripheral neurons.

4.2 Clinical, molecular and functional properties of Kv7.3 F534Ifs*15 variant

4.2.1 Clinical features of the proband

Thanks to our international collaborations with clinical centers in Europe, one family with a unique genetic transmission patterns of a previously-unknown Kv7.3 variant has come to our attention. In particular, Dr. Moutton (Dijon University Hospital) identified a proband (Individual II-3; Fig. 28), who is a French 9 year-old female born to consanguineous healthy parents. At age 2 days, she presented with both focal (affecting either the left or right hemi-body) and generalized convulsions associated with hypotonia, cyanosis, and clonic movements of the four limbs. The first electroencephalograms (EEGs), performed in the following days, revealed electrical seizures characterized by central and temporal slow waves prevailing on the right side, not always associated with clinical manifestations. At 7 months of age, sodium valproate monotherapy was effective in controlling seizures; interruption of sodium valproate treatment at the age of 3-4 years resulted in seizure recurrence during late night, including febrile episodes, with left hemispheric spikes and waves recorded on the EEG; valproate therapy was therefore reintroduced and the girl is still treated with good response, showing the characteristics of a pharmacodependent epilepsy (Rosati et al., 2015). Brain MRI performed at day 15 revealed a suspected mild cortical dysplasia of the right frontal and temporal lobes, but a further MRI at age 6 years and 5 months was normal, as well as a brain CT scan. At age 8 years, she started to produce short rudimentary word associations. At age 6.5 years, her psychomotor development was estimated around 22 months. She did not exhibit behavioral disturbances. At last examination (age 9 years), no abnormal morphological features were noted and neurological examination was normal apart from divergent strabismus increased in superior gaze. She has a moderate intellectual disability with poor vocabulary and little autonomy in daily life.

Familial history revealed that a maternal uncle who had mild cognitive disabilities with some degree of learning (reading and writing) difficulties also suffered from transient neonatal seizures, requiring a specialized pediatric

follow-up in the first 6 months of life (Fig. 28). However, he has a milder phenotype than his niece as he could achieve a relatively good autonomy in daily life. The parents and one of the brother (individuals I-1, I-2 and II-2, respectively, Fig. 28) were heterozygous carriers for the same Kv7.3 variant; the eldest brother carried two copies of the wild-type allele (individual II-1, Fig. 28); the maternal uncle was unavailable for genetic analysis. All other members of the family had normal psychomotor and cognitive development with no history of seizures (Fig.28).

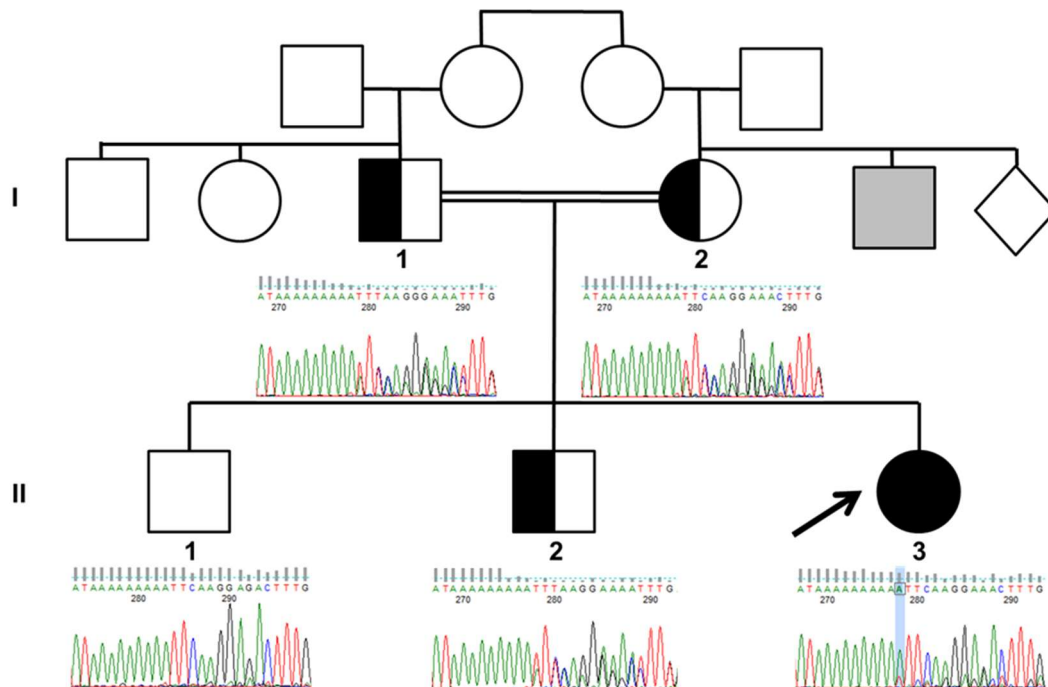


Fig. 28. Pedigree of the investigated family and Kv7.3 Sanger sequencing of all available individuals.

Individuals I-1, I-2 and II-2: heterozygous carriers for the Kv7.3 variant. Individual II-1: homozygous wild-type. The arrow indicates the proband. In grey, a maternal uncle with ID and epilepsy. The Kv7.3 F534Ifs*15 variant is shown using as a reference the minus DNA strand, from which the mRNA is transcribed.

4.2.2 Genetic data

Exome sequencing was performed on the proband (Individual II-3, Fig. 28) and revealed a homozygous single base duplication (chr8:g133150233dup in GRCh37, NM 004519.3:c.1599dup) in exon 12 (135/138 reads detected the variant) which resulted in a shift in the open reading frame p.(Phe534Ilefs*15) (Fig. 29, top panel). This mutation is due to an insertion of an adenine at c.1599, leading to a frameshift with the consequent introduction of 15 extra amino acids before a stop codon (Fig. 29, bottom panel), causing the premature termination codon (PTC) at position 549, possibly leading to the synthesis of a truncated protein deleted of a large part of the C-terminal region.

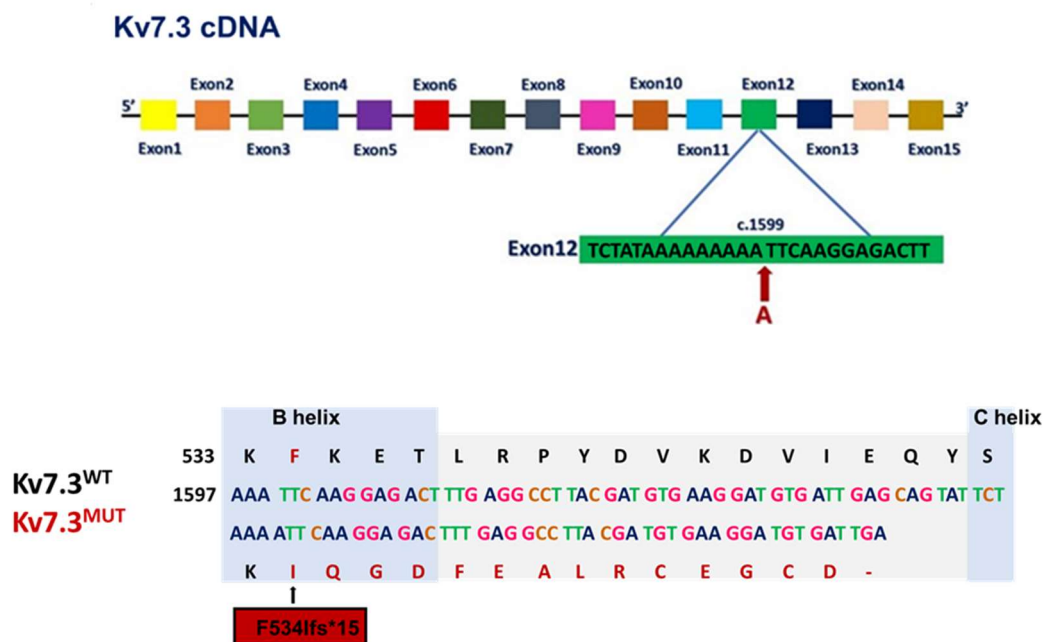


Fig. 29. Kv7.3 cDNA and partial alignment of primary sequences of wild-type and mutant Kv7.3 subunits.

In the top, the variant F534Ilefs*15 is caused by an insertion of an adenine at position c.1599 in exon 12 of Kv7.3 cDNA. In the bottom, partial alignment of primary sequences of wild-type and mutant Kv7.3 subunits. This mutation results in a frameshift and the occurrence of a premature termination codon (PTC) at position 549.

4.2.3 Kv7.3 F534Ifs*15 mRNA is expressed at lower levels in proband's fibroblasts when compared to unaffected noncarrier brother fibroblasts

The frameshift mutation found in Individual II-3 led to the introduction of a presumed premature termination codon (PTC) in the protein, and it is well known that transcripts with PTCs are degraded by the quality control systems of the cell via a process known as *non-sense mediated RNA decay* (NMD) (Lykke-Andersen et Jensen, 2015). However, not all PTCs trigger NMD pathway: in fact, the mRNAs in which the distance from the PTC to the exon-exon junction closest to the 3'-end is less than 55 nucleotides are non-NMD targets. Instead, if the distance from the PTC to the exon-exon to the 3'-end is more than 55 nucleotides, the mRNAs will be identified as putative NMD targets and degraded by the NMD pathway.(Fig. 30).

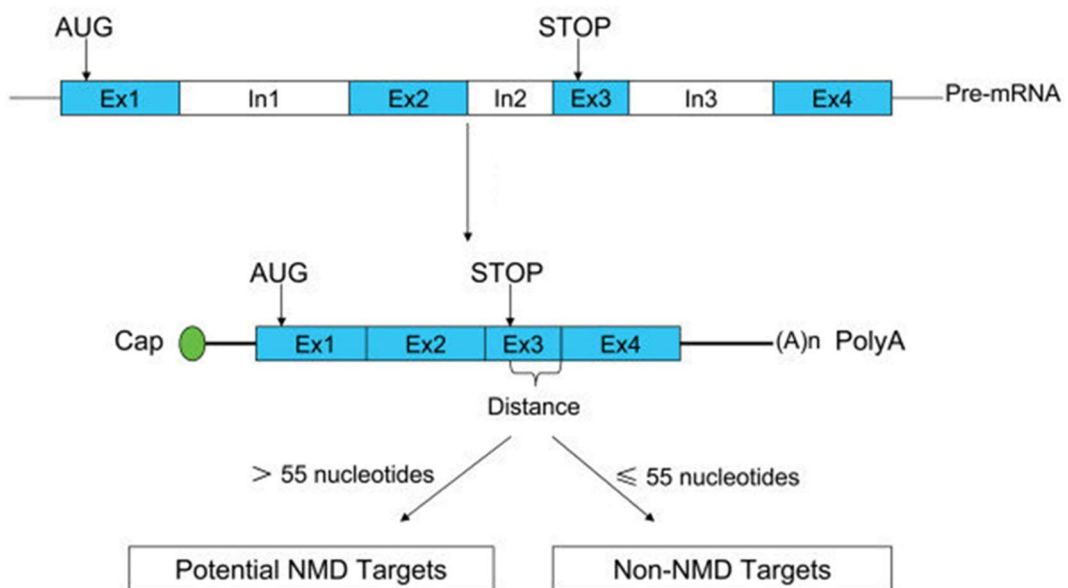


Fig. 30. Non-sense mRNA decay pathway.

Mammalian genes are transcribed from the genome, which produces the precursor of mRNA (pre-mRNA). Pre-mRNA still contains exons (Ex) and introns (In), and is subject to processes including capping, polyadenylation and splicing. The splicing step removes the introns from pre-mRNA and ligates the exons.

AUG: start codon; STOP: premature termination codon; Distance: distance from the stop codon to the exon-exon junction closest to the 3'-end (adapted from Zhanget al., 2009).

In the mutation Kv7.3 F534Ifs*15 , since this distance from the PTC to the exon-exon junction closest to the 3'-end is more than 55 nucleotides (about 1017 nucleotides), we hypothesized Kv7.3 F534Ifs*15 mRNA as a putative target for NMD. Therefore I next investigated the consequences of the newly-identified mutation on the mRNA levels in the proband's tissues. Since no brain tissue was obviously available from the proband and in view of the fact that fibroblasts were known to express (although at low levels) Kv7.3 mRNA, we therefore used primary fibroblasts for qRT-PCR experiments. For these studies, fibroblasts from the noncarrier brother (Individual II-1), who carried both wild-type Kv7.3 alleles, was used as control. The probes used to evaluate Kv7 mRNA expression levels are listed in the following Table 5; notably, these primers were chosen to allow amplification of all possible transcripts transcribed from the Kv7.3 gene (see paragraphe *The KCNQ3 gene* in the introduction). A similar approach was used when selecting primers used in qRT-PCR experiments to amplify all other Kv7 gene members.

Table 5. Probes characteristics used for qRT-PCR

Gene	Expected size of the amplified region	Exons	Reference sequence
Kcnq1	1620	11-12	NM_000218.2
Kcnq2	2015	14-15	NM_004518.5
Kcnq3	451	4-5	NM_001204824_1
Kcnq4	1697	11-12	NM_004700.3
Kcnq5	1474	7-8	NM_001160130.1

All values were normalized to that of Ubiquitin C (UBC), a housekeeping gene used as comparator (Poulet, 2014). As shown in Fig. 31, in cells from the proband, Kv7.3 transcript levels were reduced to ~22% when compared to those in control cells; a quantitatively similar decrease in transcript levels was also observed for Kv7.4, whereas those for Kv7.2 were markedly increased.

No significant difference was instead observed when comparing Kv7.1 and Kv7.5 transcript abundance between proband and control primary fibroblasts (Fig. 31).

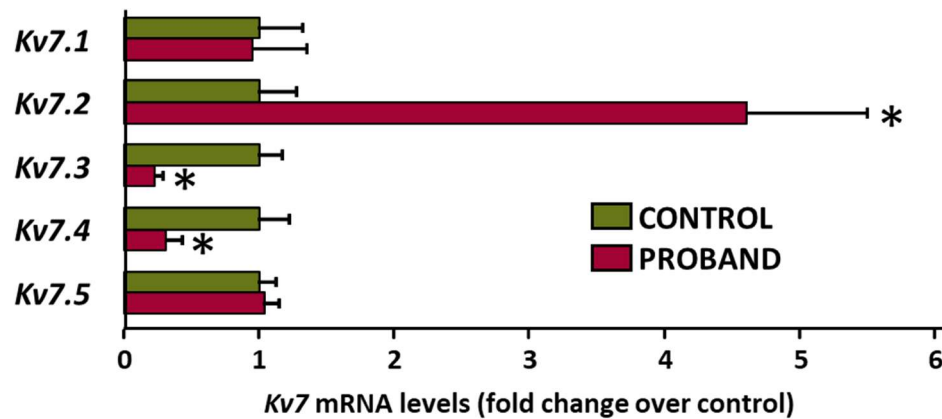


Fig. 31. Kv7 mRNA expression levels in fibroblasts from the proband and unaffected noncarrier brother.

Data are expressed as cycle threshold values for each Kv7 transcript to that of UBC; after normalization, data from control (Individual II-1) fibroblasts were expressed as one, and data from proband (Individual II-3) fibroblasts were expressed relative to control. Asterisks indicate values statistically significant ($p < 0.05$) from respective controls.

4.2.4 In-vitro (in CHO cells) and ex-vivo (in primary fibroblasts) biochemical studies on Kv7.3 mutant subunits

To investigate whether the decrease of mRNA expression levels of Kv7.3 F534Ifs*15 variant observed in fibroblasts also led to alteration in the protein levels, immunofluorescence experiments were performed in primary fibroblasts from the proband (Individual II-3, fig. 28) and the unaffected non-carrier brother (Individual II-1, fig 28), using N-Kv7.3 primary antibodies; these antibodies recognized an epitope in the N-terminus which is putatively unaffected by the newly-found mutation located of the 5'-end of the truncation point.

Western-blot experiments on total lysates derived from CHO cells expressing wild-type or mutant Kv7.3 subunits were performed to validate these N-Kv7.3 antibodies. In these experiments, both proteins were detected by the same anti-Kv7.3 antibodies, but with a different molecular weight (MW): in fact, a band of 100 kDa was detected in the lanes where lysates from cells expressing wild-type Kv7.3 subunits had been run, whereas a band of 60 kDa was detected in the lanes relative to the lysates of cells expressing mutant Kv7.3 subunits; this lower value of MW is consistent with the predicted MW of the mutant protein. These results validated the ability of the N-Kv7.3 antibodies in detecting both wild-type and mutant protein, also revealing the expression of a truncated protein in the CHO heterologous expression system (Fig. 32A, left panel); in addition, these experiments also revealed that, in this heterologous cellular system, the mutant protein was expressed at lower levels when compared to the wild type Kv7.3 protein (Fig. 32A, left panel). In addition, western-blotting experiments were performed on total lysates from CHO cells expressing wild-type or mutant Kv7.3 subunits using a different antibody recognizing instead a C-terminal epitope located downstream the PTC at position 549 (C-Kv7.3). As largely predicted, C-Kv7.3 antibodies were able to detect a 100 kDa band in CHO cells transfected with wild-type Kv7.3 cDNA, whereas they failed to detect any specific signal in cells transfected with the mutant Kv7.3 plasmid (Fig. 32A, right panel). These results suggested that both N-Kv7.3 and C-Kv7.3 antibodies were able to detect wild-type Kv7.3, whereas only N-Kv7.3 antibodies could be used when attempting to biochemically identify the mutant Kv7.3 protein.

Immunocytochemistry experiments using N-Kv7.3 antibodies revealed a Kv7.3-specific mainly cytosolic signal in primary fibroblasts from both proband and unaffected non-carrier brother, (Fig. 32B, right and left panels, respectively), although the intensity of the former was lower than the latter.

Additional western blot experiments were performed in primary fibroblasts from proband and control samples with either antibodies. N-Kv7.3 and C-Kv7.3 antibodies failed to detect specific signals corresponding to wild-type or mutant Kv7.3 proteins, possibly because of the low endogenous protein abundance in these cells.

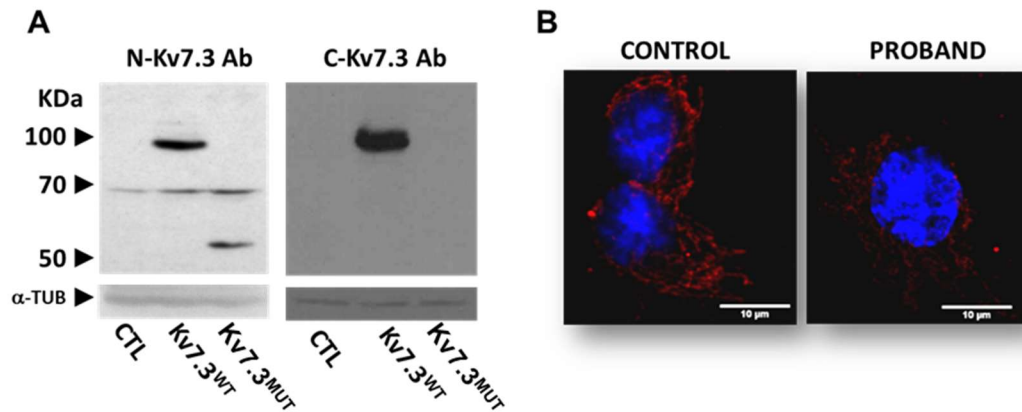


Fig. 32. Kv7.3 protein expression levels in CHO cells transiently transfected and primary fibroblasts.

A) Western-blot performed on protein lysates from CHO transiently transfected using N- and C-Kv7.3 antibodies. α -tubulin (α -TUB) served as a loading control. Each data is the mean-SEM of 10 cells in at least three separate experimental sessions. B) Confocal images of fibroblasts from the proband (Individual II-3) and the healthy brother (Individual II-1) stained with N-Kv7.3 primary antibodies (in red) and a nuclear marker, Hoechst (in blue).

Data obtained in primary fibroblasts from the proband suggest that the F534Ifs*15 variant led to a significant decrease in Kv7.3 transcription and protein levels, a result consistent with *non-sense mediated mRNA decay* (Lykke-Andersen et Jensen, 2015; Kurosaki et al., 2014).

Despite transcript expression pattern in fibroblasts might not parallel that in neurons, the observation that in primary fibroblasts the mutant protein was expressed (although lower) at detectable levels, prompted further studies to evaluate its functional properties.

4.2.5 Electrophysiological and pharmacological characterization of Kv7.2, Kv7.3 or Kv7.2/Kv7.3 currents in CHO cells

The measurement of currents elicited by wild-type or mutant channels were performed in CHO cells, which do not express these voltage-gated potassium channels: in fact, after the application of a classical voltage protocol for K⁺ currents recordings in these cells, no current was measured. Instead, when these cells were transfected with the cDNAs encoding for Kv7.2 and/or Kv7.3

subunits, sizeable outward K⁺ currents were recorded in response to incremental depolarizing voltage steps from -80 to + 40 mV. In particular, homomeric wild-type Kv7.2 channels generated robust K⁺ selective currents (42.2±9.7 pA/pF) and exhibited a half-activation potential ($V_{1/2}$) at -20 to -30 mV, whereas currents carried by Kv7.3 homomeric channels were rather small (11.5±4.8 pA/pF), also showing a more hyperpolarized $V_{1/2}$ (-35 to -45 mV); by contrast, cells co-expressing Kv7.2 and Kv7.3 subunits generated currents whose amplitude was larger than that expected from the simple summation of homomeric Kv7.2 and Kv7.3 currents (~117.6±15.1 pA/pF), and exhibited intermediate $V_{1/2}$ of -20 to -27 mV. In all cases (Kv7.2, Kv7.3, Kv7.2/7.3) expressed currents showed slow activation and deactivation kinetics and absence of inactivation. Different processes underline this Kv7.2/7.3 current potentiation (Etxeberria et al., 2004). Kv7.2/7.3 coexpression is responsible of the increase of channel number at the membrane, due to heteromerization of the C-terminal regions, and resulting in a concomitant increase in the current levels (Schwake et al., 2000). The subunit interaction domain (SID) on the α helical C and D of the C-terminal region mediates the Kv7.2 and Kv7.3 assembly, allowing to enhance the expression of heteromeric channels. The SID corresponds to the region between amino acids 528 and 623 on Kv7.2 sequence, and to the region between amino acids 535 and 650 of the Kv7.3 sequence.

Homomeric Kv7.2 and Kv7.3 channels, and heteromeric Kv7.2/7.3 channels also displaying significant difference in their pharmacological sensitivity to a blocker, tetraethylammonium (TEA), or an activator, retigabine (RTG). Kv7.2 is highly sensitive to TEA (IC₅₀=0.3 mM), whereas Kv7.3 is TEA-insensitive (IC₅₀=30 mM); by contrast heteromeric Kv7.2/7.3 channels show an intermediate sensitivity (IC₅₀=3 mM) (Hadley et al., 2000). The high TEA sensitivity of Kv7.2 might result from the presence of a tyrosine residue in the pore loop of the channel (Kavanaugh et al., 1991), whereas Kv7.3 has a threonine which confers low sensitivity to TEA (MacKinnon et Yellen, 1990). By contrast, RTG is an activator of neuronal Kv7 channels. Among channels formed by distinct Kv7 subunit combinations, Kv7.3 homomers display the longest sensitivity to RTG (EC₅₀=0.6 μ M), in contrast to Kv7.2 homomers (EC₅₀=2.5 μ M). Instead, the half maximal effective concentration of RTG on

Kv7.2/7.3 channel subunits is 1.6 μM . RTG acts by accelerating activation and decelerating deactivation kinetics, hyperpolarizing the $V_{1/2}$ (Wuttke et al., 2005; Tatulian et Brown, 2003), stabilizing the open conformation of Kv7.2 and Kv7.3 channel subunits. The putative binding site for RTG is located at the intracellular side of the central pore domain of Kv7.2 and Kv7.3 subunits (Schenzer et al., 2005; Wuttke et al., 2005): a tryptophan at position 236 in Kv7.2, corresponding to 265 in Kv7.3, plays a critical role in retigabine binding.

4.2.6 Kv7.3 F534Ifs*15 mutation induces loss-of-function effects on Kv7.3 currents

In the first series of experiments, patch-clamp recordings were performed in CHO cells transfected only with wild-type or mutant Kv7.3 cDNA. CHO cells transfected with wild-type Kv7.3 cDNA produced K^+ currents as shown in Figure 33; by contrast, cells transfected with Kv7.3 F534Ifs*15 cDNA did not elicit currents above background levels, causing a complete *loss-of-function* (LoF) effect (Fig. 33 and Table 6).

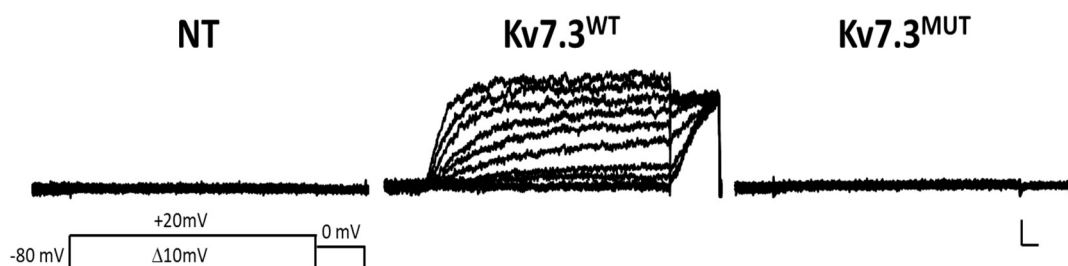


Fig. 33. Macroscopic currents measured in CHO cells expressing wild-type or mutant Kv7.3 homomeric channels.

Representative current traces from non-transfected cells (NT, $n=10$; left panel) or from cells expressing wild-type Kv7.3- (Kv7.3^{WT}, $n=9$; middle panel) or Kv7.3 F534Ifs*15-encoding plasmids (Kv7.3^{MUT}, $n=9$; right panel) in response to the voltage protocol shown in the bottom part. Horizontal scale bar: 100ms; vertical scale bar: 2pA/pF.

However, as previously described, in most neurons, the M-current is formed by Kv7.2 and Kv7.3 subunit assembly in heteromeric channels. Therefore, to reproduce the genetic status of all family members, patch-clamp recordings were performed on CHO cells transfected according to following scheme:

- 1- Kv7.2+Kv7.3 (transfection ratio 1:1) to reproduce the genetic status of unaffected non-carrier brother (Individual II-1);
- 2- Kv7.2+Kv7.3^{MUT} (transfection ratio 1:1) to reproduce the genetic status of proband who carries the mutant allele in homozygosity (Individual II-3);
- 3- Kv7.2+Kv7.3+Kv7.3^{MUT} (transfection ratio 1:0.5:0.5) to reproduce the genetic balance of family members who carry the mutant allele in heterozygosity (Individual I-1, I-2, and II-2).

When Kv7.3 mutant subunits were co-transfected with wild-type Kv7.2 subunits, maximal current densities were reduced compare to those measured in the control group, Kv7.2+Kv7.3 subunits, suggesting loss-of-function effect as the pathogenetic mechanism for this mutation (Table 6).

These functional results indicated that Kv7.3 F534Ifs*15 subunits prompted a dramatic reduction on Kv7.2/7.3 current density. Pharmacological experiments with tetraethylammonium (TEA) were performed to investigate Kv7.3 F534Ifs*15 subunits incorporation into heteromeric channels with Kv7.2 subunits. In particular, the ability of mutant subunits to form heteromeric channels with wild-type subunits was studied by measuring current inhibition upon perfusion of 3 mM TEA.

As shown in Table 6 and in Figure 34, CHO-transfected cells with Kv7.2 and Kv7.3 F534Ifs*15 plasmids failed to enhance current density and to modify the V_{1/2}. Moreover, Kv7.2/Kv7.3^{MUT}-transfected cells displayed a sensitivity to blockade by 3 mM TEA higher than that of Kv7.2/7.3-transfected cells, and identical to that of Kv7.2-only transfected cells. Because 3 mM TEA should selectively block primarily Kv7.2/7.3 heteromers and Kv7.2 homomers (IC₅₀=0.3 mM), but not Kv7.3 homomers (IC₅₀=30 mM) (Wang et al., 1998, Hadley et al., 2000, Lerche et al., 2000), these results suggested that Kv7.3 F534Ifs*15 mutant subunits did not appear to be incorporated into heteromeric channels with Kv7.2 subunits.

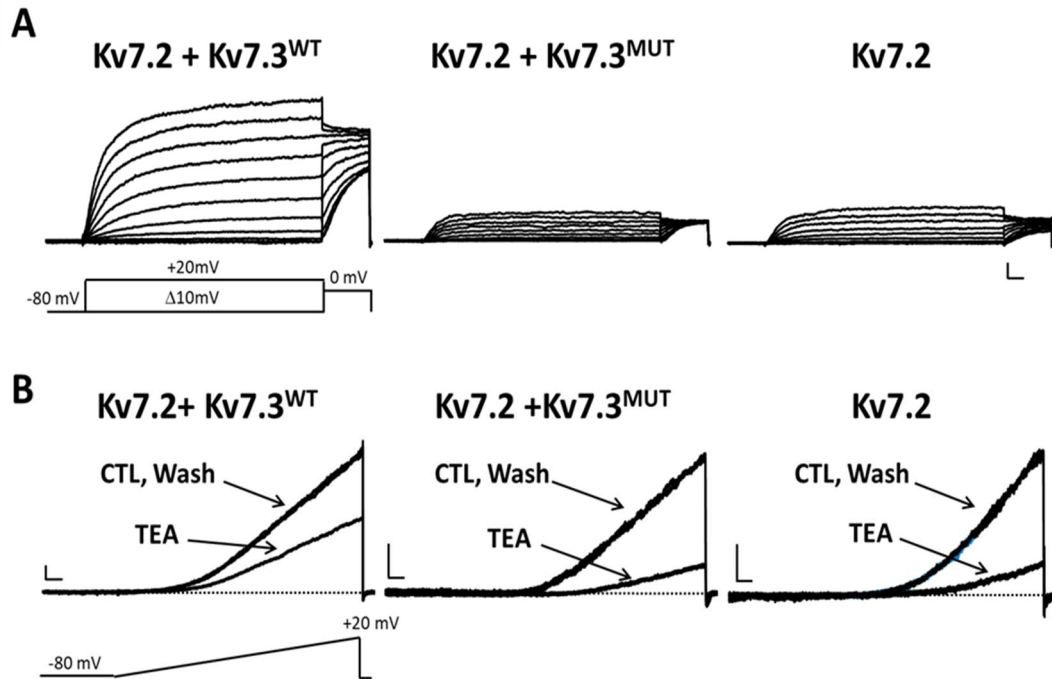


Fig. 34. Functional and pharmacological characterization of heteromeric channels carrying Kv7.3 F534Ifs*15 subunits.

A) Representative current traces recorded in CHO cells expressing the indicated subunits, in response to the voltage protocol shown in bottom part. Horizontal scale bar: 100 ms; vertical scale bar: 20 pA/pF. B) Representative current traces from CHO cells expressing the indicated subunits in response to the indicated voltage ramp protocol before TEA exposure (CTL, control), during TEA exposure (TEA, 3 mM), and upon drug washout (Wash). Horizontal scale bar: 200 ms; vertical scale bar: 10 pA/pF.

This view seems also confirmed by the observation that current levels measured in CHO cells transiently transfected with Kv7.2+Kv7.3+Kv7.3^{MUT} cDNAs were lower than those measured in the control group (Table 6). Indeed, CHO transiently transfected with Kv7.2+Kv7.2+Kv7.3^{MUT} showed biophysical and pharmacological properties of Kv7.2/7.3 wild-type heteromers, but a reduced current density when compared to that recorded in cells transfected with a full dose of Kv7.3. Moreover, the pharmacological and functional properties of the currents recorded in cell transfected with Kv7.2, Kv7.3, and Kv7.3 F534Ifs*15 plasmids were compared to Kv7.2+Kv7.3+pcDNA3-expressing cells at same transfection ratio (1:0.5:0.5 cDNA ratio): current properties were identical for both CHO-transfected cells groups.

Table 6. Biophysical and pharmacological properties of wild-type and mutant Kv7.3 subunits.

	cDNA transfected (μg)	n	$V_{1/2}$ (mV)	k (mV/efold)	Current density (pA/pF at 0 mV)	Blockade by 3mM TEA (%)
Non-transfected CHO cells	---	10	---	---	0.5 \pm 0.1	---
Kv7.3	3	9	-41.9 \pm 1.5*, **	8.2 \pm 0.9*, **	11.5 \pm 4.8*, **	8.0 \pm 2.1*, **
Kv7.3 F534Ifs*15	3	9	---	---	0.3 \pm 0.1	---
Kv7.2+pcDNA3	1.5+1.5	11	-21.7 \pm 1.9	13.2 \pm 0.8	21.7 \pm 5.1*	---
Kv7.2	3	13	-23.0 \pm 1.5	12.0 \pm 0.5	42.2 \pm 9.7	93.8 \pm 0.01**
Kv7.2+Kv7.3	1.5+1.5	23	-35.1 \pm 1.6	13.0 \pm 0.7	117.6 \pm 15.1	56.1 \pm 0.06
Kv7.2+Kv7.3 F534Ifs*15	1.5+1.5	20	-23.9 \pm 1.9**	15.4 \pm 1.5	17.5 \pm 2.5**	90.0 \pm 0.02**
Kv7.2+Kv7.3 +pcDNA3	1.5+0.75+0.75	13	-27.5 \pm 1.0**	13.0 \pm 0.7	33.6 \pm 6.9**	62.0 \pm 0.03*
Kv7.2+Kv7.3 +Kv7.3 F534Ifs*15	1.5+0.75+0.75	24	-29.5 \pm 1.8**	12.8 \pm 0.7	39.6 \pm 6.1**	62.2 \pm 0.03*

*p<0.05 versus Kv7.2 (3 μg); **p<0.05 versus Kv7.2+Kv7.3 (1.5+1.5 μg); TEA: tetraethylammonium. Student's t test. Each data is the mean-SEM of cells recorded in at least three separate experimental sessions.

Furthermore, I next explored whether a channel activator, retigabine, was able to rescue the loss of channel function caused by the Kv7.3 F534Ifs*15 variant. In these experiments, retigabine was used at a concentration 1 μM on CHO transfected cells with:

- 1- Kv7.2+Kv7.3 (transfection ratio 1:1) to reproduce the genetic status of unaffected non-carrier brother (Individual II-1);
- 2- Kv7.2+Kv7.3^{MUT} (transfection ratio 1:1) to reproduce the genetic status of proband who carries the mutant allele in homozygosity (Individual II-3).

In CHO cells transiently transfected with Kv7.2+Kv7.3 cDNAs, RTG was able to enhance current density and caused a leftward shift in the voltage-dependent (Table 7). Instead, application of RTG in CHO transfected with Kv7.2+Kv7.3^{MUT} although caused an increased current density, the values were still lower when compared to those from Kv7.2+Kv7.3 transfected cells.

However, as shown in Table 7, the retigabine is able to restore the $V_{1/2}$ on cells-transfected with Kv7.2+Kv7.3^{MUT} plasmids.

Table 7. Biophysical and pharmacological properties of wild-type and mutant Kv7.3 subunits.

	cDNA transfected (μ g)	n	$V_{1/2}$ (mV)	k (mV/efold)	Current density (pA/pF at 0 mV)
Kv7.2+Kv7.3	1.5+1.5	23	-35.1 \pm 1.6	13.0 \pm 0.7	117.6 \pm 15.1
Kv7.2+Kv7.3(RTG 1 μ M)	1.5+1.5	10	-51.9 \pm 2.4	12.3 \pm 1.4	176.6 \pm 32.4*
Kv7.2+Kv7.3 F534Ifs*15	1.5+1.5	20	-23.9 \pm 1.9	15.4 \pm 1.5	17.5 \pm 2.5*
Kv7.2+Kv7.3 F534Ifs*15 (RTG 1 μ M)	1.5+1.5	9	-40.7 \pm 2.7**	14.1 \pm 0.9	31.1 \pm 3.1*,**

*p<0.05 versus Kv7.2+Kv7.3; **p<0.05 versus Kv7.2+Kv7.3 F534Ifs*15; RTG: retigabine. Student's t test. Each data is the mean-SEM of cells recorded in at least three separate experimental sessions.

Overall, the present functional characterization of the variant suggests a LoF effect and underline the inability of mutant Kv7.3 subunits to form heteromeric channels with wild-type subunits. In addition, the application of retigabine is not able to restore the functional changes caused by the Kv7.3 pathogenic variant.

The results obtained demonstrated that, despite a possible involvement of the NMD pathway for the presence of PTC at position 549, in proband's fibroblasts lower Kv7.3^{MUT} mRNA expression levels was detected. Additionally, *ex vivo* and *in vitro* biochemical experiments revealed a decrease in mutated protein abundance and a diffuse cytoplasmatic expression of Kv7.3 F534Ifs*15 channels. Functional characterization of CHO transiently transfected with mutant Kv7.3 cDNA revealed a loss-of-function effect; moreover mutant Kv7.3 subunits did not incorporate into functional heteromeric channels when co-expressed with Kv7.2 subunits, a result consistent with the deletion of a significant portion of the long C-terminus in this Kv7.3 pathogenic variant, causing the loss of critical domains responsible for homomeric and heteromeric subunit assembly, such as subunit interacting domain (SID).

4.3. Clinical, functional and structural properties of the Kv7.3 R227Q and R230C/S/H variants

4.3.1 Clinical features of the patients

This part of my work has been performed thanks to our international collaborations with clinical centers which interact each other through the Rational Intervention for KCNQ2/3 Epileptic Encephalopathy (RIKEE) database. The RIKEE database, currently curated at Baylor College of Medicine under an institutional review board (IRB)-approved research protocol, collects information about patients where genetic tests show KCNQ2 and KCNQ3 sequence variants, their phenotypes, and related lab studies (website: www.rikee.org).

The patients of this cohort, carrying heterozygous Kv7.3 *de novo* variants, are 11 and are affected by neurodevelopmental delay (NDD) and autism spectrum disorders (ASD), or autistic features. Although one of the patients was previously reported with minimal clinical details as part of an Epi4K epileptic encephalopathy cohort (Allen et al., 2013), the others have not been previously reported. They included 3 patients with R230H, 5 patients with R230C, 1 patient with R230S, and 2 patients with R227Q mutations in Kv7.3 channels. All patients had some degree of intellectual disability (ID) and delays across multiple developmental domains, coming to clinical attention between the ages of 4 and 18 months. Delayed language was universal, but patients often presented with concurrent or preceding gross motor delays. Patient 3 did not develop head control until after 6 months. Four patients were late to sit, and all but 2 individuals were delayed in walking. Although all patients ultimately walked, walking was often characterized as broad-based and unsteady with poor balance, variably reported as ataxic. Language development was abnormal in all cases. Three patients were nonverbal; five developed single words, but 2 of these subsequently regressed to become nonverbal. One of these patients, mosaic for R230H, and the 2 patients who carried the R227Q variant had language delay with first words at 2 or 3 years, but were ultimately able to speak in sentences. Autism spectrum disorders (ASD) was diagnosed in 5 of 11 (45%) patients, and autistic features were reported in the remaining 6. Stereotypies, mouthing nonfood objects, and

aggressive, impulsive, and self-injurious behaviors were common features. Hypotonia and strabismus were each reported in 7 of 11 (64%) individuals. Brain magnetic resonance imaging (MRI) studies were normal or showed nonspecific abnormalities. The MRI of one patient showed diminished white matter and abnormal frontal sulcation not consistent with acquired injury, although he had a history of preterm delivery at 34 weeks of gestation. Two patients were diagnosed with generalized tonic–clonic seizures from 13 years and from 10 months of age, respectively. Atonic seizures were also reported for these patients, as well as absence seizures for one patient. The remaining patients were not diagnosed with seizures (9/11, 82%). No patients had seizures in the neonatal period. All 11 patients had EEGs recorded at some point between 1 and 10 years of age, and 8 of them (73%) had focal or multifocal spikes that were markedly activated by sleep. In 6 of 9 patients (67%) with sleep EEGs between 18 months and 6 years of age, epileptiform discharges became near-continuous during sleep. For 4 of these children, parents noticed recurrent episodes of unresponsive staring or deteriorating motor function with subtle jerks or loss of tone that led to assessment with prolonged video-EEG recording. Although the events of concern could not always be captured, the spikes observed were not time-locked with jerks, loss of tone, or unresponsive staring. In 5 cases, the discovery of the markedly abnormal sleep EEG in this clinical context raised concern for epileptic encephalopathy, leading physicians to treat with antiseizure medications including high-dose diazepam with the goal of reducing or eliminating the epileptiform abnormalities. The clinical response to treatments varied; some benefits were reported, although no worsening was seen when the antiseizure medications were discontinued. Treatment with high-dose oral diazepam or corticosteroids was followed by reduction of the sleep-activated spikes on EEG, but with inconsistent effects on behavior.

4.3.2 R227Q and R230C/S/H mutations induce gain-of-function effects on Kv7.3 currents

De novo variants R227Q (R1) and R230C/S/H (R2) affect the first and the second positively charged residue, respectively, along the S4 sequence in the voltage sensor domain of Kv7.3 channels. R1 and R2 are highly conserved among Kv7 channels and correspond to R198 and R201, respectively, in Kv7.2 channels (Fig. 35).

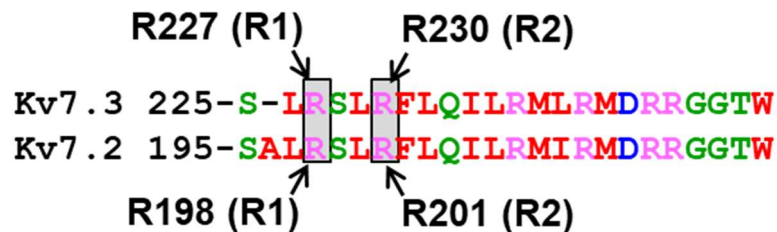


Fig. 35. Partial alignment of Kv7.3 and Kv7.2 subunits.

R1 and R2 refer to the positively charged arginines numbered according to their position along the S4 primary sequence of Kv7.2 and Kv7.3 subunits.

Previous studies have described different mutations in R1 (R198Q) and R2 (R201C/H) of Kv7.2, and in R2 (R230C) of Kv7.3, resulting in drastic effects on channel function (Millichap et al., 2017; Mulkey et al., 2017; Miceli et al., 2015): these mutations stabilize the activate state configuration of the VSD, causing a gain-of-function effects.

The functional effects of the homomeric and heteromeric mutant channels carrying the variants on residues R1 and R2 in Kv7.3 channels were characterized using transiently transfected CHO cells, similar to the previous section. As shown in Fig. 36A and in Table 8, all Kv7.3 mutations caused

GoF effects, with an almost complete loss of time-dependent current activation kinetics; as a result, the $I_{\text{Inst}}/I_{\text{steady-state}}$ ratio (ratio between the currents measured at the beginning of the depolarization step (I_{Inst}) and those at the end of the 0 mV depolarization, as show in fig.) was close to unity due to the presence of a large fraction of mutated Kv7.3 channels already open at the holding potential of -80 mV. By contrast the $I_{\text{Inst}}/I_{\text{steady-state}}$ of wild-type Kv7.3 channels was close to zero (Fig. 36A, bottom panel, and Table 8). The conductance versus voltage curve (G/V curve) of Kv7.3 channels was sigmoidal, whereas Kv7.3 mutated currents showed a mostly linear G/V between -90 mV and +20 mV, indicative of a significant loss of voltage dependent gating (Fig. 36B). Similar, although quantitatively smaller, effects were observed upon neutralization of the R227 residue with glutamine (R1Q); Kv7.3 R1Q channels retained voltage dependent gating, although with a drastic (>70mV) hyperpolarization of the voltage requirement for activation (Fig 36B).

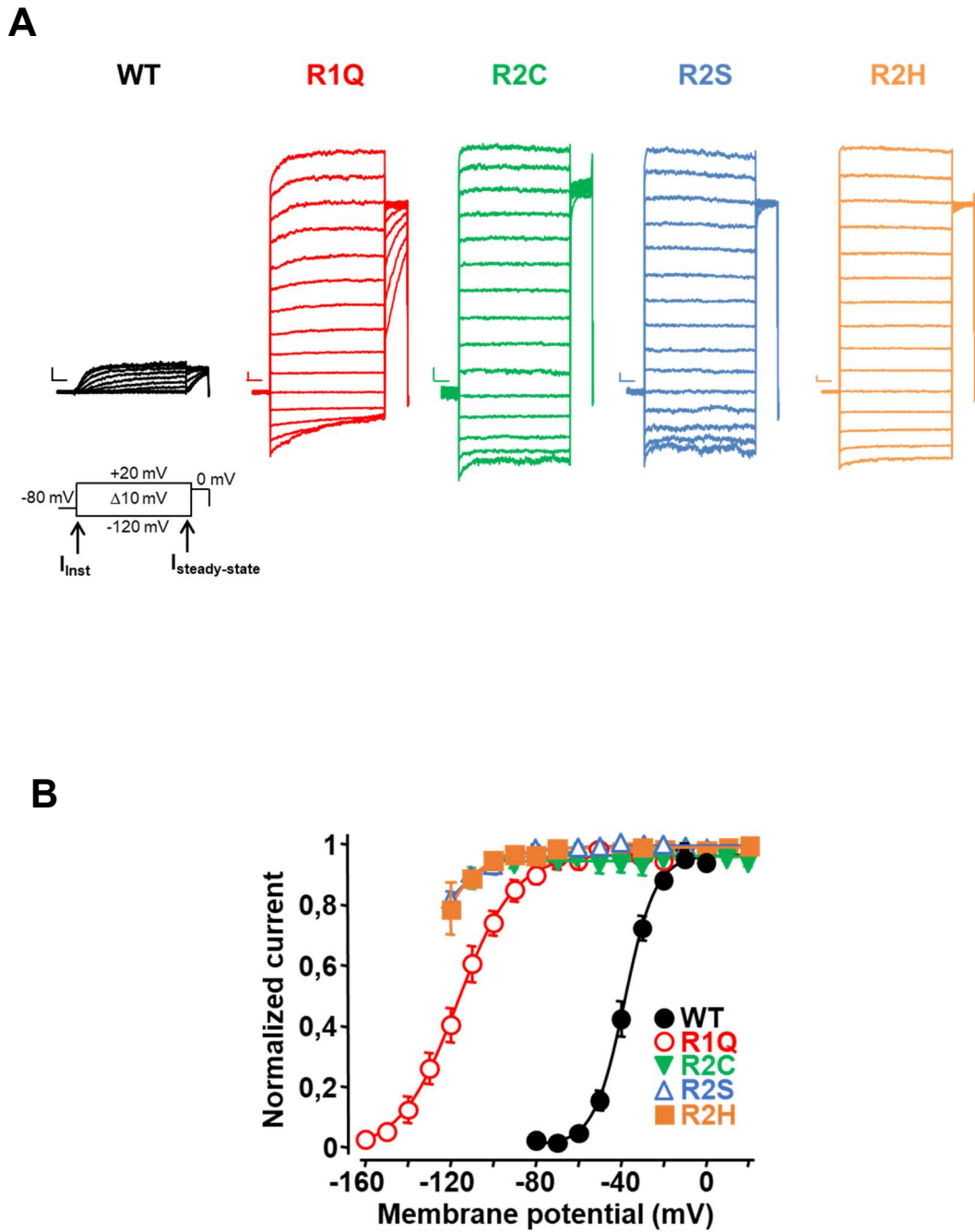


Fig. 36. Functional characterization of mutated homomeric Kv7.3 channels.

A. Representative current traces from Kv7.3 (WT, n=21), Kv7.3 R227Q (R1Q, n=9), Kv7.3 R230C (R2C, n=12), Kv7.3 R230S (R2S, n=16), or Kv7.3 R230H (R2H, n=12) homomeric channels, in response to the indicated voltage protocol. The arrows on the voltage protocol indicate the time chosen for current analysis, as explained in the text. Current scale, 100 pA; time scale, 0.2 s. B. Conductance/voltage curves for the indicated channels. Continuous lines are Boltzmann fits to the experimental data. Each data point is the mean-SEM of 9-21 cells recorded in at least three separate experimental sessions. Student's t test.

Additionally, we observed that the amplitude of K⁺ current carried by each of the 4 mutant channels at depolarized membrane potentials was increased approximately 10-fold, compared to wild-type Kv7.3 channels (Table 8). In contrast to the dramatic changes in voltage-sensitivity and current size described in all 4 mutant channels, other important properties, such as the sensitivity to blockade by tetraethylammonium (TEA), and the K⁺ reversal potential, indicative of channel selectivity for K⁺ ions, were unchanged from the wild-type (Table 8).

Table 8. Biophysical and pharmacological properties of wild-type and mutant Kv7.3 subunits.

	n	V _{1/2} (mV)	k (mV/efold)	I _{inst} / I _{steady-state}	Current density (pA/pF)	Blockade by TEA (%)		
						0.3mM	3mM	30mM
Kv7.3	21	-38.4±1.0	7.1±0.4	0.04±0.02	10.6±1.3	6.4±1.8	13.0±3.4	61.7±5.7
Kv7.3 R1Q	9	-112.0±2.4*	10.8±0.9*	0.91±0.02*	89.6±17.5*	---	---	61.1±6.8
Kv7.3 R2C	12	---	---	1.00±0.01*	121.0±21.0*	---	---	58.6±13
Kv7.3 R2S	16	---	---	0.98±0.03*	89.7±12.2*	---	---	66.1±6.1
Kv7.3 R2H	12	---	---	0.98±0.02*	132.2±20.0*	---	---	70.9±7.3
Kv7.2+Kv7.3	16	-33.6±1.2	13.6±0.4	0.04±0.02	133.5±19.0	15.6±3.1	50.5±3.1	78.8±5.6
Kv7.2+Kv7.3 +Kv7.3 R1Q	9	-39.5±3.0**	14.7±0.8	0.04±0.01	101.3±20.2	19.3±2.0	44.1±4.3	85.3±2.1
Kv7.2+Kv7.3 +Kv7.3 R2C	9	-39.9±3.7**	15.3±0.7	0.10±0.03**	108.8±16.9	14.0±6.2	47.1±9.9	77.0±7.3
Kv7.2+Kv7.3 +Kv7.3 R2S	14	-39.0±1.5**	15.0±0.6	0.07±0.02**	116.7±12.0	12.9±2.3	43.6±8.2	80.1±6.5
Kv7.2+Kv7.3 +Kv7.3 R2H	14	-39.9±1.5**	14.2±0.4	0.08±0.02**	123.0±15.5	20.8±3.1	47.4±2.5	78.8±3.2

*p<0.05 versus Kv7.3; **p<0.05 versus Kv7.2+Kv7.3; TEA: tetraethylammonium. Student's t test. Each data is the mean-SEM of cells recorded in at least three separate experimental sessions.

As described in the previous paragraph, to investigate the functional consequences in heterozygosity condition, CHO cells were transiently transfected as follow:

- 1- Kv7.2+Kv7.3 cDNAs (transfection ratio 1:1) to reproduce the genetic balance of healthy control;
- 2- Kv7.2+Kv7.3+Kv7.3 R1Q (transfection ratio 1:0.5:0.5) to reproduce the genetic balance of patients carrying the Kv7.3 R1Q variant;
- 3- Kv7.2+Kv7.3+Kv7.3 R2C/S/H (transfection ratio 1:0.5:0.5) to reproduce the genetic balance of patients carrying the Kv7.3 R2C/S/H variants, respectively.

The results obtained show that, when compared to wild-type Kv7.2/7.3 channels, heteromeric channels containing mutant subunits elicited currents with identical current densities (Fig. 37); notably, currents produced by channel incorporating mutant Kv7.3 subunits showed a statistically significant hyperpolarizing shift in the current activation, although this effect was less dramatic than that described for homomeric channels, suggesting that the extent of the observed alterations were proportional to the number of mutant Kv7.3 subunits possibly present in heteromeric channels (Fig. 37). No significant difference of TEA sensitivity was identified (Table 8).

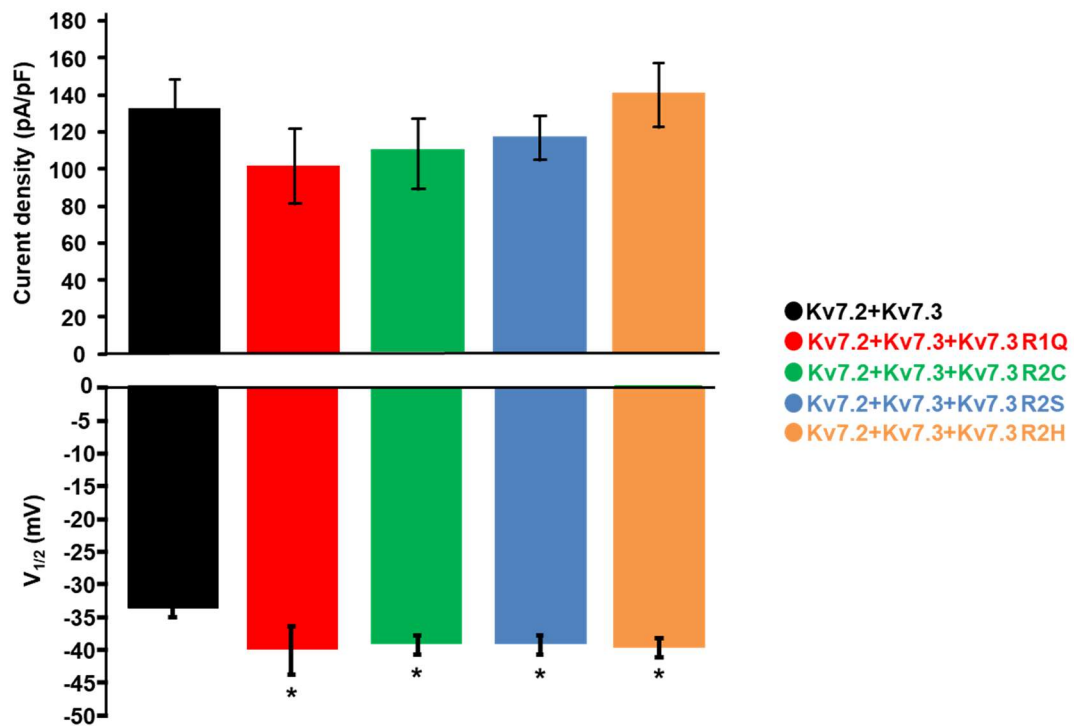


Fig. 37. Current density and $V_{1/2}$ values of mutated heteromeric channels.

Quantification of the maximal current density, in the upper part, and the $V_{1/2}$, in the bottom part, measured in CHO cells expressing indicated channels. Asterisks indicate values statistically significant ($p < 0.05$) from heteromeric Kv7.2+Kv7.3 channels. Each data point is the mean-SEM of 9-21 cells recorded in at least three separate experimental sessions. Student's t test.

Functional data obtained suggest that the mutations in Kv7.3 investigated increased channel sensitivity to voltage, leading therefore to a gain-of-function effects, suggesting a crucial role of the first and second arginine residue in Kv7.3 channel function.

4.3.3 The gain-of-function effects induced by the Kv7.3 mutations are due to destabilization of the resting state of Kv7.3 channels

To investigate the molecular mechanisms by which the R1 and R2 residues control gating in Kv7.3 channels, multistate molecular modelling of a model based on the atomic structure of Kv1.2/2.1 channels (Jensen et al, 2012) was used to characterize the interactions in which each residue in Kv7.3 VSD is involved with neighboring residues in the resting and activated states of the

VSD (Fig. 38A). In particular, we used the coordinates of the six gating states (activated, early deactivated, late deactivated, resting, early activated, and late activated) identified in Kv1.2/2.1 voltage-gated K⁺ channels by molecular dynamics simulation (Jensen et al, 2012).

As shown in figure 38, the positively charged side chains of R227 (R1) and R230 (R2) in the Kv7.3 VSD established ionized hydrogen bonds with nearby polar or charged residues: in particular, in the resting state, R227 residue interacts with C136 in S1, and R230 with E170 and D202 in S2 and S3, respectively (Fig. 38B, left panel). Such interactions disappear when the VSD is displaced outwardly upon depolarization, to occupy the fully activated state when in this configuration, no interaction occurs involving these two residues. Thus, the substitutions of the first arginine with glutamine and the second one with cysteine/serine/histidine could selectively destabilize the resting state configuration of the VSD and favoring Kv7.3 channel opening. Interestingly, the resting state of Kv7.2 channel in addition to C106 (corresponding to Kv7.3 C136), is also stabilized by the presence of a strong hydrogen bond between the same first arginine, R198, corresponding to R227 of Kv7.3 subunit, with S110 (Fig. 38B, right panel). In fact, unlike Kv7.2 channel, this position in Kv7.3 is occupied by a nonpolar residue (A140) that is unable to interact with R227, making the VSD resting state less stable in Kv7.3 when compared to Kv7.2.

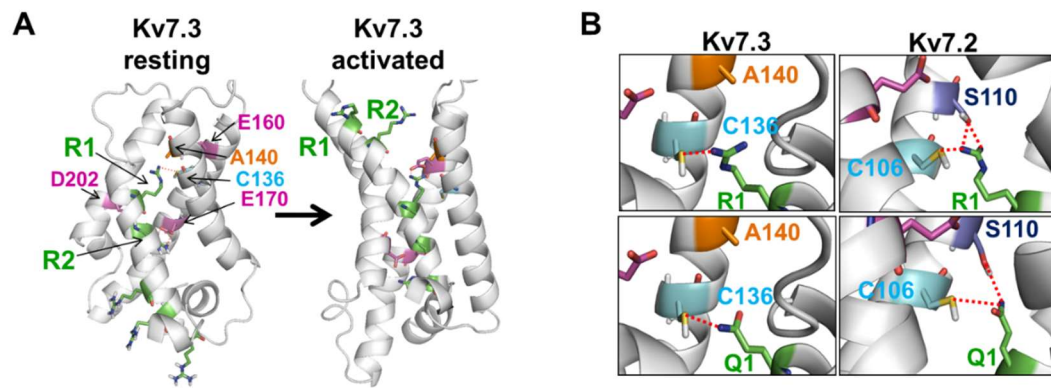


Fig. 38. Structural modeling of Kv7.3 VSD in resting and activated states.

A) Structural model of the resting (left panel) and activated (right panel) gating states of the VSD from a single Kv7.3 subunit, as indicated. Residues relevant to the present study are colored as follows: green for positively-charged, violet for negatively-charged, orange for non-polar, and blue for polar; among polar amino acids, C is in light blue, whereas S is in dark blue. R1 and R2 refer to the positively charged arginines numbered according to their position along the S4 primary sequence. B) An enlarged view of the resting state of the VSD of Kv7.3 (top, left panel) and Kv7.2 (top, right panel). In both panels, dashed red lines indicate ionic interactions between R1 and nearby polar or charged residues. Bottom panels highlight the ionic interactions established when the R1 residues are substituted with Q (Q1) in Kv7.3 (left panel) or Kv7.2 (right panel) subunits.

Altogether these data provide that GoF missense variants at R230 and R227 in Kv7.3 do not cause neonatal epilepsy, and instead result in a novel phenotype, expanding the phenotypic spectrum associated with pathogenic variants in Kv7.3, and adding KCNQ3 gene to genetic causes of autism.

5. Discussion

5.1 Kv7.3 subunits contribute to M-current heterogeneity

Kcnq3 gene encodes for neuronal Kv7.3 voltage-gated potassium channels. Kv7.3 subunits are believed to form heteromeric channels with the homologous Kv7.2 subunits which underline the so-called M-current, a prominent regulator of neuronal excitability. Different studies have shown that M-current is able to control excitability in several areas of the peripheral and central nervous system, but no evidence in cerebellum has been reported (Wang et al., 1998). The absence of I_{KM} may be explained by the different Kv7.2 and Kv7.3 channels expression in this area: indeed, while Kv7.3 channel subunits are only weakly or not expressed in cerebellum (Schroeder et al., 1998; Kanaumi et al., 2008), Kv7.2 channel subunits is strongly expressed (Yang et al., 1998).

However, Kv7.2 and Kv7.3 subunits may not be the only Kv7 members that contribute to M-current. This view seems to be confirmed by the observation that functional interactions and colocalization of Kv7.3 and Kv7.5 subunits in distinct subregions of the brain suggest that Kv7.5 subunits may form heteromeric channels with Kv7.3 (Lerche et al., 2000; Schroeder et al., 2000). Moreover, another member of Kv7 family, Kv7.4 channel subunits, also may interact with Kv7.3 (Kubisch et al., 1999), but only in some areas of the brainstem. Indeed, unlike Kv7.2 and Kv7.3 subunits that are highly expressed in the nervous system, Kv7.4 plays an important role in hearing, and its expression is restricted to nuclei and tracts of the auditory pathway (Kharkovets et al., 2000).

Despite these data suggest the hypothesis that the M-current may be mediated by the combination of other Kv7 family members in different parts of the nervous system, their contribution was not completely addressed.

5.2 Role of Kv7.3 in control of neuronal excitability

In the last decades, the expression and influence on neuronal excitability of Kv7.3 channel subunits has been intensely investigated, mainly through the use of transgenic mice. In particular, previous functional experiments were carried out to identify the role of Kv7.3 in the control of excitability in

hippocampal pyramidal neurons using a conditional Kcnq3 KO mice (Soh et al., 2014). Soh and colleagues demonstrated that, unlike Kcnq2 KO mice, the deletion of Kcnq3 in CA1 pyramidal neurons was not responsible of hyperexcitability, suggesting a minor role in the control of neuronal excitability played by Kv7.3 subunits when compared to Kv7.2 (Soh et al., 2014). Thus, while the role of Kv7.3 channels on firing properties in hippocampal neurons has previously been discussed, the contribution of Kv7.3 in the other brain areas has yet to be addressed.

In the present work we have investigated the role of Kv7.3 channel subunits in the control of neuronal excitability in subicular and CA1 pyramidal neurons, using two conditional Kcnq3 KO mice lines: a conditional kcnq3 KO mice of CA1 pyramidal neurons obtained by crossing the Kcnq3^{fl/+} mice with Emx1-ires-cre (Emx1) mice (Soh et al., 2014), and a conditional kcnq3 KO mice of the subicular neurons obtained by crossing the Kcnq3^{fl/+} mice with G5-Emx-cre (G5) mice. Interestingly, while deletion of Kcnq3 was not responsible of hyperexcitability in subicular pyramidal neurons, recordings from CA1 pyramidal neurons in Kcnq3 KO showed an increase in the number of action potentials, contrarily to the previous study carried out by Soh and colleagues (2014). This difference between the two studies could be explain by the extracellular calcium concentration and temperature used. Indeed, contrarily to Soh (2014) in which recordings from CA1 pyramidal neurons were carried out at room temperature and high calcium concentration (2.5 mM), our recordings have performed at more closely physiological conditions (1.5 mM calcium concentration and 32 °C temperature). In particular, at room temperature a hallmark of CA1 pyramidal neurons function is a physiological process known as *spike frequency adaptation*, which dictates the duration and frequency of action potential firing. As temperature increase and calcium concentration decrease, the pyramidal neuron fire results in much higher rate, revealing a prominent role of Kv7.3 channels in the CA1 hippocampal area. Furthermore, subsequent recordings were carried out to investigate the effects of retigabine (1 µM) on the spontaneous firing of subicular and CA1 pyramidal neurons of Kcnq3 KO mice. Interestingly, different consequences on firing properties after application of retigabine between two areas in Kcnq3 KO mice were observed: in fact, while in subiculum Kcnq3 deletion

substantially decreased the effects of retigabine when compared to those of the corresponding control subicular neurons, in CA1 pyramidal neurons of Kcnq3 KO mice retigabine did not show a net inhibition, but a bimodal effect, that is a decrease followed by an increase in firing. The different results obtained, between the two areas in Kcnq3 KO mice, especially at very low amount of current injection (50 pA), could be explained by the different expression of Kv7 family members, additional to Kv7.3, in subiculum and CA1 area. In particular, while Kv7.5 seems to play a relevant role in controlling CA1 excitability, this subunit in subicular neurons is not expressed (Tzingounis et al., 2010).

Altogether, these data suggest that Kv7.3 channel subunits may have a differential role in the control of neuronal excitability in different neuronal areas, underlying the possibility that the M-current could be underlined by a combination of different Kv7 family members at each neuronal site.

5.3 Kv7.3 pathogenic variants revealed novel features of Kv7.3-related disorders

The role of Kv7.3 channels in brain function has also been established after the identification of Kv7.3 pathogenic variants responsible for several disorders. Among them, different Kv7.3 *missense* mutations have been associated to several forms of epilepsies, ranging from benign (BFNE, BFIE) to severe form (EOEE, Allen et al., 2013; Ambrosino et al., 2018). Nevertheless, more recent *de novo* Kv7.3 variants have been identified in rare families with nonsyndromic sporadic intellectual disability (Rauch et al., 2012; McRae et al., 2017), and intellectual disability with seizures and cortical visual impairment (Bosch et al., 2016). The molecular mechanisms for such phenotypic heterogeneity are still debated, but the disease severity and the clinical course in affected patients is likely influenced by the Kv7.3 variant.

5.3.1 A novel homozygous Kv7.3 F534Ifs*15 frameshift variant

Clinical and ex vivo results

In the present work we reported the clinical, *ex vivo*, and *in vitro* results from a family carrying the novel frameshift Kv7.3 F534Ifs*15 variant. The mutation was found in homozygosity in a patient with non-syndromic ID and neonatal seizures. This Kv7.3 pathogenic variant led the introduction of a premature termination codon (PTC) at position 549, possibly leading to the synthesis of a truncated protein. The presence of the PTC in the mutated mRNA may be a putative target for NMD, a quality control mechanism to avoid production of truncated proteins with potentially deleterious effects, eliminating mRNA transcripts that contain premature stop codons (Baker et Parker, 2004). Therefore, we evaluated the consequences of the newly-identified mutation on the mRNA levels in the proband's primary fibroblasts, since no brain tissue was obviously available, and compared to fibroblasts from the noncarrier brother, used as control. Kv7.3 transcript levels in primary fibroblasts were reduced to ~22% when compared to those in control cells. Moreover, an increase in Kv7.2 and a reduction of Kv7.4 transcript levels were also observed when compared to those from the unaffected noncarrier brother; instead no change in Kv7.1 or Kv7.5 transcript levels were identified. These changes in expression levels of Kv7 members may be due to compensatory effects: it should be highlighted that conditional and selective ablation of Kcnq2 or Kcnq3 gene in cortical mouse tissue also modifies the expression of other members of the Kv7 family (Soh et al., 2014). Notably, immunofluorescence experiments revealed a reduced intensity of the Kv7.3 signal in primary fibroblasts from the proband; in these experiments, the Kv7.3 signal showed a diffuse cytoplasmic staining consistent with endoplasmic reticulum-Golgi localization with no remarkable difference in subcellular localization between fibroblasts from the proband or the unaffected brother.

*Functional consequences of the homozygous Kv7.3 F534Ifs*15 variant*

Despite transcript expression pattern in fibroblasts might not parallel that in neurons, the observation that in primary fibroblasts the mutant protein was

expressed (although lower) at detectable levels, prompted further studies to evaluate its functional properties. The functional experiments, carried out on CHO transiently transfected with Kv7.3 F534Ifs*15 cDNA, showed a complete LoF effect of the Kv7.3 mutant channels. Moreover, since M-current in adult neurons is underlined by Kv7.2+Kv7.3 heteromeric channels, to reproduce *in vitro* the genetic balance of proband who carries the mutant allele in homozygosity CHO were subsequently transfected with Kv7.2+Kv7.3^{MUT} plasmids. Recordings obtained demonstrated a reduced current density, comparable with that recorded from homomeric Kv7.2 channels, suggesting the inability of mutant Kv7.3 subunits to incorporate into functional heteromeric channels with Kv7.2. Infact, this mutation, localized in the long C-terminal domain, caused a deletion of subunit interacting domain (SID) responsible for homomeric and heteromeric subunit assembly and plasmembrane trafficking (Soldovieri et al., 2011; Haitin et Attali, 2008; Choveau et al., 2015). Furthermore, to reproduce *in vitro* the genetic balance of family members who carry the mutant allele in heterozygosity CHO cells were transiently transfected with an halved dose of wild-type Kv7.3 protein. These results showed that CHO transiently transfected with Kv7.2+Kv7.3+Kv7.3^{MUT} displayed biophysical and pharmacological properties of Kv7.2+Kv7.3 wild-type heteromers, but with a reduced current density when compared to that recorded in cells transfected with a full dose of Kv7.3. Therefore, unlike Kv7.2-related EOEE pathogenesis where mutant subunits carrying heterozygous missense variants are functional and able to heteromerize with wild-type subunits causing a dominant-negative mechanism (Miceli et al, 2013; Orhan, 2014), the results obtained from the functional characterization of this Kv7.3 variant indicate haploinsufficiency as the main molecular mechanism for this severe disease.

Clinical spectrum and genetic mechanisms of Kv7.3-related diseases

The role of Kv7.3 subunits in the control of neuronal excitability seems to be different than Kv7.2. This observation could be also confirmed by the fact that, unlike Kv7.3, no homozygous frameshift variant in Kv7.2 has ever been described in humans, as minimal Kv7.2 residual activity is probably essential under penalty of potential lethality. Although several potential mechanisms

may account for the more severe clinical consequences associated with Kv7.2 variants when compared to Kv7.3 ones, the fact that, in both rodents and human brains (Hadley et al., 2003; Kanaumi et al., 2008), the ratio of Kv7.3 to Kv7.2 expression is low at birth and increases during postnatal development provides a plausible explanation.

5.3.2 Gain-of-function Kv7.3 variants responsible of a non-epileptic phenotypes

Additionally to the homozygous Kv7.3 F534Ifs*15 variant, *de novo* Kv7.3 missense variants at R1 (R227Q) and R2 (R230C/S/H) positions in Kv7.3 channels were herein characterized as well. Kv7.3 pathogenic variants were found in 11 patients with different phenotypes than to epilepsy: they were affected by neurodevelopmental delay (NDD) and autism spectrum disorders (ASD), or autistic features. As for the previous Kv7.3 mutation, the functional experiments were carried out on CHO transiently transfected with mutated Kv7.3 cDNAs. Our studies revealed that that the R230C, R230H, and R230S variants all resulted in strong GoF effects, whereas similar but smaller effects were exhibited by Kv7.3 R227Q mutation, consistent with less severe clinical features of the patients carrying this *de novo* variant. Infact, *in vitro* functional properties of homomeric channels carrying Kv7.3 R227Q subunits showed a less complete loss of time-dependent current activation kinetics when compared to those carrying Kv7.3 R230C/H/S variants. Furthermore, co-expression of Kv7.3 R227Q, R230C, R230H, or R230S subunits with both Kv7.2 and Kv7.3 subunits resulted in a statistically significant hyperpolarization in activation voltage-dependence of about 6 mV, without affecting current density or TEA sensitivity, when compared to heteromeric wild-type channels.

Molecular modeling studies revealed that in the resting state R1 and R2 residues in S4 form ionized hydrogen bonds with residues in S1, S2 and S3, necessary to stabilize the resting state of the VSD in native Kv7.3 channels. Thus, mutations in R1 and R2 positions in Kv7.3, caused a loss of these interactions, destabilizing the resting state and, probably, causing the GoF effect observed.

The vast majority of Kv7.2 and Kv7.3 variants in severe infantile epilepsies are LoF, whereas about 10% of the identified variants are actually gain-of-function (GoF) (Mulkey SB et al., 2017). The intriguing issue is: how to reconcile that gain-of-function mutations also produce neuronal hyperexcitability? One possible hypothesis to explain this apparent counter intuitive result was provided by Miceli and colleagues (2015a) for the gain-of-function mutation Kv7.2 R201C, homologous to GoF variant Kv7.3 R230C. In fact, the authors have modelled an inhibitory microcircuit between interneurons and pyramidal cells, incorporating the experimentally-defined values of the kinetic and steady-state properties of the M-current obtained from Kv7.2+Kv7.3 or by Kv7.2+Kv7.2-R201C+Kv7.3 mutant channels. Under control conditions, the interneuron activity blocks more than half of action potentials that would be generated in CA1 hippocampal cell after excitatory input; by contrast, in the presence of the mutation R201C, the interneurons appear more hyperpolarized and this results in an effective disinhibition of the CA1 pyramidal cells, which appear more excitable (Miceli F et al., 2015a). To date, other GoF variants have been identified in the first and the second positively charged residues, R1 and R2, respectively, along the S4 sequence in the voltage sensor domain in Kv7.2 and Kv7.3 channels. These mutations include variants in the Kv7.2 voltage-sensing domain (R1: R198Q; R2: R201C and R201H) and one Kv7.3 variant (R2: R230C) (Mulkey et al., 2017; Miceli et al., 2015; Millichap et al., 2017).

5.4 Kv7.2 and Kv7.3 Genotypes and Phenotypes

To date, inherited LoF missense variants identified in Kv7.2 and Kv7.3 are responsible of BFNE and most *de novo* Kv7.2 LoF variants result in a severe DEE with seizure onset in the neonatal period. However, *de novo* Kv7.2 GoF variants which affected R1 and R2 residue in S4 caused different phenotypes. In particular, while Kv7.2 R198Q variant (a mild GoF) has been found recurrently in patients with West syndrome without prior neonatal seizures, R201C and R201H variants in Kv7.2 are associated with a distinct neonatal syndrome characterized by nonepileptic myoclonus, pathological breathing, and a suppression-burst EEG pattern in the absence of seizures. Herein, we reported *de novo* GoF variants at the Kv7.3 R227 and R230

positions found in 11 patients with NDD associated with ASD, or autistic features. Altogether, these findings further extend the phenotypes associated with Kv7.2 and Kv7.3 GoF variants, which have in common the absence of neonatal seizures, the main characteristic of LoF variants. The reason for the differences in phenotypes between Kv7.2 and Kv7.3 variants at homologous positions is unknown, and fuller investigation of this will likely require in vivo developmental studies. In particular, it is unclear why the LoF condition presents in the neonatal period, whereas the GoF condition results in cognitive and behavioral disturbances that only become apparent later in Kv7.3. In rodents, the ratio of Kv7.3 to Kv7.2 expression is low at birth and increases during postnatal development (Hadley et al., 2003). Similar findings have been shown in the human brain (Kanaumi et al., 2008) and may explain the earlier onset and more severe disability of Kv7.2 GoF pathogenic variants compared to Kv7.3 (Fig.31). The clinical severity of the diseases might have relevant impact on disease-management procedures, as well as on clinical course prediction and pharmacological treatment.

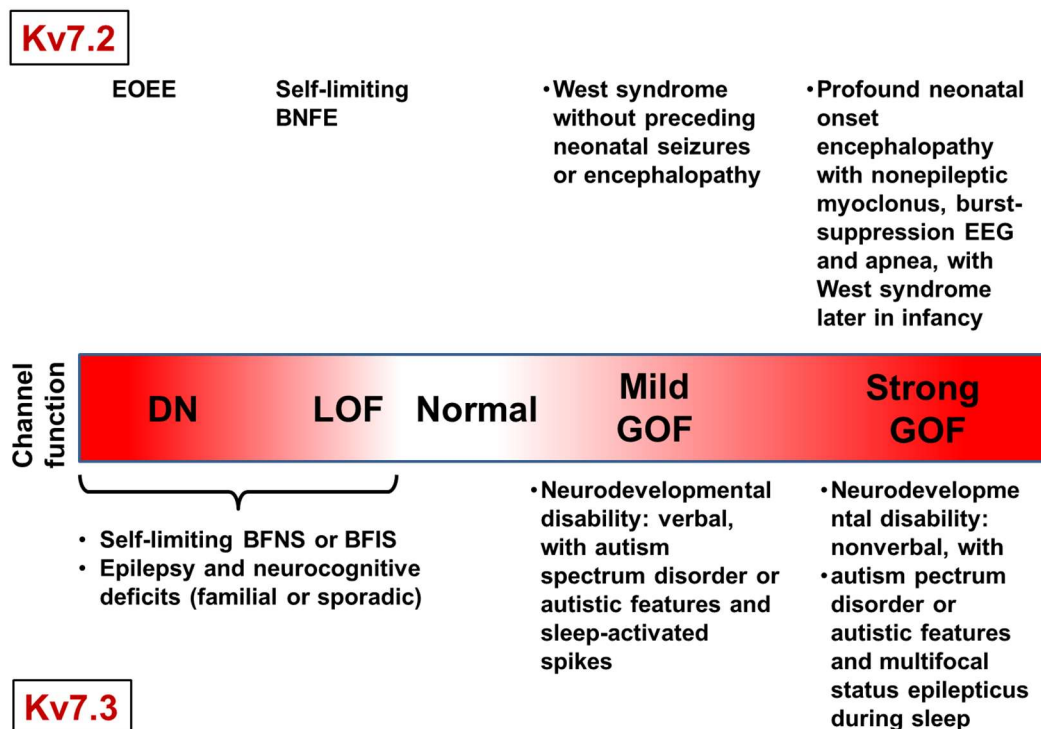


Fig. 31. Summary of genotype-phenotype correlations in Kv7.2 and Kv7.3.

5.5 Pharmacological rescue in Kv7.3-related disorders

Functional consequences prompted by Kv7.3 LoF or GoF mutations could influence the choice of activators or blockers compound pharmacological treatment: in fact, the use of anti-convulsivant drugs which enhance Kv7.3 channel function could represent a rational pharmacological strategy in those patients carrying loss-of-function mutations, such as the Kv7.3 F534Ifs*15 variant, but may be ineffective or even detrimental in patients carrying gain-of-function variants, such as the Kv7.3 R227Q or Kv7.3 R230C/S/H variants, all described in the present thesis. On the opposite, Kv7.3 channels selective blockers could be useful for the treatment of patients carrying gain-of-function Kv7.3 variants.

The identification of the pathogenetic mechanisms underlying several phenotypes possibly associated to distinct variants in this gene allows the possibility of directed therapeutic approaches (precision medicine), targeted to influence the specific functional changes caused by each pathogenic variant.

In conclusions, the present work has been aimed at investigating the role of Kv7.3 in brain function, using tools and models ranging from *kcnq3* KO mice to human mutations.

Altogether, these data provide evidence for a differential contribution of Kv7.3 subunits in controlling neuronal excitability when compared to Kv7.2, suggesting that the M-current is not always underlined by Kv7.2/7.3 heteromeric channels, and expanding the phenotypic spectrum associated with Kv7.3 variants.

References

Adams PR et al., *M-currents and other potassium currents in bullfrog sympathetic neurons*. J Physiol. 1982 Sep;330:537-72.

Adams PR et al., *Pharmacological inhibition of the M-current*. J Physiol. 1982 Nov;332:223-62.

Adams PR et Brown DA, *Luteinizing hormone-releasing factor and muscarinic agonists act on the same voltage-sensitive K⁺-current in bullfrog sympathetic neurons*. Br J Pharmacol. 1980 Mar;68(3):353-5.

Adams PR et Brown DA, *Synaptic inhibition of the M-current: slow excitatory postsynaptic potential mechanism in bullfrog sympathetic neurons*. J Physiol. 1982 Nov; 332: 263–272.

Aggarwal SK et MacKinnon R, *Contribution of the S4 segment to gating charge in the Shaker K⁺ channel*. Neuron. 1996 Jun;16(6):1169-77.

Aiken SP et al., *Reduction of spike frequency adaptation and blockade of M-current in rat CA1 pyramidal neurons by linopirdine (DuP 996), a neurotransmitter release enhancer*. Br J Pharmacol. 1995 Aug; 115(7): 1163–1168.

Alberdi A et al., *Uncoupling PIP2-calmodulin regulation of Kv7.2 channels by an assembly destabilizing epileptogenic mutation*. J Cell Sci. 2015 Nov 1;128(21):4014-23.

Allen AS et al., *Epi4K Consortium and Epilepsy Phenome/Genome Project: De novo mutations in epileptic encephalopathies*. Nature. 2013;501:217–21.

Amaral DG et Witter MP, *The three-dimensional organization of the hippocampal formation: a review of anatomical data*. Neuroscience. 1989;31(3):571-91.

Amaral DG, *Emerging principles of intrinsic hippocampal organization*. Current opinion in Neurobiology. 1993, 3:225-229.

Ambrosino P et al., *Kv7.3 Compound Heterozygous Variants in Early Onset Encephalopathy Reveal Additive Contribution of C-Terminal Residues to*

PIP2-Dependent K⁺ Channel Gating. Mol Neurobiol. 2018 Aug;55(8):7009-7024.

Andrade R et al., *The calcium-activated slow AHP: cutting through the Gordian knot*. Front Cell Neurosci. 2012 Oct 25;6:47.

Baker KE et Parker R, *Conventional 3' end formation is not required for NMD substrate recognition in Saccharomyces cerevisiae*. RNA. 2006;12:1441–1445.

Bal M et al., *Ca²⁺/calmodulin disrupts AKAP79/150 interactions with KCNQ (M-Type) K⁺ channels*. J Neurosci. 2010 Feb 10; 30(6): 2311–2323.

Battefeld A et al., *Heteromeric Kv7.2/7.3 channels differentially regulate action potential initiation and conduction in neocortical myelinated axons*. J Neurosci. 2014 March. 34(10): p. 3719-32.

Bezanilla F, *The voltage sensor in Voltage-Dependent Ion Channels*. Physiol. Rev. 2000 Apr;80(2):555-92.

Biervert C et al., *A potassium channel mutation in neonatal human epilepsy*. Science. 1998 Jan 16;279(5349):403-6.

Blom SM et al., *Differential effects of ICA-27243 on cloned K(V)7 channels*. Pharmacology, 2010. 86(3): p. 174-81.

Boehlen A et al., *The new KCNQ2 activator 4-Chlor-N-(6-chlor-pyridin-3-yl)-benzamid displays anticonvulsant potential*. Br J Pharmacol, 2013. 168(5): p. 1182-200.

Böhm C et al., *Functional Diversity of Subicular Principal Cells during Hippocampal Ripples*. J Neurosci. 2015 Oct 7;35(40):13608-18.

Börjesson SI et Elinder F, *Structure, function, and modification of the voltage sensor in voltage-gated ion channels*. Cell Biochem Biophys. 2008;52(3):149-74.

Bosch DG et al., *Novel genetic causes for cerebral visual impairment*. Eur J Hum Genet. 2016 May;24(5):660-5.

Boscia F et al., *Retigabine and flupirtine exert neuroprotective actions in organotypic hippocampal cultures*. Neuropharmacology. 2006 Aug;51(2):283-94.

Brown DA et Adams PR, *Muscarinic suppression of a novel voltage-sensitive K⁺ current in a vertebrate neurone*. Nature. 1980 Feb 14;283(5748):673-6.

Brown DA et al., *Voltage-sensitive K-currents in sympathetic neurons and their modulation by neurotransmitters*. J Auton Nerv Syst. 1982 Jul;6(1):23-35.

Brown DA et Passmore GM, *Neural KCNQ (Kv7) channels*. Br J Pharmacol. 2009 Apr;156(8):1185-95.

Bunting M et al., *Targeting genes for self-excision in the germ line*. Genes Dev. 1999 Jun 15;13(12):1524-8.

Cembrowski MS et al., *The subiculum is a patchwork of discrete subregions*. eLife 2018 Oct;7:e37701.

Charlier C et al., *A pore mutation in a novel KQT-like potassium channel gene in an idiopathic epilepsy family*. Nat Genet. 1998 Jan;18(1):53-5.

Charlier C et al., *A pore mutation in a novel KQT-like potassium channel gene in an idiopathic epilepsy family*. Nat Genet. 1998 Jan;18(1):53-5.

Cheung YY et al., *Discovery of a series of 2-phenyl-N-(2-(pyrrolidin-1yl)phenyl)acetamides as novel molecular switches that modulate modes of K(v)7.2 (KCNQ2) channel pharmacology: identification of (S)-2-phenyl-N-(2-(pyrrolidin-1yl)phenyl)butanamide (ML252) as a potent, brain penetrant K(v)7.2 channel inhibitor*. J Med Chem. 2012 Aug 9;55(15):6975-9.

Choveau FS et al., *Phosphatidylinositol 4,5-bisphosphate (PIP₂) regulates KCNQ3 K⁺ channels by interacting with four cytoplasmic channel domains*. J Biol Chem. 2018 Dec 14;293(50):19411-19428.

Choveau FS et Shapiro MS, *Regions of KCNQ K(+) channels controlling functional expression*. Front Physiol. 2012 Oct 16;3:397.

Chung HJ et al., *Polarized axonal surface expression of neuronal KCNQ channels is mediated by multiple signals in the KCNQ2 and KCNQ3 C-terminal domains*. Proc Natl Acad Sci U S A. 2006 Jun 6;103(23):8870-5.

Clark S et al., *New antiepileptic medication linked to blue discoloration of the skin and eyes*. Ther Adv Drug Saf, 2015 Feb; 6(1): 15–19.

Cooper EC et al., *Colocalization and coassembly of two human brain M-type potassium channel subunits that are mutated in epilepsy*. Proc Natl Acad Sci U S A. 2000; 97: 4914-4919.

Cooper EC et al., *M channel KCNQ2 subunits are localized to key sites for control of neuronal network oscillations and synchronization in mouse brain*. J Neurosci. 2001 Dec 15;21(24):9529-40.

Cooper EC, *Made for "anchoring": Kv7.2/7.3 (KCNQ2/KCNQ3) channels and the modulation of neuronal excitability in vertebrate axons*. Semin Cell Dev Biol. 2011 Apr;22(2):185-92.

Dahimene S et al., *The N-terminal juxtamembranous domain of KCNQ1 is critical for channel surface expression: implications in the Romano-Ward LQT1 syndrome*. Circ Res, 2006 Nov 10;99(10):1076-83.

Dalby-Brown W et al., *Characterization of a novel high-potency positive modulator of K(v)7 channels*. Eur J Pharmacol. 2013 Jun 5;709(1-3):52-63.

de Guzman et al., *Subiculum network excitability is increased in a rodent model of temporal lobe epilepsy*. Hippocampus. 2006;16(10):843-60.

Devaux JJ et al., *KCNQ2 is a nodal K⁺ channel*. J Neurosci. 2004 Feb 4;24(5):1236-44.

Doyle DA et al., *The structure of the potassium channel: molecular basis of K⁺ conduction and selectivity*. Science. 1998 Apr 3;280(5360):69-77.

Dubyak GR, *Ion homeostasis, channels, and transporters: an update on cellular mechanisms*. Adv Physiol Educ. 2004 Dec;28(1-4):143-54.

Ekberg J et al., *Regulation of the voltage-gated K⁺ channels KCNQ2/3 and KCNQ3/5 by ubiquitination. Novel role for Nedd4-2.* J Biol Chem. 2007 Apr 20;282(16):12135-42.

Etxeberria A et al., *Calmodulin regulates the trafficking of KCNQ2 potassium channels.* FASEB J. 2008 Apr;22(4):1135-43.

Etxeberria, A., et al., *Three mechanisms underlie KCNQ2/3 heteromeric potassium M-channel potentiation.* J Neurosci. 2004 Oct 13;24(41):9146-52.

Fedida D et Hesketh JC, *Gating of voltage-dependent potassium channels.* Prog Biophys Mol Biol. 2001;75(3):165-99.

Gamper N et al., *Subunit-Specific Modulation of KCNQ Potassium Channels by Src Tyrosine Kinase.* JNeurosci. 2003 Jan, 23 (1) 84-95.

Geiger J et al., *Immunohistochemical analysis of KCNQ3 potassium channels in mouse brain.* Neurosci Lett. 2006 May 29;400(1-2):101-4.

Genome Aggregation Database. Available at: <http://gnomad.broadinstitute.org/variant/8-133192492-C-T>. Accessed August 1, 2018.

Gomis-Perez C et al., *An unconventional calmodulin-anchoring site within the AB module of Kv7.2 channels.* J Cell Sci. 2015 Aug 15;128(16):3155-63.

Greene DL et al., *XE991 and Linopirdine Are State-Dependent Inhibitors for Kv7/KCNQ Channels that Favor Activated Single Subunits.* J Pharmacol Exp Ther. 2017 Jul;362(1):177-185.

Hadley JK et al., *Differential tetraethylammonium sensitivity of KCNQ1-4 potassium channels.* Br J Pharmacol. 2000 Feb;129(3):413-5.

Haitin Y et Attali B, *The C-terminus of Kv7 channels: a multifunctional module.* J Physiol. 2008 Apr 1; 586(Pt 7): 1803–1810.

Hernandez CC et al., *A carboxy-terminal inter-helix linker as the site of phosphatidylinositol 4,5-bisphosphate action on Kv7 (M-type) K⁺ channels.* J Gen Physiol. 2008 Sep;132(3):361-81.

Higashida H et al., *Protein kinase C bound with A-kinase anchoring protein is involved in muscarinic receptor-activated modulation of M-type KCNQ potassium channels*. *Neurosci Res*. 2005 Mar;51(3):231-4.

Hille, B., *Ionic Channels of Excitable Membranes*, 3rd, Ed. 2001: Sinauer Associates Inc.

Hoshi N et al., *AKAP150 signaling complex promotes suppression of the M-current by muscarinic agonists*. *Nat Neurosci*. 2003 Jun;6(6):564-71.

Hoshi N et al., *Distinct enzyme combinations in AKAP signalling complexes permit functional diversity*. *Nat Cell Biol*. 2005 Nov;7(11):1066-73.

Hu HN et al., *Discovery of a retigabine derivative that inhibits KCNQ2 potassium channels*. *Acta Pharmacol Sin*. 2013 Oct;34(10):1359-66.

Jarsky T et al., *Distribution of bursting neurons in the CA1 region and the subiculum of the rat hippocampus*. *J. Comp. Neurol*. 2008;506:535–547.

Jensen MO et al., *Mechanism of voltage gating in potassium channels*. *Science*. 2012;336, 229–233.

Jiang Y et al., *X-ray structure of a voltage-dependent K⁺ channel*. *Nature*. 2003 May 1;423(6935):33-41.

Kalappa BI et al., *Potent KCNQ2/3-specific channel activator suppresses in vivo epileptic activity and prevents the development of tinnitus*. *J Neurosci*. 2015 Jun 10;35(23):8829-42.

Kanaumi T et al., *Developmental changes in KCNQ2 and KCNQ3 expression in human brain: possible contribution to the age-dependent etiology of benign familial neonatal convulsions*. *Brain Dev*. 2008 May;30(5):362-9.

Kavanaugh MP et al., *Interaction between tetraethylammonium and amino acid residues in the pore of cloned voltage-dependent potassium channels*. *J. Biol. Chem*. 1991;266:7583–7587.

Kharkovets T et al., *KCNQ4, a K⁺ channel mutated in a form of dominant deafness, is expressed in the inner ear and the central auditory pathway*. *Proc Natl Acad Sci U S A*. 2000 Apr 11;97(8):4333-8.

Kim KS et al., *Hippocalcin and KCNQ Channels Contribute to the Kinetics of the Slow Afterhyperpolarization*. *Biophys J*. 2012 Dec 19; 103(12): 2446–2454.

Kim KS et al., *The Voltage Activation of Cortical KCNQ Channels Depends on Global PIP2 Levels*. *Biophys J*. 2016 Mar 8; 110(5): 1089–1098.

Kim Y et Spruston N, *Target-specific output patterns are predicted by the distribution of regular-spiking and bursting pyramidal neurons in the subiculum*. *Hippocampus*. 2012 Apr;22(4):693-706.

Kim Y et Spruston N. *Target-specific output patterns are predicted by the distribution of regular-spiking and bursting pyramidal neurons in the subiculum*. *Hippocampus*. 2012 Apr;22(4):693-706.

Klein F et al., *Flupirtine-induced hepatic failure requiring orthotopic liver transplant*. *Exp Clin Transplant*. 2011 Aug;9(4):270-2.

Kornilov P et al., *Promiscuous gating modifiers target the voltage sensor of K(v)7.2, TRPV1, and H(v)1 cation channels*. *FASEB J*. 2014 Jun;28(6):2591-602.

Kothur K et al., *Diagnostic yield of targeted massively parallel sequencing in children with epileptic encephalopathy*. *Seizure*. 2018 Jul;59:132-140.

Kothur K et al., *Diagnostic yield of targeted massively parallel sequencing in children with epileptic encephalopathy*. *Seizure*. 2018; 59: 132-140.

Kubisch C et al., *KCNQ4, a novel potassium channel expressed in sensory outer hair cells, is mutated in dominant deafness*. *Cell*. 1999 Feb 5;96(3):437-46.

Kumar M et al., *Synthesis and Evaluation of Potent KCNQ2/3-Specific Channel Activators*. *Mol Pharmacol*. 2016 Jun;89(6):667-77.

Kurata HT et Fedida D, *A structural interpretation of voltage-gated potassium channel inactivation*. *Prog Biophys Mol Biol*. 2006 Oct;92(2):185-208.

Kurosaki et al., *A post-translational regulatory switch on UPF1 controls targeted mRNA degradation*. *Genes Dev*. 2014 Sep 1; 28(17): 1900–1916.

Lanzafame M et al., *Reference genes for gene expression analysis in proliferating and differentiating human keratinocytes*. *Exp Dermatol*. 2015 Apr;24(4):314-6.

Lauritano A et al., *A novel homozygous KCNQ3 loss-of-function variant causes non-syndromic intellectual disability and neonatal-onset pharmacodependent epilepsy*. *Epilepsia Open*. 2019 Aug 11;4(3):464-475.

Lehmann-Horn F et Jurkat-Rott K, *Voltage-gated ion channels and hereditary disease*. *Physiol Rev*. 1999 Oct;79(4):1317-72.

Lerche C et al., *Molecular cloning and functional expression of KCNQ5, a potassium channel subunit that may contribute to neuronal M-current diversity*. *J Biol Chem*. 2000 22395–22400.

Li Y et al., *Regulation of Kv7 (KCNQ) K⁺ Channel Open Probability by Phosphatidylinositol 4,5-Bisphosphate*. *JNeurosci*. 2005 Oct, 25 (43) 9825-9835.

Long SB et al., *Crystal structure of a mammalian voltage-dependent Shaker family K⁺ channel*. *Science*. 2005 Aug 5;309(5736):897-903.

Luo L et al., *Centipedes subdue giant prey by blocking KCNQ channels*. *Proc Natl Acad Sci U S A*, 2018 Feb. 115(7): p. 1646-1651.

Lykke-Andersen S et Jensen TH, *Nonsense-mediated mRNA decay: an intricate machinery that shapes transcriptomes*. *Nat Rev Mol Cell Biol*. 2015, 16: 665677.

MacKinnon R et Yellen G., *Mutations affecting TEA blockade and ion permeation in voltage-activated K⁺ channels*. *Science*. 1990; 250: 276--279.

MacKinnon R, *Potassium channels*. *FEBS Lett*. 2003 Nov 27;555(1):62-5.

Maljevic S et al., *C-terminal interaction of KCNQ2 and KCNQ3 K⁺ channels*. *J Physiol*. 2003 Apr 15; 548(Pt 2): 353–360.

Maljevic S et al., *KV7 channelopathies*. *Pflugers Arch*. 2010 Jul;460(2):277-88.

Martire M et al., *Involvement of KCNQ2 subunits in [3H]dopamine release triggered by depolarization and pre-synaptic muscarinic receptor activation from rat striatal synaptosomes*. J Neurochem. 2007;102(1):179-93.

Martire M et al., *M channels containing KCNQ2 subunits modulate norepinephrine, aspartate, and GABA release from hippocampal nerve terminals*. J. Neurosci. 2004 Jan 21;24(3):592-7.

McRae JF et al., *Prevalence and architecture of de novo mutations in developmental disorders*. Nature. 2017;542:433–8.

Miceli F et al., (Ed) GeneReviews® [Internet]. 2017 Seattle (WA): University of Washington, Seattle. available at <https://www.ncbi.nlm.nih.gov/books/NBK201978/>. Accessed March 15, 2019.

Miceli F et al., *A novel KCNQ3 mutation in familial epilepsy with focal seizures and intellectual disability*. Epilepsia. 2015b Feb;56(2):e15-20.

Miceli F et al., *Early-onset epileptic encephalopathy caused by gain-of-function mutations in the voltage sensor of Kv7.2 and Kv7.3 potassium channel subunits*. J Neurosci. 2015a Mar 4;35(9):3782-93.

Miceli F et al., *Gating currents from neuronal KV7.4 Channels: General features and correlation with the ionic conductance*. Channels. 2009 Aug. 3:4, 277-286.

Miceli F et al., GeneReviews® [Internet]. Seattle (WA): University of Washington, Seattle; 1993-2019.

Miceli F et al., *Genotype-phenotype correlations in neonatal epilepsies caused by mutations in the voltage sensor of K(v)7.2 potassium channel subunits*. Proc Natl Acad Sci U S A. 2013 Mar 12;110(11):4386-91.

Miceli F et al., *The Voltage-Sensing Domain of K(v)7.2 Channels as a Molecular Target for Epilepsy-Causing Mutations and Anticonvulsants*. Front Pharmacol. 2011 Feb 1;2:2.

Michel MC et al., *Unexpected frequent hepatotoxicity of a prescription drug, flupirtine, marketed for about 30 years.* Br J Clin Pharmacol. 2012 May;73(5):821-5.

Millichap JJ et al., *Infantile spasms and encephalopathy without preceding neonatal seizures caused by KCNQ2 R198Q, a gain-of-function variant.* Epilepsia. 2017 Jan;58(1):e10-e15.

Millichap JJ et al., *KCNQ2 encephalopathy: Features, mutational hot spots, and ezogabine treatment of 11 patients.* Neurol Genet. 2016 Aug 22;2(5):e96.

Mulkey SB et al., *Neonatal nonepileptic myoclonus is a prominent clinical feature of KCNQ2 gain-of-function variants R201C and R201H.* Epilepsia. 2017 Mar;58(3):436-445.

Naber PA et al., *Reciprocal connections between the entorhinal cortex and hippocampal fields CA1 and the subiculum are in register with the projections from CA1 to the subiculum.* Hippocampus. 2001;11(2):99-104.

Okada M et al., *Age-dependent modulation of hippocampal excitability by KCNQ-channels.* Epilepsy Res. 2003 Feb;53(1-2):81-94.

Orhan G et al., *Dominant-negative effects of KCNQ2 mutations are associated with epileptic encephalopathy.* Ann Neurol. 2014 Mar;75(3):382-94.

Padilla K et al., *The KCNQ2/3 selective channel opener ICA-27243 binds to a novel voltage-sensor domain site.* Neurosci Lett, 2009. 465(2): p. 138-42.

Pan Z et al., *A common ankyrin-G-based mechanism retains KCNQ and NaV channels at electrically active domains of the axon.* J Neurosci. 2006 Mar 8;26(10):2599-613.

Pan Z et al., *A common ankyrin-G-based mechanism retains KCNQ and NaV channels at electrically active domains of the axon.* J Neurosci. 2006 Mar 8;26(10):2599-613.

Peretz A et al., *Meclofenamic acid and diclofenac, novel templates of KCNQ2/Q3 potassium channel openers, depress cortical neuron activity and exhibit anticonvulsant properties*. Mol Pharmacol, 2005. 67(4): p. 1053-66.

Plouin, P, *Benign idiopathic neonatal convulsions (familial and non-familial): open questions about these syndromes*. In: Wolf P (Hrsg) Epileptic seizures and syndromes. London, S 193–201. John Libbey, 1994.

Poulet C et al., *Altered physiological functions and ion currents in atrial fibroblasts from patients with chronic atrial fibrillation*. Physiol Rep. 2016; 4.pii: e12681.

Provence A et al., *The Novel KV7.2/KV7.3 Channel Opener ICA069673 Reveals Subtype-Specific Functional Roles in Guinea Pig Detrusor Smooth Muscle Excitability and Contractility*. J Pharmacol Exp Ther, 2015. 354(3): p. 290-301.

Putney JW et Tomita T, *Phospholipase C signaling and calcium influx*. Adv Biol Regul. 2012 Jan;52(1):152-64.

Rauch A et al., *Range of genetic mutations associated with severe non-syndromic sporadic intellectual disability: an exome sequencing study*. Lancet. 2012 Nov 10;380(9854):1674-82.

Regev N et al., *Selective interaction of syntaxin 1A with KCNQ2: possible implications for specific modulation of presynaptic activity*. PLoS One. 2009 Aug 13;4(8):e6586.

Rockwood K et al., *A randomized, controlled trial of linopirdine in the treatment of Alzheimer's disease*. Can J Neurol Sci. 1997. 24(2): p. 140-5.

Roeloffs R et al., *In vivo profile of ICA-27243 [N-(6-chloro-pyridin-3-yl)-3,4-difluorobenzamide], a potent and selective KCNQ2/Q3 (Kv7.2/Kv7.3) activator in rodent anticonvulsant models*. J Pharmacol Exp Ther, 2008. 326(3): p. 818-28.

Rosati A et al., *Antiepileptic Drug Treatment in Children with Epilepsy*. CNS Drugs. 2015;29(10):847-63.

- Sands TT et al., *Autism and developmental disability caused by KCNQ3 gain-of-function variants*. Ann Neurol. 2019 Aug;86(2):181-192.
- Sanguinetti MC et al., *Coassembly of K(V)LQT1 and minK (IsK) proteins to form cardiac I(Ks) potassium channel*. Nature. 1996 Nov 7;384(6604):80-3.
- Schenzer A et al., *Molecular determinants of KCNQ (Kv7) K⁺ channel sensitivity to the anticonvulsant retigabine*. J Neurosci 18 maggio 2005; 25 (20): 5051-60.
- Schroeder BC et al., *A constitutively open potassium channel formed by KCNQ1 and KCNE3*. Nature. 2000 Jan 13;403(6766):196-9.
- Schroeder BC et al., *Moderate loss of function of cyclic-AMP-modulated KCNQ2/KCNQ3 K⁺ channels causes epilepsy*. Nature. 1998 Dec 17;396(6712):687-90.
- Schwake M et al., *Structural determinants of M-type KCNQ (Kv7) K⁺ channel assembly*. J Neurosci. 2006 Apr 5;26(14):3757-66.
- Schwake M et al., *Surface expression and single channel properties of KCNQ2/KCNQ3, M-type K⁺ channels involved in epilepsy*. J Biol Chem. 2000 May 5;275(18):13343-8.
- Schwarz JR et al., *KCNQ channels mediate I_{Ks}, a slow K⁺ current regulating excitability in the rat node of Ranvier*. J Physiol. 2006 May 15;573(Pt 1):17-34.
- Schwiening C., *A brief historical perspective: Hodgkin and Huxley*. J Physiol. 2012 Jun 1;590(11):2571-5.
- Selyanko AA et al., *Properties of single M-type KCNQ2/KCNQ3 potassium channels expressed in mammalian cells*. J Physiol. 2001 Jul 1;534(Pt 1):15-24.
- Seyfarth EA, *Julius Bernstein (1839-1917): pioneer neurobiologist and biophysicist*. Biol Cybern. 2006 Jan;94(1):2-8.

Shao LR, Dudek FE. *Detection of increased local excitatory circuits in the hippocampus during epileptogenesis using focal flash photolysis of caged glutamate*. *Epilepsia*. 2005;46(Suppl 5):100–106.

Shapiro MS et al., *Reconstitution of muscarinic modulation of the KCNQ2/KCNQ3 K(+) channels that underlie the neuronal M current*. *J Neurosci*. 2000 Mar 1;20(5):1710-21.

Singh NA et al., *Mouse models of human KCNQ2 and KCNQ3 mutations for benign familial neonatal convulsions show seizures and neuronal plasticity without synaptic reorganization*. *J Physiol* 586.14 (2008) pp 3405–3423.

Soh H et al., *Conditional deletions of epilepsy-associated KCNQ2 and KCNQ3 channels from cerebral cortex cause differential effects on neuronal excitability*. *J Neurosci*, 2014 Apr 9;34(15):5311-21.

Soh H et al., *Deletion of KCNQ2/3 potassium channels from PV+ interneurons leads to homeostatic potentiation of excitatory transmission*. *eLife*. 2018; 7: e38617.

Soh H et Tzingounis AV, *The specific slow afterhyperpolarization inhibitor UCL2077 is a subtype-selective blocker of the epilepsy associated KCNQ channels*. *Mol Pharmacol*. 2010 Dec; 78(6): 1088–1095.

Soldovieri MV et al., *Driving with no brakes: molecular pathophysiology of Kv7 potassium channels*. *Physiology (Bethesda)*. 2011 Oct;26(5):365-76.

Soldovieri MV et al., *Driving with no brakes: molecular pathophysiology of Kv7 potassium channels*. *Physiology (Bethesda)*. 2011 Oct;26(5):365-76.

Staff NP et al., *Resting and active properties of pyramidal neurons in subiculum and CA1 of rat hippocampus*. *J. Neurophysiol*. 2000;84:2398–2408.

Stafstrom CE et Carmant L, *Seizures and Epilepsy: An Overview for Neuroscientists*. *Cold Spring Harb Perspect Med*. 2015 Jun; 5(6): a022426.

Suh BC et Hille B, *Recovery from muscarinic modulation of M current channels requires phosphatidylinositol 4,5-bisphosphate synthesis*. *Neuron*. 2002 Aug 1;35(3):507-20.

Sun J et al., *Structural and mechanistic insights into Mcm2-7 double-hexamer assembly and function*. *Genes Dev*. 2014 Oct 15;28(20):2291-303. doi: 10.1101/gad.242313.114.

Sun J et MacKinnon R, *Cryo-EM Structure of a KCNQ1/CaM Complex Reveals Insights into Congenital Long QT Syndrome*. *Cell*. 2017 Jun 1;169(6):1042-1050.e9.

Tang QY et al., *Epilepsy-Related Slack Channel Mutants Lead to Channel Over-Activity by Two Different Mechanisms*. *Cell Rep*. 2016 Jan 5;14(1):129-139.

Tatulian L et al., *Activation of expressed KCNQ potassium currents and native neuronal M-type potassium currents by the anti-convulsant drug retigabine*. *J Neurosci*. 2001 Aug 1;21(15):5535-45.

Tatulian L et Brown DA, *Effect of the KCNQ potassium channel opener retigabine on single KCNQ2/3 channels expressed in CHO cells*. *J Physiol*. 2003 May 15;549(Pt 1):57-63.

Taube JS. *Electrophysiological properties of neurons in the rat subiculum in vitro*. *Exp Brain Res*. 1993;96:304–318.

Thomas KR et Capecchi MR, *Site-directed mutagenesis by gene targeting in mouse embryo-derived stem cells*. *Cell*. 1987 Nov 6;51(3):503-12.

Tinel N et al., *The KCNQ2 potassium channel: splice variants, functional and developmental expression. Brain localization and comparison with KCNQ3*. *FEBS Lett*. 1998 Nov 6;438(3):171-6.

Tombola F et al., *How does voltage open an ion channel?* *Annu Rev Cell Dev Biol*. 2006;22:23-52.

Topsakal V et al., *Phenotype determination guides swift genotyping of a DFNA2/KCNQ4 family with a hot spot mutation (W276S)*. Otol Neurotol. 2005 26:52–58.

Treven M et al., *The anticonvulsant retigabine is a subtype selective modulator of GABAA receptors*. Epilepsia, 2015 Apr;56(4):647-57.

Tzingounis AV et al., *The KCNQ5 potassium channel mediates a component of the afterhyperpolarization current in mouse hippocampus*. Proc Natl Acad Sci U S A. 2010 Jun 1;107(22):10232-7.

Tzingounis AV et Nicoll RA, *Contribution of KCNQ2 and KCNQ3 to the medium and slow afterhyperpolarization currents*. Proc Natl Acad Sci U S A. 2008 Dec 16;105(50):19974-9.

Wang H et al., *Localization of Kv1.1 and Kv1.2, two K channel proteins, to synaptic terminals, somata, and dendrites in the mouse brain*. J Neurosci. 1994 Aug;14(8):4588-99.

Wang HS et al., *KCNQ2 and KCNQ3 potassium channel subunits: molecular correlates of the M-channel*. Science. 1998 Dec 4;282(5395):1890-3.

Wang HS et al., *KCNQ2 and KCNQ3 potassium channel subunits: Molecular correlates of the M-channel*. Science. 1998 Dec 4;282(5395):1890-3.

Wang Q et al., *Positional cloning of a novel potassium channel gene: KVLQT1 mutations cause cardiac arrhythmias*. Nat Genet. 1996 Jan;12(1):17-23.

Weber YG et al., *Immunohistochemical analysis of KCNQ2 potassium channels in adult and developing mouse brain*. Brain Res. 2006 Mar 10;1077(1):1-6.

Wen H et Levitan IB, *Calmodulin is an auxiliary subunit of KCNQ2/3 potassium channels*. J Neurosci, 2002 Sep 15;22(18):7991-8001.

Wickenden AD et al., *N-(6-chloro-pyridin-3-yl)-3,4-difluoro-benzamide (ICA-27243): a novel, selective KCNQ2/Q3 potassium channel activator*. Mol Pharmacol, 2008. 73(3): p. 977-86.

Wu YJ et al., *(S)-N-[1-(4-cyclopropylmethyl-3,4-dihydro-2H-benzo[1,4]oxazin-6-yl)ethyl]-3-(2-fluoro-phenyl)-acrylamide is a potent and efficacious KCNQ2 opener which inhibits induced hyperexcitability of rat hippocampal neurons*. *Bioorg Med Chem Lett*, 2004. 14(8): p. 1991-5.

Wu YJ et al., *Discovery of (S,E)-3-(2-fluorophenyl)-N-(1-(3-(pyridin-3yloxy)phenyl)ethyl)-acrylamide as a potent and efficacious KCNQ2 (Kv7.2) opener for the treatment of neuropathic pain*. *Bioorg Med Chem Lett*, 2013. 23(22): p. 6188-91.

Wu YJ et al., *Synthesis and KCNQ2 opener activity of N-(1-benzo[1,3]dioxol-5-yl-ethyl, N-[1-(2,3-dihydro-benzofuran-5-yl)-ethyl, and N-[1-(2,3-dihydro-1H-indol-5-yl)-ethyl acrylamides*. *Bioorg Med Chem Lett*, 2004. 14(17): p. 4533-7.

Wua YJ et Dworetzky SI, *Recent developments on KCNQ potassium channel openers*. *Curr Med Chem*. 2005;12(4):453-60.

Wuttke TV et al., *Neutralization of a negative charge in the S1-S2 region of the KV7.2 (KCNQ2) channel affects voltage-dependent activation in neonatal epilepsy*. *J Physiol*. 2008 Jan 15;586(2):545-55.

Wuttke TV et al., *The new anticonvulsant retigabine favors voltage-dependent opening of the Kv7.2 (KCNQ2) channel by binding to its activation gate*. *Mol Pharmacol*. 2005 Apr;67(4):1009-17.

Xu X et al., *Noncanonical connections between the subiculum and hippocampal CA1*. *J Comp Neurol*. 2016 Dec 1;524(17):3666-3673.

Yu H et al., *Identification of a novel, small molecule inhibitor of KCNQ2 channels*, in *Probe Reports from the NIH Molecular Libraries Program*. 2010: Bethesda (MD).

Yue C et Yaari Y, *KCNQ/M Channels Control Spike Afterdepolarization and Burst Generation in Hippocampal Neurons*. *J Neurosci*. 2004 May 12; 24(19): 4614–4624.

Yus-Najera E et al., *The identification and characterization of a noncontinuous calmodulin-binding site in noninactivating voltage-dependent KCNQ potassium channels.* J Biol Chem. 2002 Aug 9;277(32):28545-53.

Zaczek R et al., *Two new potent neurotransmitter release enhancers, 10,10-bis(4-pyridinylmethyl)-9(10H)-anthracenone and 10,10-bis(2-fluoro-4-pyridinylmethyl)-9(10H)-anthracenone: comparison to linopirdine.* J Pharmacol Exp Ther. 1998 May;285(2):724-30.

Zhang J et al., *AKAP79/150 signal complexes in G-protein modulation of neuronal ion channels.* J Neurosci. 2011 May 11;31(19):7199-211.

Zheng Y et al., *Activation of peripheral KCNQ channels relieves gout pain.* Pain, 2015 Jun;156(6):1025-35.

Appendix: Published papers

- *A novel homozygous KCNQ3 loss-of-function variant causes non-syndromic intellectual disability and neonatal-onset pharmacodependent epilepsy*
- *Autism and developmental disability caused by KCNQ3 gain-of-function variants*

FULL-LENGTH ORIGINAL RESEARCH

A novel homozygous KCNQ3 loss-of-function variant causes non-syndromic intellectual disability and neonatal-onset pharmacodependent epilepsy

Anna Lauritano¹ | Sebastien Moutton^{2,3}  | Elena Longobardi¹ |
 Frédéric Tran Mau-Them^{3,4} | Giusy Laudati¹ | Piera Nappi¹ |
 Maria Virginia Soldovieri⁵ | Paolo Ambrosino⁶ | Mauro Cataldi¹ | Thibaud Jouan^{3,4} |
 Daphné Lehalle^{2,3} | Hélène Maurey⁷ | Christophe Philippe^{3,4} | Francesco Miceli¹ |
 Antonio Vitobello^{3,4} | Maurizio Tagliatela¹ 

¹Division of Pharmacology, Department of Neuroscience, University of Naples “Federico II”, Naples, Italy

²Reference Center for Developmental Anomalies, Department of Medical Genetics, Dijon University Hospital, Dijon, France

³INSERM U1231, LNC UMR1231 GAD, Burgundy University, Dijon, France

⁴Laboratoire de Génétique, Innovation en Diagnostic Génomique des Maladies Rares UF6254, Plateau Technique de Biologie, CHU Dijon, Dijon, France

⁵Department of Medicine and Health Science “V. Tiberio”, University of Molise, Campobasso, Italy

⁶Division of Pharmacology, Department of Science and Technology, University of Sannio, Benevento, Italy

⁷Service de Neurologie Pédiatrique, APHP, Hôpital Universitaire Bicêtre, Le Kremlin-Bicêtre, France

Correspondence

Maurizio Tagliatela, Department of Neuroscience, University of Naples “Federico II”, Via Pansini 5, 80131, Naples, Italy.
 Email: mtagliat@unina.it

Funding information

Ministero dell’Istruzione, dell’Università e della Ricerca, Grant/Award Number: PRIN 2017ALCR7C to MT and MVS, PRIN 2017YH3SXX to FM and RBS11444EM to FM; Fondazione Telethon, Grant/Award Number: GGPI5113 to MT; Ministero della Salute, Grant/Award Number: GR-2016-02363337 to MVS; Università degli Studi di Napoli Federico II, Grant/Award Number: 6-CSP-UNINA-120 to FM

Abstract

Objective: Heterozygous variants in *KCNQ2* or, more rarely, *KCNQ3* genes are responsible for early-onset developmental/epileptic disorders characterized by heterogeneous clinical presentation and course, genetic transmission, and prognosis. While familial forms mostly include benign epilepsies with seizures starting in the neonatal or early-infantile period, de novo variants in *KCNQ2* or *KCNQ3* have been described in sporadic cases of early-onset encephalopathy (EOEE) with pharmacoresistant seizures, various age-related pathological EEG patterns, and moderate/severe developmental impairment. All pathogenic variants in *KCNQ2* or *KCNQ3* occur in heterozygosity. The aim of this work was to report the clinical, molecular, and functional properties of a new *KCNQ3* variant found in homozygous configuration in a 9-year-old girl with pharmacodependent neonatal-onset epilepsy and non-syndromic intellectual disability. **Methods:** Exome sequencing was used for genetic investigation. *KCNQ3* transcript and subunit expression in fibroblasts was analyzed with quantitative real-time PCR and Western blotting or immunofluorescence, respectively. Whole-cell patch-clamp electrophysiology was used for functional characterization of mutant subunits.

Lauritano, Moutton, and Longobardi contributed equally.

This is an open access article under the terms of the Creative Commons Attribution License, which permits use, distribution and reproduction in any medium, provided the original work is properly cited.

© 2019 University of Naples Federico II. *Epilepsia Open* published by Wiley Periodicals Inc. on behalf of International League Against Epilepsy.

Results: A novel single-base duplication in exon 12 of *KCNQ3* (NM_004519.3:c.1599dup) was found in homozygous configuration in the proband born to consanguineous healthy parents; this frameshift variant introduced a premature termination codon (PTC), thus deleting a large part of the C-terminal region. Mutant *KCNQ3* transcript and protein abundance was markedly reduced in primary fibroblasts from the proband, consistent with nonsense-mediated mRNA decay. The variant fully abolished the ability of *KCNQ3* subunits to assemble into functional homomeric or heteromeric channels with *KCNQ2* subunits.

Significance: The present results indicate that a homozygous *KCNQ3* loss-of-function variant is responsible for a severe phenotype characterized by neonatal-onset pharmacodependent seizures, with developmental delay and intellectual disability. They also reveal difference in genetic and pathogenetic mechanisms between *KCNQ2*- and *KCNQ3*-related epilepsies, a crucial observation for patients affected with EOEE and/or developmental disabilities.

KEYWORDS

early-onset epileptic encephalopathy, homozygous loss-of-function variant, intellectual disability, *KCNQ3*, next-generation sequencing, nonsense-mediated mRNA decay

1 | INTRODUCTION

Next-generation sequencing (NGS) technologies have revolutionized diagnostic procedures in developmental disorders, intellectual disability (ID), and pediatric epilepsies, allowing early identification of the molecular defects in an ever-growing number of human disease-causing genes.¹ Early genetic diagnosis is critical for prognostic assessment, genetic counseling, and, in some cases, personalized treatment attempts.²

Pathogenic variants in *KCNQ2* and *KCNQ3* genes coding for Kv7.2 and Kv7.3 neuronal voltage-gated potassium (K⁺) channel subunits cause early-onset epilepsies with wide phenotypic heterogeneity.^{3–5} At the benign end of this spectrum is benign familial neonatal seizures (BFNS), an autosomal dominant self-limiting neonatal epilepsy with seizures beginning in otherwise healthy infants in the first days of life and spontaneously disappearing in the following months, with mostly normal neurocognitive development and unremarkable neuroimaging.^{3,6,7} On the other hand, sporadic cases of early-onset epileptic encephalopathy (EOEE) with cognitive disability, various age-related pathological EEG patterns such as suppression-burst/multifocal epileptic activity/hypsarrhythmia,^{8,9} and distinct neuroradiological features have been more recently described in association to *KCNQ2* variants.^{10,11}

When compared to *KCNQ2*, pathogenic variants in *KCNQ3* have been more rarely described, mostly in families affected with familial forms of benign epilepsies with

Key Points

- Heterozygous variants in *KCNQ2* or, more rarely, *KCNQ3* genes are responsible for early-onset developmental/epileptic disorders
- We describe a patient with severe epilepsy and intellectual disability carrying a homozygous frameshift loss-of-function variant in *KCNQ3*
- Familial members who are heterozygous carriers of the *KCNQ3* variant are unaffected
- The present results highlight difference in genetic and pathogenetic mechanisms between *KCNQ2*- and *KCNQ3*-related epilepsies

seizures starting in the neonatal (BFNS)^{6,12,13} or early-infantile (benign familial infantile seizures, BFIS) period.^{14,15} Fewer than twenty families with BFNS and three families with BFIS with a heterozygous *KCNQ3* pathogenic variant have been reported to date.¹⁶ In addition, de novo variants in *KCNQ3* have been described in few children with EOEE,^{17–20} ID apparently without epilepsy,^{21,22} and cortical visual impairment.²³

Notably, all pathogenic variants in *KCNQ2* and *KCNQ3*, except one,²⁴ occur in heterozygosity. In the present manuscript, we report the clinical, molecular, and functional properties of a new *KCNQ3* variant found in homozygous configuration

in a 9-year-old girl with pharmacodependent neonatal-onset epilepsy and non-syndromic ID; the variant, a single-base duplication in exon 12 of *KCNQ3* (chr8:g.133150233dup in GRCh37; NM_004519.3:c.1599dup), is predicted to result in a frameshift p.(Phe534Ilefs*15) which could lead to either mRNA degradation by the nonsense-mediated mRNA decay (NMD) machinery²⁵ and/or a truncation of a large part of the C-terminus. Ex vivo results showed that *KCNQ3* transcript levels were markedly reduced in primary fibroblasts from the proband when compared to those from the unaffected non-carrier brother, and in vitro studies revealed that the variant fully abolished the ability of *KCNQ3* subunits to assemble into functional homomeric or heteromeric channels with *KCNQ2* subunits. The present results provide the first clinical, genetic, and functional evidence for a severe phenotype associated with a homozygous loss-of-function (LoF) variant in *KCNQ3* and highlight previously unrecognized difference in genetic and pathogenetic mechanisms between *KCNQ2*- and *KCNQ3*-related epilepsies.

2 | MATERIALS AND METHODS

2.1 | Informed patient consent

Written informed consent was obtained from all study participants or from parents/authorized legal guardians. The study was performed within the framework of the Genetique des Anomalies du Développement (GAD) collection performed at Equipe Inserm U1231 of the Université de Bourgogne in Dijon (FR), approved by institutional review board (no DC2011-1332).

2.2 | Exome sequencing

Singleton exome sequencing was performed using an Agilent CRE capture kit (Agilent Technologies) and a HiSeq 4000 sequencer (Illumina); exome data analysis and variant filtering were performed as previously described²⁶ using the following annotation databases and software versions: dbsnp 149, clinvar 2016_11_03, cosmic COSMICv79, omim 2016_11_29, refseq_annotation 2016_11_27, FASTQC 2015_12_15, TRIMMOMATIC 0.35, BWA_0.7.12, PICARD_2.0.1, GATK_3.5, samtools_1.2, IGVTools_2.3.67, reference genome GRCh37/hg19, refseq 2015_07_30. Reads alignment resulted in coverage of at least 10× for 96.5% of the bases on target and an average sequencing depth of 116.01×.

2.3 | Cell culture

Chinese hamster ovary (CHO) cells were grown in Dulbecco's Modified Eagle's Medium (DMEM) containing 10% fetal bovine serum (FBS), 2 mmol/L L-glutamine, penicillin (50 U/mL), and streptomycin (50 µg/mL) in a humidified

atmosphere at 37°C with 5% CO₂. Primary fibroblasts were obtained from punch skin biopsies. Tissue was cut into small pieces (1 × 3 mm), and cells were cultivated in a fibroblast growth medium consisting of AmnioMax (Gibco, Thermo Fisher) supplemented with 20% FBS. For long-term culture, fibroblasts were maintained in DMEM supplemented with 10% FBS.

2.4 | Mutagenesis and heterologous expression of *KCNQ2* or *KCNQ3* cDNAs

The variant of interest was engineered in *KCNQ3* human cDNA cloned into pcDNA3.1 (variant 1; NM_004519.3; 872 aa) by QuikChange site-directed mutagenesis (Agilent Technologies). Channel subunits were expressed in CHO cells by transient transfection using Lipofectamine 2000 (Invitrogen);^{27,28} when two or more cDNAs were cotransfected, their molar ratio was modified such that total cDNA in the transfection mixture was kept constant at 3 µg. Enhanced green fluorescent protein (1 µg; Clontech) was used as transfection marker.

2.5 | Western blot experiments

KCNQ3 subunits in total protein lysates from CHO cells obtained 24 hours post-transfection were analyzed by Western blotting on 8% SDS-PAGE using two primary rabbit anti-*KCNQ3* polyclonal antibodies: (a) the first directed against a C-terminal epitope (rat aa 668-686; accession number O88944; C-*KCNQ3*) (clone APC-051, dilution 1:1000; Alomone Labs) and (b) the second raised against an N-terminal epitope (rat aa 1-71; N-*KCNQ3*) (PA1-930; dilution 1:1000; Thermo Scientific). Both antibodies also recognized human *KCNQ3* subunits. Following exposure to primary antibodies, filters were incubated with HRP-conjugated anti-rabbit secondary antibodies (NA934V; dilution 1:5,000; GE Healthcare) and reactive bands visualized by chemiluminescence. Data acquisition and analysis were performed with the Gel Doc Imaging System (Bio-Rad) and ImageLab software (version 4.1; Bio-Rad), respectively.

2.6 | RNA isolation, reverse transcription, and quantitative PCR

Isolation and purification of RNA was performed using the TriReagent (Sigma). 1 µg of total RNA was retrotranscribed with the High Capacity cDNA RT Kit (Applied Biosystem, Thermo Fisher Scientific). For quantitative PCR, cDNA was amplified with the TaqMan Gene Expression assay in a 7500 Fast Real-Time PCR System thermocycler (Applied Biosystems, Thermo Fisher Scientific). Commercially available probes were used to amplify *KCNQ1*, *KCNQ2*, *KCNQ3*, *KCNQ4*, and *KCNQ5* mRNAs (Applied Biosystem TaqMan

gene expression, codes *KCNQ1*: hs00923522_m1; *KCNQ2*: hs01548339_m1; *KCNQ3*: hs01120412_m1; *KCNQ4*: hs00542548_m1; *KCNQ5*: hs01068536_m1). The comparative $\Delta\Delta CT$ method was used to quantify transcript abundance using the ubiquitin-conjugating enzyme (UBC; hs05002522_g1) gene as control.²⁹ Three separate experiments, each in triplicate, were performed for each probe.

2.7 | Immunofluorescence

Cells were fixed with 4% paraformaldehyde in PBS for 10 minutes at room temperature (RT). After permeabilization with 0.1% Tween-20 for 5 minutes and blocking with 0.5% BSA for 1 hour at RT, cells were incubated overnight at 4°C with the N-KCNQ3 antibody (1:300), followed by a 1 hour incubation with donkey anti-rabbit Cy3-conjugated secondary antibody (Applied Biosystems, Thermo Fisher Scientific) at RT. Nuclei were visualized using Hoechst 33258 (1:5000) in PBS. Coverslips were mounted in Fluoromount G (eBioscience, Hatfield, Hertfordshire, UK); images were acquired with a Zeiss inverted LSM 700 confocal laser scanning microscope (Carl Zeiss) and analyzed with ImageJ (NIH). Slides in which the primary antibody was omitted were used as controls in all experiments.

2.8 | Whole-cell electrophysiology

Macroscopic current recordings from transiently transfected CHO cells, as well as data processing and analysis, were performed as described.^{27,28} Currents from CHO cells were recorded at room temperature with the whole-cell configuration of the patch-clamp technique, using glass micropipettes of 3–5 M Ω resistance. The extracellular solution contained (in mmol/L) the following: 138 NaCl, 5.4 KCl, 2 CaCl₂, 1 MgCl₂, 10 glucose,

and 10 HEPES, pH 7.4 with NaOH. The pipette (intracellular) solution contained (in mmol/L) the following: 140 KCl, 2 MgCl₂, 10 EGTA, 10 HEPES, and 5 Mg-ATP, pH 7.3–7.4 with KOH. The pCLAMP software (version 10.0.2) was used for data acquisition and analysis. Linear cell capacitance (C) and series-resistance (RS) calculation were performed as described previously.³⁰ In the experiments with tetraethylammonium, currents were activated by 3-second voltage ramps from –80 mV to +40 mV at 0.08 Hz frequency. Fast solution exchanges (<1 second) were achieved by means of a cFlow 8 flow controller attached to a cF-8VS eight-valve switching apparatus (Cell MicroControls).

2.9 | Statistics

Data are expressed as the mean \pm SEM. Data reported in Table 1 are average values of at least 9 individual measurements, recorded in at least 3 separate experimental sessions (transfections). Statistically significant differences between the data were evaluated with Student's *t* test (*P* < .05).

3 | RESULTS

3.1 | Clinical features

The proband (individual II-3; Figure 1A) is a French 9-year-old female originary from Morocco born to consanguineous healthy parents after an uneventful pregnancy and delivery, apart from a transient prematurity risk at 35 weeks. She was delivered at term (38 weeks 4 days), and birth parameters were normal: 3040 g weight, 46.5 cm length, and 34 cm occipito-frontal head circumference (OCF). At the age of 2 days, she presented with both focal (affecting either the left or right hemi-body) and generalized convulsions associated with

TABLE 1 Biophysical and pharmacological properties of currents recorded in CHO cells transfected with the indicated plasmid combinations

	cDNA transfected (μ g)	n	$V_{1/2}$ (mV)	K (mV/efold)	Current density (pA/pF at 0 mV)	Blockade by 3 mmol/L TEA (%)
Nontransfected	-	10	-	-	0.5 \pm 0.1	-
<i>KCNQ3</i>	3	9	-41.9 \pm 1.5***	8.2 \pm 0.9***	11.5 \pm 4.8***	8.0 \pm 2.1***
<i>KCNQ3</i> p.(Phe534Ilefs*15)	3	9	-	-	0.3 \pm 0.1	-
<i>KCNQ2</i> + pcDNA3	1.5 + 1.5	11	-21.7 \pm 1.9	13.2 \pm 0.8	21.7 \pm 5.1*	-
<i>KCNQ2</i>	3	13	-23.0 \pm 1.5	12.0 \pm 0.5	42.2 \pm 9.7	94.0 \pm 1.0**
<i>KCNQ2</i> + <i>KCNQ3</i>	1.5 + 1.5	23	-35.1 \pm 1.6	13.0 \pm 0.7	117.6 \pm 15.1	56.1 \pm 6.6
<i>KCNQ2</i> + <i>KCNQ3</i> p.(Phe534Ilefs*15)	1.5 + 1.5	20	-23.9 \pm 1.9**	15.4 \pm 1.5	17.5 \pm 2.5**	90.0 \pm 1.5**
<i>KCNQ2</i> + <i>KCNQ3</i> + pcDNA3	1.5 + 0.75 + 0.75	13	-27.5 \pm 1.0**	13.0 \pm 0.7	33.6 \pm 6.9**	62.0 \pm 4.3*
<i>KCNQ2</i> + <i>KCNQ3</i> + <i>KCNQ3</i> p.(Phe534Ilefs*15)	1.5 + 0.75 + 0.75	24	-29.5 \pm 1.8**	12.8 \pm 0.7	39.6 \pm 6.1**	62.2 \pm 3.2*

**P* < 0.05 vs *KCNQ2* (3 μ g).

***P* < 0.05 vs *KCNQ2* + *KCNQ3* (1.5 + 1.5 μ g).

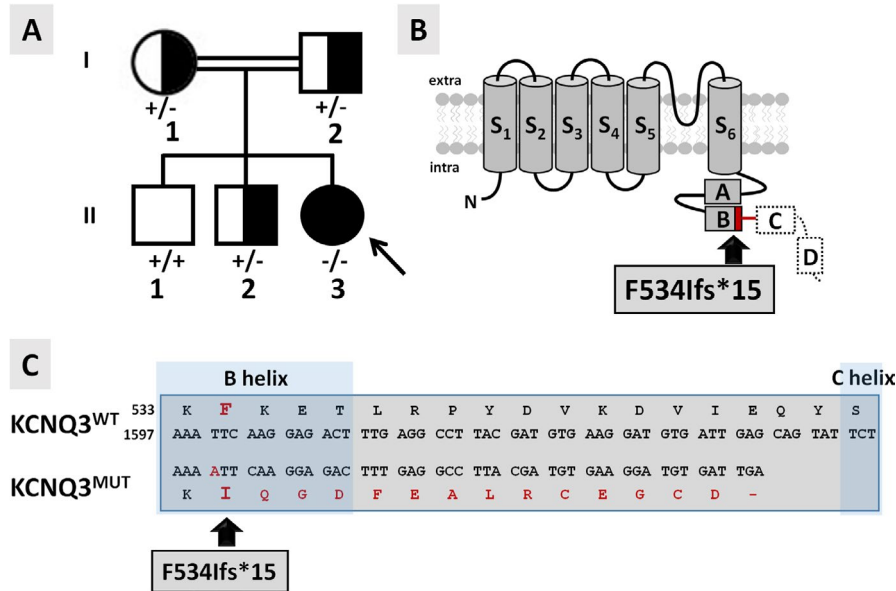


FIGURE 1 Pedigree of the investigated family and topological models of the mutant KCNQ3 subunit. A, Pedigree of the family investigated. ‘+’ indicates the wild-type *KCNQ3* allele; ‘-’ indicates the mutant *KCNQ3* p.(Phe534Iifs*15) allele. The arrow indicates the proband. B, Schematic topology of a KCNQ3 subunit: S₁-S₆ refer to the six transmembrane segments, while boxes labeled from A to D depict the four α -helical regions in the intracellular C-terminus. The p.(Phe534Iifs*15) variant located in the helix B is indicated by the arrow. The aa sequence deleted in the mutant KCNQ3 protein is indicated by a dashed line. The red line indicates the amino acid sequence altered by the frameshift variant. C, Partial alignments of the primary sequences of KCNQ3 and KCNQ3 p.(Phe534Iifs*15, indicated as KCNQ3^{MUT}) subunits. The B and C helices are highlighted with darker blue boxes.

hypotonia, cyanosis, and clonic movements of the four limbs. Biochemical and metabolic screening was noncontributive. Initial neurological examination and tonus were normal. The first electroencephalograms (EEGs), performed in the following days, revealed electrical seizures characterized by central and temporal slow waves prevailing on the right side not always associated with clinical manifestations. Biotin, pyridoxine, and folic acid were ineffective. At the age of 2 months, convulsions were controlled with phenytoin and vigabatrin; ocular contact was poor; and the tonus was insufficient. At 7 months of age, sodium valproate monotherapy was effective in controlling seizures; a marked strabismus was noted requiring specialized management including botulinum toxin injection. Interruption of sodium valproate treatment at the age of 3-4 years resulted in seizure recurrence during late night, including febrile episodes, with left hemispheric spikes and waves recorded on the EEG; valproate therapy was therefore reintroduced. Since then, she exhibited rare tonic-clonic seizures, and all subsequent EEG recordings were normal, the last one at age 6 years. She is currently treated with sodium valproate with good response, and her epilepsy shows the characteristics of a pharmacodependent epilepsy.³¹ Brain MRI performed at day 15 revealed a suspected mild cortical dysplasia of the right frontal and temporal lobes, but a further MRI at age 6 years and 5 months was normal, as well as a brain CT scan. The proband acquired head control

at age 6-7 months, could sit unsupported at age 12 months, and walked independently around age 30-36 months. At age 3 years, she could speak 2 words and required speech therapy, including Makaton technique while verbal language was insufficient; she attended specialized educational institution at age 5 years and started to produce short rudimentary word associations since age 6 years, with about 10 words in her vocabulary; sentences were still incompletely produced at age 8 years. At age 6.5 years, her psychomotor development was estimated around 22 months. She did not exhibit behavioral disturbances. At last examination (age 9 years), no abnormal morphological features were noted and neurological examination was normal apart from divergent strabismus increased in superior gaze. She has a moderate intellectual disability with poor vocabulary and little autonomy in daily life; she still attends a medical institute with little schooling abilities. Growth charts showed regular evolution of length, weight, and OFC between median and -1 SD. Familial history revealed that a maternal uncle who had mild cognitive disabilities with some degree of learning (reading and writing) difficulties also suffered from transient neonatal seizures, requiring a specialized pediatric follow-up in the first 6 months of life. However, he has a milder phenotype than his niece as he could achieve a relatively good autonomy in daily life. All other members of the family had normal psychomotor and cognitive development with no history of seizures.

3.2 | Genetic data

Array-CGH, *KCNQ2*-targeted sequencing, and gene panel sequencing in the proband (individual II-3) were normal; exome sequencing was therefore performed. The analysis on OMIM morbid genes responsible for mental retardation associated or not with epileptic encephalopathy highlighted the presence of two rare heterozygous variants, one in *HERC2*, associated with an autosomal recessive form of mental retardation (MIM 615516), and one in *FRAS1*, associated with autosomal recessive Fraser syndrome 1 (MIM 219000). Both variants were not retained as causative because the mode of inheritance was not compatible with the genotype of our patient. A variant of *DYNC1H1*, gene associated with Mental Retardation autosomal dominant 13 (MIM 614563), was not retained as causal as this variant has been reported 77 times in the healthy population (gnomAD 2.1.1). No further variants were retained using a sporadic mode of inheritance. The homozygosity analysis obtained through HomozygosityMapper³² using default parameters revealed relatively small regions of homozygosity in chr1, chr9, chr10, chr14, chr16, and chr22 compatible with the consanguinity between the parents (the 2 grandmothers of the proband are sisters, see expanded pedigree shown as Figure S1). Within these regions, we identified a rare variant of the *DMBT1* gene at the homozygous state, not retained as causal because it was found at the homozygous state in 7 individuals in the healthy population. Outside the regions of homozygosity, the analysis on OMIM morbid genes at the recessive state retained an homozygous variant of the *KCNQ3* gene absent from public databases as the only candidate compatible with the clinical presentation of the proband. This variant (ClinVar submission number SUB5837801) is a homozygous single-base duplication (chr8:g133150233dup in GRCh37, NM_004519.3:c.1599dup) in exon 12 (135/138 reads detected the variant) which results in a shift in the open reading frame p.(Phe534Ilefs*15) and the occurrence of a premature termination codon (PTC) at position 549, possibly leading to the synthesis of a truncated protein deleted of a large part of the C-terminal region (Figure 1B,C). The parents and one of the brothers (individuals I-1, I-2, and II-2, respectively) were heterozygous carriers for the *KCNQ3* variant; the eldest brother (individual II-1) carried two copies of the wild-type allele (Figure 1A); and the maternal uncle was unavailable for genetic analysis.

3.3 | The *KCNQ3* mutant allele is expressed at lower levels when compared to healthy control

Premature termination codons often result in mRNA instability and precocious degradation by nonsense-mediated

mRNA decay (NMD).²⁵ *KCNQ3* expression was previously reported in human fibroblasts³³; therefore, the effect of the NM_004519.3:c.1599dup variant on *KCNQ3* transcript levels was evaluated in primary fibroblasts from the proband (II-3, carrying two copies of the mutant allele) and a control member of the family (II-1, carrying two copies of the wild-type allele), using qRT-PCR. In control cells, the Ct values for the different *KCNQ3* transcripts are the following: *KCNQ1*: 36; *KCNQ2*: 28; *KCNQ3*: 28; *KCNQ4*: 32; and *KCNQ5*: 31; all these values are considerably higher than that of UBC, the housekeeping gene used as comparator (Ct value of 25), consistent with the described low expression levels for these transcripts.³³

As shown in Figure 2A, in cells from the proband, *KCNQ3* transcript levels were reduced to ~22% when compared to those in control cells; a quantitatively similar decrease in transcript levels was also observed for *KCNQ4*, whereas those for *KCNQ2* were markedly increased. No significant difference was instead observed when comparing *KCNQ1* and *KCNQ5* transcript abundance between proband and control primary fibroblasts.

To investigate whether such decrease in *KCNQ3* mRNA levels also led to changes in *KCNQ3* protein expression, immunofluorescence experiments using N-*KCNQ3* primary antibodies were performed in primary fibroblasts from the proband and the noncarrier, unaffected brother. These antibodies were validated in Western blots on lysates from CHO cells transiently transfected with wild-type *KCNQ3* or *KCNQ3* p.(Phe534Ilefs*15)-encoding plasmids (*KCNQ3*^{MUT}; Figure 2B, left panel). In these experimental groups, N-*KCNQ3* antibodies specifically recognized a ~100 kDa or a ~60 kDa protein band, respectively. These values are consistent with the molecular masses expected for wild-type or mutant *KCNQ3* proteins, respectively. Western blot experiments also revealed that, in this heterologous cellular system, the mutant protein was expressed at lower levels when compared to the wild-type *KCNQ3* protein (Figure 2B, left panel). As expected, C-*KCNQ3* antibodies targeting a C-terminal epitope located downstream the predicted premature termination site introduced by the variant, while detecting the 100kDa band corresponding to the wild-type *KCNQ3* protein, failed to recognize any specific signal in cells transfected with the mutant plasmid (Figure 2B, right panel). Western blot experiments performed in primary fibroblasts from proband and control samples with both antibodies failed to detect specific signals corresponding to either wild-type or mutant *KCNQ3* proteins, possibly because of the low abundance of the endogenous protein in these cells (data not shown). Immunocytochemistry experiments using N-*KCNQ3* antibodies performed in primary fibroblasts from the proband (individual II-3) and the wild-type brother (individual II-1) (Figure 2C, right and left panels, respectively) revealed a

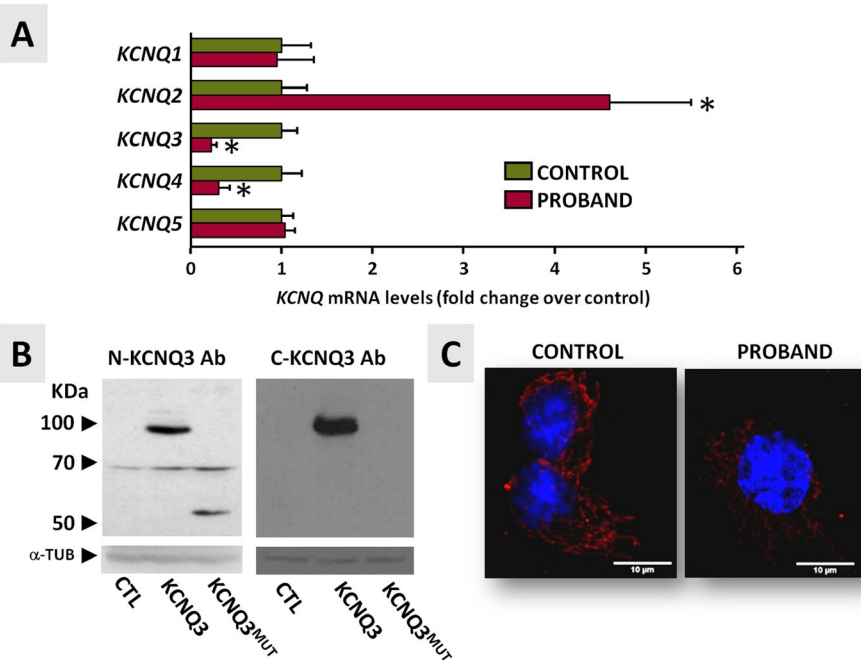


FIGURE 2 KCNQ transcript and protein expression profile in primary fibroblasts from the proband (individual II-3) and healthy brother (individual II-1). **A**, *KCNQ1-5* qRT-PCR data from primary fibroblasts. Data are expressed as cycle threshold values for each *KCNQ* transcript normalized to that of *UBC*; after normalization, data from control fibroblasts were expressed as one (green bars), and data from proband fibroblasts were expressed relative to controls (red bars). Asterisks indicate values statistically different ($P < 0.05$) from respective controls. **B**, Western blot performed on protein lysates from transiently transfected CHO cells using N- and C-KCNQ3 antibodies. CHO cells were transfected with wild-type (*KCNQ3*) or mutant (*KCNQ3^{MUT}*) *KCNQ3* cDNA, and total lysates were analyzed with N-KCNQ3 (left panel) or C-KCNQ3 (right panel) antibodies. α -tubulin (α -TUB) served as a loading control. **C**, Confocal images of fibroblasts from the proband (individual II-3) and the healthy brother (individual II-1) stained with N-KCNQ3 primary antibodies (in red) and a nuclear marker (Hoechst, in blue)

KCNQ3-specific signal in both groups, although the intensity was lower in the former when compared to the latter. Notably, in fibroblasts from both individuals, the immunofluorescent signal was mainly cytosolic, showing a subcellular distribution consistent with an endoplasmic reticulum localization.

3.4 | Functional and pharmacological characterization of homomeric and heteromeric channels carrying KCNQ3 p.(Phe534Ilefs*15) mutant subunits

Previously shown data obtained in primary fibroblasts from the proband suggest that the p.(Phe534Ilefs*15) truncating variant led to a significant decrease in *KCNQ3* transcript and protein levels, a result consistent with NMD.²⁵ However, transcript expression pattern in fibroblasts might not parallel that in neurons; moreover, a significant, although reduced in abundance, fraction of *KCNQ3* protein was still detected in fibroblasts. Therefore, electrophysiological recordings in transiently transfected CHO cells were carried out to evaluate the effects prompted by the p.(Phe534Ilefs*15) variant on *KCNQ3* channel function.

Heterologous expression of wild-type *KCNQ3* subunits led to the appearance of voltage-dependent K^+ -selective

currents characterized by a slow time course of activation and deactivation and a threshold for current activation around -50 mV.^{5,7} By contrast, no currents could be recorded in cells transfected with the *KCNQ3* p.(Phe534Ilefs*15) plasmid, consistent with the variant causing a complete loss-of-function (LoF) effect (Figure 3A and Table 1).

In adult neuronal cells, *KCNQ3* subunits assemble into heteromeric channels with *KCNQ2* to form I_{KM} .⁵ To investigate the functional consequences of mutant *KCNQ3* subunits when coexpressed with *KCNQ2* subunits, CHO cells were cotransfected with *KCNQ2* and *KCNQ3* cDNAs at a 1:1 ratio (to mimic the genetic balance of the noncarrier Individual II-1) or with *KCNQ2* and *KCNQ3* p.(Phe534Ilefs*15) at 1:1 ratio (to mimic the genetic balance of the proband, Individual II-3). Coexpression of wild-type *KCNQ3* subunits and *KCNQ2* subunits markedly increased current size when compared to *KCNQ2*- or *KCNQ3*-only expressing cells (Table 1); in addition, *KCNQ2/3* heteromeric channels display a significant leftward shift in the activation $V_{1/2}$ and a decrease in current sensitivity to blockade by TEA (Table 1).^{5,28,34} By contrast, coexpression of *KCNQ3* p.(Phe534Ilefs*15) with *KCNQ2* subunits failed to enhance current density and to modify the $V_{1/2}$ (Figure 3B and Table 1). Currents recorded in *KCNQ2* + *KCNQ3*

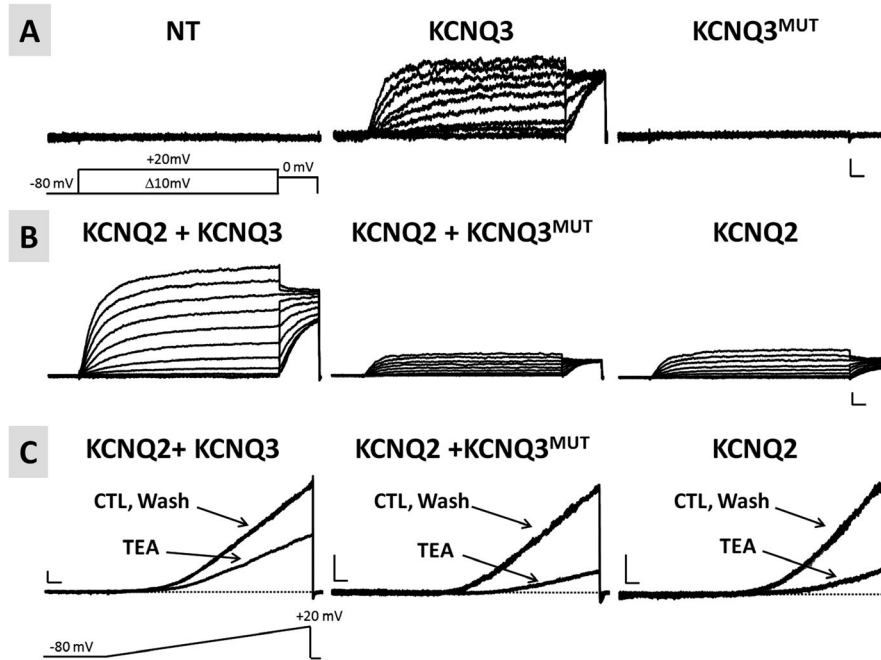


FIGURE 3 Functional characterization of homomeric or heteromeric channels incorporating KCNQ3 p.(Phe534Ilefs*15) subunits. A, Representative current traces from nontransfected cells (NT; left panel) or from cells transfected with either wild-type KCNQ3- (KCNQ3; middle panel) or KCNQ3 p.(Phe534Ilefs*15)-encoding plasmids (KCNQ3^{MUT}; right panel) in response to the voltage protocol shown. Horizontal scale bar: 100 ms; vertical scale bar: 2 pA/pF. B, Representative current traces recorded in cells expressing the indicated subunits, in response to the same voltage protocol shown in A. Horizontal scale bar: 100 ms; vertical scale bar: 20 pA/pF. C, Representative current traces from cells expressing the indicated subunits in response to the indicated voltage ramp protocol before TEA exposure (CTL, control), during TEA exposure (TEA, 3 mmol/L), and upon drug washout (Wash). Horizontal scale bar: 200 ms; vertical scale bar: 10 pA/pF

p.(Phe534Ilefs*15)-transfected cells displayed a sensitivity to blockade by 3 mmol/L TEA higher than that of KCNQ2/KCNQ3-transfected cells and identical to that of KCNQ2-only transfected cells (Figure 3C, Table 1). These results suggest that mutant KCNQ3 subunits fail to form functional heteromeric channels with KCNQ2 subunits.

To replicate in vitro genetic combination occurring in the family members who are heterozygous carriers of the mutant allele (Individuals I-1, I-2, and II-2), functional studies were also carried out upon transfection of KCNQ2, KCNQ3, and KCNQ3 p.(Phe534Ilefs*15) plasmids in a 1:0.5:0.5 cDNA ratio; for these experiments, cells transfected with an identical (1:0.5:0.5) cDNA ratio of KCNQ2 + KCNQ3+pcDNA plasmids served as controls. The results obtained suggest that the presence of an halved dose of functional/wild-type KCNQ3 allele is sufficient to generate currents displaying the biophysical and pharmacological properties of KCNQ2/KCNQ3 heteromers, although with a reduced density when compared to that recorded in cells transfected with a full dose of KCNQ3 (1:1 KCNQ2:KCNQ3 cDNA ratio). Notably, the pharmacological and functional properties of the currents recorded in cell transfected with KCNQ2, KCNQ3, and KCNQ3 p.(Phe534Ilefs*15) plasmids (1:0.5:0.5 cDNA ratio) were identical to KCNQ2 + KCNQ3+pcDNA-expressing cells (1:0.5:0.5 cDNA ratio) (Table 1).

4 | DISCUSSION

4.1 | Epilepsy and ID caused by a novel homozygous KCNQ3 frameshift variant: clinical and ex vivo results

We herein report the clinical, ex vivo, and in vitro results from a family carrying the novel frameshift p.(Phe534Ilefs*15) variant in *KCNQ3* (NM_004519.3:c.1599dup). The proband is a 9-year-old girl diagnosed with neonatal-onset and pharmacosensitive seizures and non-syndromic ID; she was found to be a homozygous carrier for this variant. While our study was in progress, another family with three siblings affected with neonatal-onset seizures (reported as pharmacosensitive in one of them) and ID of variable severity due to a different homozygous frameshift variant in *KCNQ3* (c.1220_1221delCT; p.(Ser407Phefs*27)) has been described in a large cohort of children suffering from epileptic encephalopathy.²⁴ In this family, where no functional analyses were performed, neonatal seizures or neurodevelopmental problems did not occur in consanguineous parents or extended family members who were heterozygous carriers for the *KCNQ3* mutant allele. One of the affected sibling in Kothur et al.²⁴ exhibited severe developmental delay, while the two others presented with mild ID; since genetic analysis was only limited to a

restricted epileptic encephalopathy gene panel, it is unknown whether additional genetic defects, potentially enabled by consanguinity, could account for the more severe phenotype in this particular sibling.

PTC-containing mRNAs often undergo NMD when the PTC is located upstream the ~50-55th nucleotide before the last exon-intron junction,³⁵ as it occurs with the presently described variant. NMD represents a quality control mechanism to avoid production of truncated proteins with potentially deleterious effects.^{25,36} *KCNQ3* transcript levels in primary fibroblasts³³ from the proband were markedly decreased when compared to those from the unaffected noncarrier brother II-1, a result consistent with NMD; the reduction in *KCNQ3* mutant transcript levels was accompanied by an increase in *KCNQ2*, a reduction of *KCNQ4*, and no change in *KCNQ1* or *KCNQ5* transcript levels. It remains to be determined whether these changes are due to compensatory effects or uncover a more complex coordination of gene expression. In this regard, whether the transcriptional repressor RE1 silencing transcription factor (REST), which has been shown to regulate *KCNQ2* and *KCNQ3*³⁷ as well as *KCNQ4*³⁸ expression, participates in this coordination is currently unknown; moreover, it should be highlighted that conditional and selective ablation of *Kcnq2* or *Kcnq3* in cortical mouse tissue also modifies the expression of other members of the *Kcnq* subfamily.³⁹ Notably, immunofluorescence experiments also revealed a reduced intensity of the *KCNQ3* signal in primary fibroblasts from the proband; in these experiments, the *KCNQ3* signal showed a diffuse cytoplasmic staining consistent with endoplasmic reticulum-Golgi localization with no remarkable difference in subcellular localization between fibroblasts from the proband or the control brother. A diffuse staining pattern on both cell surface and intracellular components was also detected for *KCNQ3* in rat⁴⁰ and human⁴¹ hippocampal and cortical pyramidal neurons.

4.2 | Functional consequences of the *KCNQ3* p.(Phe534Ilefs*15) variant

Our results indicate that transcript and protein levels encoded by the mutant *KCNQ3* allele are detectable, prompting investigation of the functional consequences of the p.(Phe534Ilefs*15) variant on *KCNQ3* subunit function. The results obtained clearly suggest the *KCNQ3* p.(Phe534Ilefs*15) protein is fully nonfunctional; indeed, homomeric expression of mutant subunits failed to generate detectable voltage-gated K⁺ currents. Moreover, mutant *KCNQ3* subunits did not incorporate into functional heteromeric channels when coexpressed with *KCNQ2* subunits, a result consistent with the variant-induced deletion of a significant portion of the long C-terminus where critical domains responsible for homomeric and heteromeric subunit assembly and plasmemembrane trafficking have been

identified.^{4,42,43} Furthermore, the presence of an halved dose of wild-type *KCNQ3* protein, an experimental condition mimicking in vitro the genetic combination of the family members who are heterozygous carriers of the mutant *KCNQ3* allele, was sufficient to generate currents displaying the biophysical and pharmacological properties of *KCNQ2/Q3* heteromers, although with a reduced density when compared to that recorded in cells transfected with a full dose of *KCNQ3*. Currents recorded in cells transfected with *KCNQ2*, *KCNQ3*, and mutant *KCNQ3* cDNAs were identical to those in cells transfected with the same cDNA amount of *KCNQ2* and *KCNQ3* cDNAs only, arguing in favor of the inability of the protein encoded by the mutant allele to heteromerize and interfere with the function of wild-type subunits. This functional result strongly suggests that haploinsufficiency is the main molecular mechanism for the severe disease in the affected proband; this is in sharp contrast to *KCNQ2*-related EOEE pathogenesis, where mutant subunits carrying heterozygous missense variants are functional and heteromerize with wild-type subunits, thereby poisoning channel function by a dominant-negative mechanism.^{27,44} Additional pathogenic mechanisms for *KCNQ2* EOEE include changes in subcellular localization,⁴⁵ and/or in calmodulin-^{46,47} or phosphatidylinositol 4,5-bisphosphate⁴⁸-dependent regulation.

4.3 | Clinical spectrum and genetic mechanisms of *KCNQ3*-related diseases

Heterozygous pathogenic variants in *KCNQ3* have been associated with neonatal-onset epilepsies showing broad clinical heterogeneity and diverse genetic transmission mechanisms.¹⁶ These range from relatively benign familial phenotypes with seizures starting in the neonatal (BFNS)^{6,12,13} or early-infantile (BFIS)^{14,15} period, to sporadic cases with severe clinical presentations characterized by developmental disabilities with or without refractory seizures^{17,19,21,22,49} or by cortical visual impairment.²³

Notably, in both familial and sporadic cases, *KCNQ3* pathogenic variants are all single missense variants, either with autosomal dominant inheritance or arising de novo, respectively (34/34; www.rikee.org).¹¹ A notable exception is a recently described EOEE patient who carries two missense variants in compound heterozygosity, each inherited from an asymptomatic parent.²⁰ Interestingly, no heterozygous pathogenic frameshift *KCNQ3* variant has ever been associated with a human phenotype, whereas haploinsufficiency due to heterozygous frameshift variants in *KCNQ2* is a frequent cause of BFNS,^{16,50} indeed, frameshift/deletion variants account for 36% (39/108) of BFNS-causing variants in the *KCNQ2* gene^{11,13,51,52} (www.rikee.org). Notably, in both families where *KCNQ3* homozygous frameshift variants were identified, that is, the presently described family and the one reported by Kothur et al.²⁴, heterozygous carriers of the

KCNQ3 frameshift variant are unaffected, with no seizures or psychomotor/cognitive impairment. Instead, no homozygous frameshift variant in *KCNQ2* has ever been described in humans, as minimal *KCNQ2* residual activity is probably essential under penalty of potential lethality. Although several potential mechanisms may account for the more severe clinical consequences associated with *KCNQ2* variants when compared to *KCNQ3* ones, the fact that, in both rodents and human brains,^{53,54} the ratio of *KCNQ3* to *KCNQ2* expression is low at birth and increases during postnatal development provides a plausible explanation; notably, deletion of *Kcnq2*, but not of *Kcnq3*, from cortical pyramidal neurons in mice is sufficient for the development of aberrant EEG activity and leads to death by the third week of life.³⁹

Noteworthy, about 10 nonsense or frameshift variants leading to *KCNQ3* truncation spread throughout the gene are reported in public databases such as ClinVar⁵⁵ or gnomAD.⁵⁶ Among these variants, only one, found in an individual in the gnomAD's non-neuro-samples from individuals who were not ascertained for having a neurological condition in a neurological case/control study, was interpreted as pathogenic (although the phenotype is unknown), while the others were associated with an uncertain clinical significance.

5 | CONCLUSIONS

This is the first study exploring the functional consequences of a novel *KCNQ3* homozygous LoF variant responsible for a severe phenotype characterized by neonatal-onset pharmacodependent seizures, with developmental delay and ID. Ex vivo and in vitro experiments revealed a decrease in transcript abundance proportional to variant expression levels and an impaired ability of mutant subunits to assemble into functional homomeric or heteromeric channels with *KCNQ2*. A lesser degree of channel dysfunction occurs when a single copy of the mutant allele is present, a result possibly contributing to the lack of neurodevelopmental phenotype in heterozygous carriers. The described LoF mechanism allows to hypothesize that, in close analogy to LoF variants found in *KCNQ2*-EOEE-affected patients,^{50,57} *KCNQ* activators such as retigabine may be useful precision medicines to counteract the channel dysfunction triggered by the herein described novel *KCNQ3* variant as well as similar variants that may be identified in the future.

ACKNOWLEDGMENTS

We are deeply indebted to: Dr. Thomas J. Jentsch, Department of Physiology and Pathology of Ion Transport, Leibniz-Institut für Molekulare Pharmakologie (FMP),

Berlin (Germany) for sharing *KCNQ2* and *KCNQ3* cDNAs. The present work was also supported by the following projects: the Telethon Foundation (grant number GGP15113) and the Italian Ministry for University and Research (MIUR) (PRIN 2017ALCR7C) to MT; MIUR (Scientific Independence of Researchers Project 2014 RBSI1444EM and PRIN 2017YH3SXX), PRIN (2017YH3SXX), and the University of Naples "Federico II" and Compagnia di San Paolo within the STAR Program "Sostegno Territoriale alle Attività di Ricerca" (project number 6-CSP-UNINA-120) to FM; and the Italian Ministry of Health (Project GR-2016-02363337) and MIUR (PRIN 2017ALCR7C) to MVS. We thank the family members who participated to the study.

CONFLICT OF INTEREST

The authors declare no competing financial interests. The Authors confirm that they have read the Journal's position on issues involved in ethical publication and affirm that this report is consistent with those guidelines.

ORCID

Sebastien Moutton  <https://orcid.org/0000-0002-8942-6731>

Maurizio Tagliatela  <https://orcid.org/0000-0002-8202-0560>

REFERENCES

1. Moller RS, Dahl HA, Helbig I. The contribution of next generation sequencing to epilepsy genetics. *Expert Rev Mol Diagn.* 2015;15:1531–8.
2. Demarest ST, Brooks-Kayal A. From molecules to medicines: the dawn of targeted therapies for genetic epilepsies. *Nat Rev Neurol.* 2018;14:735–45.
3. Jentsch TJ *KCNQ* potassium channels: physiology and role in disease. *Nat Rev Neurosci.* 2000;1:21–30.
4. Soldovieri MV, Miceli F, Tagliatela M. Driving with no brakes: molecular pathophysiology of Kv7 potassium channels. *Physiology (Bethesda).* 2011;26:365–76.
5. Wang HS, Pan Z, Shi W, Brown BS, Wymore RS, Cohen IS, et al. *KCNQ2* and *KCNQ3* potassium channel subunits: molecular correlates of the M-channel. *Science.* 1998;282:1890–3.
6. Singh NA, Westenskow P, Charlier C, Pappas C, Leslie J, Dillon J, et al. *KCNQ2* and *KCNQ3* potassium channel genes in benign familial neonatal convulsions: expansion of the functional and mutation spectrum. *Brain.* 2003;126:2726–37.
7. Soldovieri MV, Castaldo P, Iodice L, Miceli F, Barrese V, Bellini G, et al. Decreased subunit stability as a novel mechanism for potassium current impairment by a *KCNQ2* C terminus mutation causing benign familial neonatal convulsions. *J Biol Chem.* 2006;281:418–28.
8. Weckhuysen S, Ivanovic V, Hendrickx R, VanCoster R, Hjalgrim H, Møller RS, et al. Extending the *KCNQ2* encephalopathy spectrum: clinical and neuroimaging findings in 17 patients. *Neurology.* 2013;81(19):1697–703.

9. Millichap JJ, Miceli F, De Maria M, Keator C, Joshi N, Tran B, et al. Infantile spasms and encephalopathy without preceding neonatal seizures caused by KCNQ2 R198Q, a gain-of-function variant. *Epilepsia*. 2017;58:e10–e15.
10. Weckhuysen S, Mandelstam S, Suls A, Audenaert D, Deconinck T, Claes L, et al. KCNQ2 encephalopathy: emerging phenotype of a neonatal epileptic encephalopathy. *Ann Neurol*. 2012;71:15–25.
11. Joshi N, Tagliatalata M, Weckhuysen S, Nesbitt G, Cooper EC. An informatics infrastructure for KCNQ2 encephalopathy research including a patient registry, database, curation platform, and website. Annual Meeting of the American Epilepsy Society. 2016;Abstract:3.329.
12. Charlier C, Singh NA, Ryan SG, Lewis TB, Reus BE, Leach RJ, et al. A pore mutation in a novel KQT-like potassium channel gene in an idiopathic epilepsy family. *Nat Genet*. 1998;18:53–5.
13. Soldovieri MV, Boutry-Kryza N, Milh M, Doummar D, Heron B, Bourel E, et al. Novel KCNQ2 and KCNQ3 mutations in a large cohort of families with benign neonatal epilepsy: first evidence for an altered channel regulation by syntaxin-1A. *Hum Mutat*. 2014;35:356–67.
14. Heron SE, Ong YS, Yendle SC, McMahon JM, Berkovic SF, Scheffer IE, et al. Mutations in PRR2 are not a common cause of infantile epileptic encephalopathies. *Epilepsia*. 2013;54:e86–e89.
15. Zara F, Specchio N, Striano P, Robbiano A, Gennaro E, Paravidino R, et al. Genetic testing in benign familial epilepsies of the first year of life: clinical and diagnostic significance. *Epilepsia*. 2013;54:425–36.
16. Miceli F, Soldovieri MV, Joshi N, Weckhuysen S, Cooper EC, Tagliatalata M. KCNQ3-related disorders. In: Pagon RA, Adam MP, Ardinger HH, Wallace SE, Amemiya A, Bean L, Bird TD, Ledbetter N, Mefford HC, Smith R, Stephens K, editors. *GeneReviews®* [Internet], Seattle (WA): University of Washington, Seattle, 2017.
17. Allen AS, Berkovic SF, Cossette P, Delanty N, Dlugos D, Eichler EE, et al. De novo mutations in epileptic encephalopathies. *Nature*. 2013;501:217–21.
18. Miceli F, Striano P, Soldovieri MV, Fontana A, Nardello R, Robbiano A, et al. A novel KCNQ3 mutation in familial epilepsy with focal seizures and intellectual disability. *Epilepsia*. 2015;56:e15–e20.
19. Grozeva D, Carss K, Spasic-Boskovic O, Tejada M-I, Gecz J, Shaw M, et al. Targeted next-generation sequencing analysis of 1,000 individuals with intellectual disability. *Hum Mutat*. 2015;36:1197–204.
20. Ambrosino P, Freri E, Castellotti B, Soldovieri MV, Mosca I, Manocchio L, et al. Compound heterozygous variants in early onset encephalopathy reveal additive contribution of C-terminal residues to PIP2-dependent K⁺ channel gating. *Mol Neurobiol*. 2018;55:7009–24.
21. Rauch A, Wiczorek D, Graf E, Wieland T, Ende S, Schwarzmayr T, et al. Range of genetic mutations associated with severe non-syndromic sporadic intellectual disability: an exome sequencing study. *Lancet*. 2012;380:1674–82.
22. McRae JF, Clayton S, Fitzgerald TW, Kaplanis J, Prigmore E, Rajan D, et al. Prevalence and architecture of de novo mutations in developmental disorders. *Nature*. 2017;542:433–8.
23. Bosch D, Boonstra FN, de Leeuw N, Pfundt R, Nillesen WM, de Ligt J, et al. Novel genetic causes for cerebral visual impairment. *Eur J Hum Genet*. 2016;24:660–5.
24. Kothur K, Holman K, Farnsworth E, Ho G, Lorentzos M, Troedson C, et al. Diagnostic yield of targeted massively parallel sequencing in children with epileptic encephalopathy. *Seizure*. 2018;59:132–40.
25. Lykke-Andersen S, Jensen TH. Nonsense-mediated mRNA decay: an intricate machinery that shapes transcriptomes. *Nat Rev Mol Cell Biol*. 2015;16:665–77.
26. Thevenon J, Duffourd Y, Masurel-Paulet A, Lefebvre M, Feillet F, El Chehadeh-Djebbar S, et al. Diagnostic odyssey in severe neurodevelopmental disorders: toward clinical whole-exome sequencing as a first-line diagnostic test. *Clin Genet*. 2016;89:700–7.
27. Miceli F, Soldovieri MV, Ambrosino P, Barrese V, Migliore M, Cilio MR, et al. Genotype-phenotype correlations in neonatal epilepsies caused by mutations in the voltage sensor of K(v)7.2 potassium channel subunits. *Proc Natl Acad Sci USA*. 2013;110:4386–91.
28. Miceli F, Soldovieri MV, Ambrosino P, De Maria M, Migliore M, Migliore R, et al. Early-onset epileptic encephalopathy caused by gain-of-function mutations in the voltage sensor of Kv7.2 and Kv7.3 potassium channel subunits. *J Neurosci*. 2015;35:3782–93.
29. Lanzafame M, Botta E, Teson M, Fortugno P, Zambruno G, Stefanini M, et al. Reference genes for gene expression analysis in proliferating and differentiating human keratinocytes. *Exp Dermatol*. 2015;24:314–6.
30. Soldovieri MV, Cilio MR, Miceli F, Bellini G, Miraglia del Giudice E, Castaldo P, et al. Atypical gating of M-type potassium channels conferred by mutations in uncharged residues in the S4 region of KCNQ2 causing benign familial neonatal convulsions. *J Neurosci*. 2007;27:4919–28.
31. Rosati A, De Masi S, Guerrini R. Antiepileptic drug treatment in children with epilepsy. *CNS Drugs*. 2015;29:847–63.
32. Seelow D, Schuelke M, Hildebrandt F, Nürnberg P. HomozygosityMapper—an interactive approach to homozygosity mapping. *Nucleic Acids Res*. 2009;37:W593–599.
33. Poulet C, Künzel S, Büttner E, Lindner D, Westermann D, Ravens U. Altered physiological functions and ion currents in atrial fibroblasts from patients with chronic atrial fibrillation. *Physiol Rep*. 2016;4.pii:e12681.
34. Hadley JK, Noda M, Selyanko AA, Wood IC, Abogadie FC, Brown DA. Differential tetraethylammonium sensitivity of KCNQ1–4 potassium channels. *Br J Pharmacol*. 2000;129:413–5.
35. Hwang J, Sato H, Tang Y, Matsuda D, Maquat LE. UPF1 association with the cap-binding protein, CBP80, promotes nonsense mediated mRNA decay at two distinct steps. *Mol Cell*. 2010;39:396–409.
36. Hug N, Longman D, Cáceres JF. Mechanism and regulation of the nonsense-mediated decay pathway. *Nucleic Acids Res*. 2016;44:1483–95.
37. Mucha M, Ooi L, Linley JE, Mordaka P, Dalle C, Robertson B, et al. Transcriptional control of KCNQ channel genes and the regulation of neuronal excitability. *J Neurosci*. 2010;30:13235–45.
38. Iannotti FA, Barrese V, Formisano L, Miceli F, Tagliatalata M. Specification of skeletal muscle differentiation by repressor element-1 silencing transcription factor (REST)-regulated Kv7.4 potassium channels. *Mol Biol Cell*. 2013;24:274–84.
39. Soh H, Pant R, LoTurco JJ, Tzingounis AV. Conditional deletions of epilepsy-associated KCNQ2 and KCNQ3 channels from cerebral cortex cause differential effects on neuronal excitability. *J Neurosci*. 2014;34:5311–21.
40. Shah MM, Mistry M, Marsh SJ, Brown DA, Delmas P. Molecular correlates of the M-current in cultured rat hippocampal neurons. *J Physiol*. 2002;544:29–37.

41. Cooper EC, Aldape KD, Abosch A, Barbaro NM, Berger MS, Peacock WS, et al. Colocalization and coassembly of two human brain M-type potassium channel subunits that are mutated in epilepsy. *Proc Natl Acad Sci USA*. 2000;97:4914–9.
42. Haitin Y, Attali B. The C-terminus of Kv7 channels: a multifunctional module. *J. Physiol*. 2008;586:1803–10.
43. Choveau FS, Zhang J, Bierbower SM, Sharma R, Shapiro MS. The role of the carboxyl terminus helix C-D linker in regulating KCNQ3 K⁺ current amplitudes by controlling channel trafficking. *PLoS ONE*. 2015;10:e0145367.
44. Orhan G, Bock M, Schepers D, Ilina EI, Reichel SN, Löffler H, et al. Dominant-negative effects of KCNQ2 mutations are associated with epileptic encephalopathy. *Ann Neurol*. 2014;75:382–94.
45. Abidi A, Devaux JJ, Molinari F, Alcaraz G, Michon FX, Suter-Sardo J, et al. A recurrent KCNQ2 pore mutation causing early onset epileptic encephalopathy has a moderate effect on M current but alters subcellular localization of Kv7 channels. *Neurobiol Dis*. 2015;80:80–92.
46. Ambrosino P, Alaimo A, Bartollino S, Manocchio L, De Maria M, Mosca I, et al. Epilepsy-causing mutations in Kv7.2 C-terminus affect binding and functional modulation by calmodulin. *Biochim Biophys Acta*. 2015;1852:1856–66.
47. Kim EC, Zhang J, Pang W, Wang S, Lee KY, Cavaretta JP, et al. Reduced axonal surface expression and phosphoinositide sensitivity in K_v7 channels disrupts their function to inhibit neuronal excitability in Kcnq2 epileptic encephalopathy. *Neurobiol Dis*. 2018;118:76–93.
48. Soldovieri MV, Ambrosino P, Mosca I, De Maria M, Moretto E, Miceli F, et al. Early-onset epileptic encephalopathy caused by a reduced sensitivity of Kv7.2 potassium channels to phosphatidylinositol 4,5-bisphosphate. *Sci Rep*. 2016;6:38167.
49. Sands TT, Miceli F, Lesca G, Beck AE, Sadleir LG, Arrington DK, et al. Autism and developmental disability caused by KCNQ3 gain-of-function variants. *Ann Neurol*. 2019;86:181–92.
50. Millichap JJ, Park KL, Tsuchida T, Ben-Zeev B, Carmant L, Flamini R, et al. (2016) KCNQ2 encephalopathy: features, mutational hot spots, and ezogabine treatment of 11 patients. *Neurol Genet*. 2016;2:e96.
51. Goldberg-Stern H, Kaufmann R, Kivity S, Afawi Z, Heron SE. Novel mutation in KCNQ2 causing benign familial neonatal seizures. *Pediatr Neurol*. 2009;41:367–70.
52. Grinton BE, Heron SE, Pelekanos JT, Zuberi SM, Kivity S, Afawi Z, et al. Familial neonatal seizures in 36 families: Clinical and genetic features correlate with outcome. *Epilepsia*. 2015;56:1071–80.
53. Hadley JK, Passmore GM, Tatulian L, Al-Qatari M, Ye F, Wickenden AD, et al. Stoichiometry of expressed KCNQ2/KCNQ3 potassium channels and subunit composition of native ganglionic M channels deduced from block by tetraethylammonium. *J Neurosci*. 2003;23:5012–9.
54. Kanaumi T, Takashima S, Iwasaki H, Itoh M, Mitsudome A, Hirose S. Developmental changes in KCNQ2 and KCNQ3 expression in human brain: possible contribution to the age-dependent etiology of benign familial neonatal convulsions. *Brain Dev*. 2008;30:362–9.
55. Landrum MJ, Lee JM, Benson M, Brown GR, Chao C, Chitipiralla S, et al. ClinVar: improving access to variant interpretations and supporting evidence. *Nucleic Acids Res*. 2018;46:D1062–D1067. (retrieved from <https://www.ncbi.nlm.nih.gov/clinvar/?term=KCNQ3%5Bgene%5D>).
56. Karczewski KJ, Francioli LC, Tiao G, Cummings BB, Alföldi J, Wang Q, et al. Variation across 141,456 human exomes and genomes reveals the spectrum of loss-of-function intolerance across human protein-coding genes. *bioRxiv* 531210; doi: <http://dx.doi.org/10.1101/531210>. (retrieved from <https://gnomad.broadinstitute.org/gene/ENSG00000184156>).
57. Weckhuysen S, Ivanovic V, Hendrickx R, Van Coster R, Hjalgrim H, Moller RS, et al. Extending the KCNQ2 encephalopathy spectrum: clinical and neuroimaging findings in 17 patients. *Neurology*. 2013;81:1697–703.

SUPPORTING INFORMATION

Additional supporting information may be found online in the Supporting Information section at the end of the article.

How to cite this article: Lauritano A, Moutton S, Longobardi E, et al. A novel homozygous KCNQ3 loss-of-function variant causes non-syndromic intellectual disability and neonatal-onset pharmacodependent epilepsy. *Epilepsia Open*. 2019;4:464–475. <https://doi.org/10.1002/epi4.12353>

Autism and Developmental Disability Caused by *KCNQ3* Gain-of-Function Variants

Tristan T. Sands, MD, PhD ^{1,2*} Francesco Miceli, PhD,^{3*} Gaetan Lesca, MD, PhD,^{4,5,6} Anita E. Beck, MD, PhD,^{7,8} Lynette G. Sadleir, MBChB, MD,⁹ Daniel K. Arrington, MD,¹⁰ Bitten Schönewolf-Greulich, MD,^{11,12} Sébastien Moutton, MD,¹³ Anna Lauritano, BS,³ Piera Nappi, BS,³ Maria Virginia Soldovieri, PhD,¹⁴ Ingrid E. Scheffer, MBBS, PhD,¹⁵ Heather C. Mefford, MD, PhD,⁷ Nicholas Stong, PhD,² Erin L. Heinzen, PhD ² David B. Goldstein, PhD,² Ana Grijalvo Perez, MD,¹⁶ Eric H. Kossoff, MD,¹⁷ Amber Stocco, MD,¹⁸ Jennifer A. Sullivan, MS, CGC,¹⁹ Vandana Shashi, MD,¹⁹ Benedicte Gerard, PharmD, PhD, CGC,²⁰ Christine Francannet, MD,²¹ Anne-Marie Bisgaard, MD, PhD,¹¹ Zeynep Tümer, MD, PhD, DMSc,^{12,22} Marjolaine Willems, MD,²³ François Rivier, MD, PhD,²⁴ Antonio Vitobello, PhD,²⁵ Kavita Thakkar, MD,²⁶ Deepa S. Rajan, MD,²⁶ A. James Barkovich, MD,²⁷ Sarah Weckhuysen, MD, PhD,^{28,29} Edward C. Cooper, MD, PhD,^{30*} Maurizio Tagliatela, MD, PhD,^{3*} and M. Roberta Cilio, MD, PhD^{16,31*}

View this article online at wileyonlinelibrary.com. DOI: 10.1002/ana.25522

Received Jan 20, 2019, and in revised form Jun 3, 2019. Accepted for publication Jun 6, 2019.

Address correspondence to Dr Cooper, Departments of Neurology, Neuroscience, and Molecular and Human Genetics, Baylor College of Medicine, Houston, TX, E-mail: ecc1@bcm.edu; Dr Tagliatela, Section of Pharmacology, Department of Neuroscience, University of Naples "Federico II," Naples, Italy, E-mail: mtagliat@unina.it; or Dr Cilio, Departments of Pediatrics and Institute of Experimental and Clinical Research, University of Louvain, Brussels, Belgium, E-mail: roberta.cilio@uclouvain.be

*T.T.S. and F.M. contributed equally. E.C.C., M.T., and M.R.C contributed equally.

From the ¹Department of Neurology, Columbia University Medical Center, New York, NY; ²Institute for Genomic Medicine, Columbia University Medical Center, New York, NY; ³Section of Pharmacology, Department of Neuroscience, University of Naples "Federico II," Naples, Italy; ⁴Department of Medical Genetics, Reference Center for Developmental Anomalies, Civil Hospices of Lyon, Lyon, France; ⁵French Institute of Health and Medical Research U1028, French National Center for Scientific Research UMR5292, Center for Research in Neuroscience in Lyon, Genetics of Neurodevelopment Team, Claude Bernard University Lyon 1, Lyon, France; ⁶Claude Bernard University Lyon 1, Lyon, France; ⁷Division of Genetic Medicine, Department of Pediatrics, University of Washington, Seattle, WA; ⁸Seattle Children's Hospital, Seattle, WA; ⁹Department of Paediatrics and Child Health, University of Otago, Wellington, New Zealand; ¹⁰Children's Neurology, St Luke's Children's Hospital, Boise, ID; ¹¹Center for Rett Syndrome, Department of Pediatrics and Adolescent Medicine, National Hospital, Copenhagen, Denmark; ¹²Kennedy Center, Department of Clinical Genetics, Copenhagen University Hospital, Rigshospitalet and Department of Clinical Medicine, University of Copenhagen, Copenhagen, Denmark; ¹³French Institute of Health and Medical Research U1231, Laboratory of Cognitive Neuroscience UMR1231, Genetics of Developmental Anomalies, Burgundy University, F-21000, Dijon, France; ¹⁴Department of Medicine and Health Sciences "Vincenzo Tiberio", University of Molise, Campobasso, Italy; ¹⁵University of Melbourne, Austin Health, Royal Children's Hospital, Florey and Murdoch Institutes, Melbourne, Victoria, Australia; ¹⁶Department of Neurology, University of California, San Francisco, San Francisco, CA; ¹⁷Departments of Pediatrics and Neurology, Johns Hopkins School of Medicine, Baltimore, MD; ¹⁸Pediatric Neurology, INTEGRIS Baptist Medical Center, Oklahoma City, OK; ¹⁹Division of Medical Genetics, Department of Pediatrics, Duke University, Durham, NC; ²⁰Molecular Genetic Unit, Strasbourg University Hospital, Strasbourg, France; ²¹Genetics Department, Reference Center for Developmental Anomalies, Clermont-Ferrand University Hospital, Clermont-Ferrand, France; ²²Department of Clinical Medicine, Faculty of Health and Medical Sciences, University of Copenhagen, Copenhagen, Denmark; ²³Reference Center for Developmental Disorders, Department of Medical Genetics, Arnaud de Villeneuve Hospital, Montpellier University Hospital, Montpellier, France; ²⁴Department of Pediatric Neurology, University Hospital of Montpellier, and Physiology and Experimental Medicine of Heart and Muscle Unit, University of Montpellier, National Institute for Health and Medical Research, French National Center for Scientific Research, Montpellier, France; ²⁵Functional Unit 12, Innovation in Genomic Diagnosis of Rare Diseases, University Hospital Dijon-Bourgogne, Dijon, France; ²⁶Division of Neurology, Department of Pediatrics, Children's Hospital of Pittsburgh and University of Pittsburgh School of Medicine, Pittsburgh, PA; ²⁷Department of Radiology and Biomedical Imaging, University of California, San Francisco, San Francisco, CA; ²⁸Neurogenetics Group, University of Antwerp, Antwerp, Belgium; ²⁹Neurology Department, University Hospital Antwerp, Antwerp, Belgium; ³⁰Departments of Neurology, Neuroscience, and Molecular and Human Genetics, Baylor College of Medicine, Houston, TX; and ³¹Departments of Pediatrics and Institute of Experimental and Clinical Research, University of Louvain, Brussels, Belgium

Objective: Recent reports have described single individuals with neurodevelopmental disability (NDD) harboring heterozygous *KCNQ3* de novo variants (DNVs). We sought to assess whether pathogenic variants in *KCNQ3* cause NDD and to elucidate the associated phenotype and molecular mechanisms.

Methods: Patients with NDD and *KCNQ3* DNVs were identified through an international collaboration. Phenotypes were characterized by clinical assessment, review of charts, electroencephalographic (EEG) recordings, and parental interview. Functional consequences of variants were analyzed in vitro by patch-clamp recording.

Results: Eleven patients were assessed. They had recurrent heterozygous DNVs in *KCNQ3* affecting residues R230 (R230C, R230H, R230S) and R227 (R227Q). All patients exhibited global developmental delay within the first 2 years of life. Most (8/11, 73%) were nonverbal or had a few words only. All patients had autistic features, and autism spectrum disorder (ASD) was diagnosed in 5 of 11 (45%). EEGs performed before 10 years of age revealed frequent sleep-activated multifocal epileptiform discharges in 8 of 11 (73%). For 6 of 9 (67%) recorded between 1.5 and 6 years of age, spikes became near-continuous during sleep. Interestingly, most patients (9/11, 82%) did not have seizures, and no patient had seizures in the neonatal period. Voltage-clamp recordings of the mutant *KCNQ3* channels revealed gain-of-function (GoF) effects.

Interpretation: Specific GoF variants in *KCNQ3* cause NDD, ASD, and abundant sleep-activated spikes. This new phenotype contrasts both with self-limited neonatal epilepsy due to *KCNQ3* partial loss of function, and with the neonatal or infantile onset epileptic encephalopathies due to *KCNQ2* GoF.

ANN NEUROL 2019;86:181–192

KCNQ2 and *KCNQ3* encode voltage-gated ion channel subunits mediating a subthreshold potassium current, called M-current (I_{KM}), important in limiting neuronal excitability.¹ Missense loss-of-function (LoF) variants in *KCNQ3* cause benign familial neonatal epilepsy (BFNE), characterized by seizures in the neonatal period with normal development,² although rare families with more severe epilepsy phenotypes have also been described.^{3,4} LoF variants in *KCNQ2* also cause BFNE, and de novo variants (DNVs) that result in more profound disruption of *KCNQ2* function (eg, through dominant negative effects)⁵ lead to *KCNQ2* encephalopathy, a severe developmental and epileptic encephalopathy (DEE) characterized by seizures with onset in the neonatal period and global neurodevelopmental disability (NDD).⁶

Voltage-gated potassium channel subunits contain 6 transmembrane segments (S_1 – S_6) and cytoplasmic N- and C-termini. Within the S_1 – S_4 voltage-sensing domain (VSD), the S_4 transmembrane segment includes a series of positively charged arginine residues that allows the channel to change its opening probability in response to changes in membrane potential.⁷ Missense DNVs at the 2 outermost arginines of the *KCNQ3* S_4 segment (R1: R227Q; R2: R230C/S) have surfaced in heterogeneous cohorts studied by exome sequencing for DEE, NDD, or intellectual disability (ID)^{8–10} and cortical visual impairment.¹¹ Interestingly, DNVs in the corresponding residues in *KCNQ2* (R1: R198; R2: R201) were shown to result in gain of function (GoF)¹² with distinct DEE phenotypes. Patients with the *KCNQ2* R1 variant, R198Q, present in midinfancy with West syndrome, without preceding seizures in the neonatal period,¹³ whereas patients with the *KCNQ2* R2 variants, R201C and R201H, present with neonatal onset encephalopathy without seizures and later develop infantile spasms.¹⁴ The phenotypic spectrum associated with *KCNQ3* R227 and R230 variants has not yet been described.

Here, we delineate the novel electroclinical phenotype in 11 patients with 4 different heterozygous GoF DNVs at R227 and R230 in *KCNQ3*. In contrast to previously described patients with *KCNQ3* LoF, we found that these patients do not present with seizures in the neonatal period. Instead, within the first 2 years of life, they demonstrate global NDD and autism spectrum disorder (ASD) or autistic features. For 6 of 9 (67%) recorded between 1.5 and 6 years of age, spikes became near-continuous during sleep, raising concerns for epileptic encephalopathy. Sleep-activated spikes in 2 patients demonstrated a marked response to high-dose diazepam therapy, providing insight into a possible therapeutic intervention. Patch clamp analysis of each of the *KCNQ3* variants revealed GoF effects, including increased maximal current density and increased opening at membrane potentials where the channel would normally be inactive.

Patients and Methods

Patients

Patients with variants at R230 and R227 in *KCNQ3* were identified by epilepsy gene panel or exome sequencing in clinical and research settings. All sites received prior approval by their human research ethics committee when indicated, and parental informed consent was obtained for each subject. Groups were connected through the Rational Intervention for *KCNQ2/3* Epileptic Encephalopathy database (www.rikee.org), which is curated at Baylor College of Medicine under an institutional review board–approved research protocol.¹⁵ One of the patients (Patient 6) was previously reported with minimal clinical details as part of an Epi4K epileptic encephalopathy cohort;¹⁶ the others have not been previously reported. Pediatric epileptologists (T.T.S. and M.R.C.) reviewed the genetic test results and clinical reports, and evaluated the electroencephalographic (EEG) recordings, where

available. T.T.S., M.R.C., and E.C.C. communicated with treating physicians and/or parents of all patients. Patients were considered to have sleep-activated spikes if the abundance of spikes increased by more than twice that of the awake state. Near-continuous was defined as present for >70% of the sleep record.

Mutagenesis of *KCNQ3* cDNA and Heterologous Expression

Variants were introduced in *KCNQ3* human cDNA cloned into pcDNA3.1 by QuikChange site-directed mutagenesis (Agilent Technologies, Milan, Italy), as previously described.¹² Channel subunits were expressed in Chinese hamster ovary (CHO) cells by transient transfection using Lipofectamine 2000 (Invitrogen, Carlsbad, CA) according to the manufacturer's protocol.¹⁷ A plasmid encoding enhanced green fluorescent protein (Clontech Laboratories, Mountain View, CA) was used as a transfection marker; total cDNA in the transfection mixture was kept constant at 4 μ g.

Whole-Cell Electrophysiology

Currents were recorded under whole-cell patch-clamp at room temperature (20–22°C) 1 to 2 days after transfection as reported.¹² Current densities (expressed in pA/pF) were calculated as peak K⁺ currents at 0mV divided by cell capacitance. To generate conductance–voltage curves, the cells were held at –80mV, then depolarized for 1.5 seconds from –120 to +20mV in 10mV increments, followed by an isopotential pulse at 0mV of 300-millisecond duration. The current values recorded at the beginning of the 0mV pulse were measured, normalized, and expressed as a function of the preceding voltages. The data were then fit to a Boltzmann distribution of the following form: $y = \max / [1 + \exp((V_{1/2} - V)/k)]$, where V is the test potential, $V_{1/2}$ the half-activation potential, and k the slope factor.

Multistate Protein Modeling

Three-dimensional models of *KCNQ2* and *KCNQ3* channels were generated using as templates the coordinates of 6 different states of Kv1.2/2.1 paddle chimera (PDB accession number 2R9R) by SWISS-MODEL (University of Basel, Basel, Switzerland). The models were optimized through all-atom energy minimization by the GROMOS96 implementation of Swiss-PDBViewer and analyzed using both the DeepView module of Swiss-PDBViewer (v4.0.1; <http://spdbv.vital-it.ch/>) and PyMOL (<http://www.pymol.org/>), as described.^{4,12} Sequence alignment was performed using Clustal Omega (<https://www.ebi.ac.uk/Tools/msa/clustalo/>).

Statistics

The probability that a sequencing result reflected postzygotic mosaicism was assessed by the binomial exact test, based on the expectation that heterozygous germline variants will be represented in approximately 50% of read observations. Electrophysiological data are expressed as mean \pm standard error of the mean. Statistically significant differences were evaluated with the Student t test or with analysis of variance followed by the Student–Newman–Keuls test, with the threshold set at $p < 0.05$.

Results

***KCNQ3* DNVs Are Associated with a Novel Phenotype Consisting of Neurodevelopmental Delay, Autistic Features, and Sleep-Activated Near-Continuous Multifocal Spikes**

Index Case (Patient 1). A 30-month-old boy with global developmental delay and ASD presented with episodes of head nodding and stumbling that raised concern for seizures. His development had been normal through the first year, but he did not walk until 18 months and he had no expressive language. He had poor eye contact, impaired joint attention, and did not respond to his name, and his behaviors were notable for stereotypies and echolalia. One week prior to presentation, his mother became concerned by worsening balance with increased falls and more impulsive and aggressive behavior. He was admitted for evaluation with a differential diagnosis that included seizures as a cause of his exacerbated motor impairment. The events of concern were captured on long-term video-EEG monitoring and did not show an EEG correlate. His EEG background, however, was diffusely slow with frequent multifocal spike-and-wave discharges, most prominent in the posterior leads. These discharges increased in amplitude (to >300 μ V) and in abundance during sleep, becoming present for >80% of the sleep record. Given these findings in the clinical context of worsened behaviors and motor performance, the treating physicians were concerned for an epileptic encephalopathy. Treatment with high-dose oral diazepam (1mg/kg) led to rapid resolution of the epileptiform abnormalities, and improvements were subsequently noted across multiple developmental domains by his parents and therapists. Trio exome sequencing revealed a heterozygous *KCNQ3* de novo variant predicted to result in the missense change R230H.

Cohort Genotypes and Phenotypes

We identified 10 other patients with NDD and variants in *KCNQ3* predicted to change R230 and R227 (Tables 1 and 2). These included 2 additional patients with R230H, 5 patients with R230C, 1 patient with R230S, and 2 patients with R227Q. Next generation sequencing revealed mosaicism

TABLE 1. Clinical Features of KCNQ3 Gain-of-Function Variants

Case	Variant	Age, yr/Sex	Neurodevelopment	Other Features	Brain MRI
1	c.689G>A, p.R230H	4/M	Walked at 18 mo, ataxic gait; few words; ASD diagnosis at 21 mo, ID, echolalia; impulsive, aggressive behavior; stereotypies	Hypotonia, esotropia	Normal at 37 mo
2	c.688C>A, p.R230S	23/M	Walked at 23 mo; ataxic gait; nonverbal, autistic features	Hypotonia	Mild hypoplasia of corpus callosum, mild cerebellar atrophy at 19 mo
3	c.689G>A, p.R230H ^a	5/M	Head lag at 6 mo; sat at 13 mo; walked at 25 mo; ataxic gait; nonverbal (few words, then regressed); impulsive, repetitive behaviors, poor eye contact	Hypotonia, exotropia	Mild T2 hyperintensities in the bilateral periaxial white matter at 15 mo and 3.5 yr
4	c.688C>T, p.R230C	20/F	Sat at 12 mo; walked at 24 mo; 4–5 words; moderate ID; stereotypies; aggressive behavior	Exotropia, possible CVI	Normal at 4 yr, 6 yr, and 15 yr
5	c.688C>T, p.R230C	4/F	Sat at 13 mo; walked with assistance at 34 mo; 2 words at 34 mo; poor eye contact	Birth at 34 wk, hypotonia, strabismus	Diminished white matter, right > left, and abnormal frontal sulcation at 13 mo and 32 mo
6	c.688C>T, p.R230C	11/M	Walked at 23 mo; ASD diagnosis at 3 yr; nonverbal (few words then regressed); impulsive; self-injurious behavior	Strabismus	Normal at 10 mo
7	c.689G>A, p.R230H, 18% mosaic	5/M	Walked at 14 mo, ataxic gait; fine motor impairment; words by 2 yr; sentences by 3 yr; ASD diagnosis at 3 yr	Hypotonia, strabismus	Normal at 4 yr
8	c.688C>T, p.R230C	21/M	Walked by 18 mo; nonverbal; ASD; severe ID	Left esotropia	Normal at 3 yr
9	c.688C>T, p.R230C	8/M	Sat at 12 mo; walked at 26 mo; nonverbal; anxiety, aggressive behavior; autistic features (stereotypies, poor eye contact)	Hypotonia	Nonspecific white matter lesions at 18 mo
10	c.680G>A, p.R227Q	9/F	Walked at 22 mo; speaks in 2–3-word sentences; ASD diagnosis at 2 yr; stereotypies, echolalia	Hypotonia	Normal at 9 yr and 12 yr
11	c.680G>A, p.R227Q	18/F	Walked at 12 mo; words at 3 yr, sentences by 6 yr; echolalia, stereotypies, sensory issues; dysarthria; FSIQ 42; assistance to brush teeth, comb hair		Normal at 6 yr

^aUnaffected mother with low-level mosaicism (5%–6%).

ASD = autism spectrum disorder; CVI = cortical visual impairment; F = female; FSIQ = full-scale intelligence quotient; ID = intellectual disability; M = male; MRI = magnetic resonance imaging.

TABLE 2. Electroclinical Features of Patients with KCNQ3 Gain-of-Function Variants

Patient/Variant	EEG	Seizures	AEDs
1/R230H	Diffusely slow with posterior spikes in wakefulness; MSES in sleep (posterior predominant EDs) at 30 mo	No (staring and jerks recorded at 30 mo)	For MSES at 30 mo: DZP (++), CLB (++)
2/R230S	Spikes (L) at 12 mo; MSES at 18 mo and 4 yr (R>L); spikes (R>L) at 8 yr; no spikes (awake) at 12 yr and 19 yr	Staring spells at 3 yr	VPA
3/R230H	Diffusely slow with posterior spikes in wakefulness; MSES at 3.5 yr and 4.5 yr (posterior predominant EDs)	No (staring spells recorded at 3 yr)	LEV at 3.5 yr; DZP (++) for MSES at 4.5 yr
4/R230C	Normal at 4.5 yr; diffusely slow electrical activity at 16 yr	GTC from 13 yr; atonic seizures at 15 yr	VPA, CLB, LCM (all for seizures)
5/R230C	Frequent sleep-activated L posterior > R central EDs at 3 yr	No	None
6/R230C	MSES at 6 yr (L>R central and temporal EDs)	GTC from 10 mo; atonic seizures; absence seizures	VPA, LEV, OXC, RUF, KD (all for seizures)
7/R230H mosaic	Normal at 4.5 yr	No	None
8/R230C	Diffusely slow with posterior spikes in wakefulness; MSES at 30 mo, 3.5 yr, 4 yr, 4.5 yr, and 5 yr (posterior predominant EDs)	Staring spells reported at 2 yr	VPA for staring spells; for MSES: LTG, CS (+), CLB
9/R230C	Diffusely slow in wakefulness; MSES at 3.5 yr, 4 yr, 4.5 yr, 5.5 yr, 6.5 yr	No	For MSES: CS (+), ETX, CLB
10/R227Q	Frequent sleep-activated L frontotemporal EDs at 9 yr	No	None
11/R227Q	Normal at 2.5 yr (awake only); normal at 18 yr (awake only)	Staring spells reported at 2.5 yr	None

+ = partial response; ++ = response; AEDs = antiepileptic drugs; CLB = clobazam; CS = corticosteroids; DZP = diazepam; EDs = epileptiform discharges; EEG = electroencephalogram; ETX = ethosuximide; GTC = generalized tonic-clonic seizure; KD = ketogenic diet; L = left; LCM = lacosamide; LEV = levetiracetam; LTG = lamotrigine; MSES = multifocal status epilepticus during sleep; OXC = oxcarbazepine; R = right; RUF = rufinamide; VPA = valproic acid.

in 1 parent and 1 proband. The asymptomatic mosaic mother of Patient 3 carried the variant in 3 of 50 reads (6%, $p < 10^{-8}$, binomial exact test). Aside from Patient 3, all variants were confirmed to be absent in parental samples. The DNA sequencing of Patient 7 showed R230H in 22 of 121 reads (18%, $p < 10^{-8}$). R227Q, R230C, and R230S were absent from the population database gnomAD.¹⁸ Interestingly, 1 of 122,950 individuals in the gnomAD dataset showed mosaic presence of R230H (45/145 reads, 31%, $p = 2.9 \times 10^{-6}$),^{18,19}

similar to Patient 7. Clinical information was not available regarding the gnomAD mosaic individual. In silico analysis predicted each of these variants to be deleterious with high probability (PolyPhen-2 > 0.999, SIFT = 0, CADD score > 30).²⁰⁻²²

For genome-wide significance as an NDD gene, our 11 patients would need to have been observed from a cohort no larger than 47,000 individuals ($p = 2.40e-06$, CCDS22).²³ Patient 6 was identified in an Epi4K cohort of 264

individuals,¹⁶ but the method of ascertainment of most our other patients made precise determination of the denominator impossible, precluding formal calculation.

All 11 patients had some degree of ID and delays across multiple developmental domains, coming to clinical attention between the ages of 4 and 18 months. Delayed language was universal, but patients often presented with concurrent or preceding gross motor delays. Patient 3 did not develop head control until after 6 months. Four patients were late to sit, and all but 2 individuals (Patients 7 and 11) were delayed in walking. Although all patients ultimately walked, walking was often characterized as broad-based and unsteady with poor balance, variably reported as ataxic.

Language development was abnormal in all cases. Three patients were nonverbal. Five developed single words, but 2 of these subsequently regressed to become nonverbal. Patient 7, mosaic for R230H, and the 2 patients (10 and 11) who carried the R227Q variant had language delay with first words at 2 or 3 years, but were ultimately able to speak in sentences.

ASD was diagnosed in 5 of 11 (45%) patients, and autistic features were reported in the remaining 6. Stereotypies, mouthing nonfood objects, and aggressive, impulsive, and self-injurious behaviors were common features. Hypotonia and strabismus were each reported in 7 of 11 (64%) individuals. Brain magnetic resonance imaging (MRI) studies were normal or showed nonspecific abnormalities. The MRI of Patient 5 showed diminished white matter and abnormal frontal sulcation not consistent with acquired injury, although he had a history of preterm delivery at 34 weeks of gestation.

Two patients (4 and 6) were diagnosed with generalized tonic-clonic seizures from 13 years and from 10 months of age, respectively. Atonic seizures were also reported for these patients, as well as absence seizures for Patient 6. The remaining patients were not diagnosed with seizures (9/11, 82%). No patients had seizures in the neonatal period.

All 11 patients had EEGs recorded at some point between 1 and 10 years of age, and 8 of them (73%) had focal or multifocal spikes that were markedly activated by sleep. In 6 of 9 patients (67%) with sleep EEGs between 18 months and 6 years of age, epileptiform discharges became near-continuous during sleep. For 4 of these children (Patients 1, 2, 3, and 8), parents noticed recurrent episodes of unresponsive staring or deteriorating motor function with subtle jerks or loss of tone that led to assessment with prolonged video-EEG recording. Although the events of concern could not always be captured, the spikes observed were not time-locked with jerks, loss of tone, or unresponsive staring. In 5 cases (Patients 1, 2, 3, 8, and 9), the discovery of the markedly abnormal sleep EEG in

this clinical context raised concern for epileptic encephalopathy, leading physicians to treat with antiseizure medications including high-dose diazepam with the goal of reducing or eliminating the epileptiform abnormalities. The clinical response to treatments varied; some benefits were reported, although no worsening was seen when the antiseizure medications were discontinued. Treatment with high-dose oral diazepam (Patients 1 and 3) or corticosteroids (Patients 8 and 9) was followed by reduction of the sleep-activated spikes on EEG, but with inconsistent effects on behavior.

KCNQ3 R227 and R230 Variants Exhibit GoF with Increased Current Density and Hyperpolarized Activation Voltage Dependence

KCNQ3 R227 (R1) and R230 (R2) are the outermost of the positively charged residues of the S_4 voltage sensor (Fig 1A); in KCNQ2, R1 and R2 correspond to R198 and R201, respectively (see Fig 1B). The functional properties of channels formed by KCNQ3 R227Q or R230C/H/S variants were characterized as homomers and as heteromers with KCNQ2 subunits.

Wild-type homomeric KCNQ3 channels generated small K^+ -selective and voltage-dependent currents that activated around -60 mV and displayed a $V_{1/2}$ of -38 mV (see Fig 1C, D; Table 3). At a holding voltage of -80 mV, the vast majority of KCNQ3 channels were closed; therefore, the ratio between the currents measured at the beginning of the depolarization step (I_{Inst}) and those at the end of the 0 mV depolarization ($I_{steady-state}$) was close to zero (see Table 3). By contrast, homomeric KCNQ3 channels in which the charged side chain at R230 was substituted by cysteine, serine, or histidine residues (R2C, R2S, and R2H, respectively) showed an almost complete loss of time-dependent current activation kinetics; as a result, the $I_{Inst}/I_{steady-state}$ ratio was close to unity. Similar, although quantitatively smaller, effects were observed upon neutralization of the R227 residue with glutamine (R1Q); KCNQ3 R227Q channels retained voltage-dependent gating, although with a drastic (>70 mV) hyperpolarization of the voltage requirement for activation. Notably, this functional change is qualitatively similar but quantitatively larger than that produced by the corresponding substitution (R198Q) in KCNQ2 (-30 mV).²⁴

In addition, the amplitude of K^+ current carried by each of the 4 mutant channels at depolarized membrane potentials was increased approximately 10-fold, compared to wild-type KCNQ3 channels (see Table 3). In contrast to the dramatic changes in voltage-sensitivity and current size described in all 4 mutant channels, other important properties, such as the sensitivity to blockade by tetraethylammonium (TEA), a pharmacological feature discriminating between KCNQ3 and KCNQ2 channels, and the K^+ reversal potential,

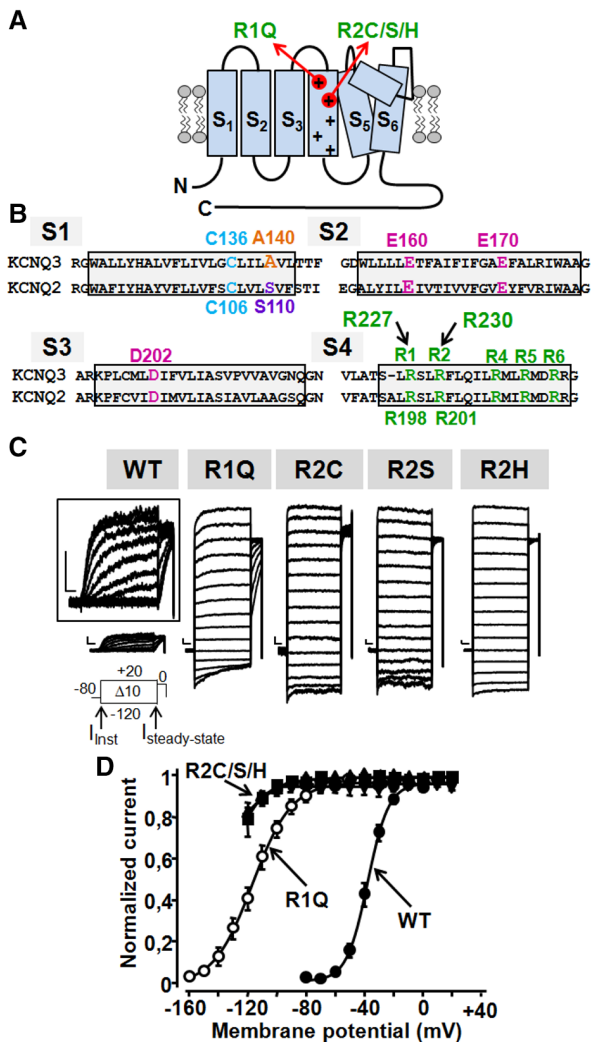


FIGURE 1: Functional consequences of the R227Q and R230C/S/H variants in KCNQ3. (A) Topological representation of a single KCNQ subunit. The red arrows highlight the position of the first 2 arginines (R1 and R2) along the S₄ primary sequence, where variants of interest in the present study are located. (B) Sequence alignment of the 4 transmembrane regions (S₁, S₂, S₃, and S₄) of the voltage-sensing domain of KCNQ3 and KCNQ2 subunits. Residues relevant to the present study are colored as follows: green for positively charged, pink for negatively charged, and orange for nonpolar. Among polar amino acids, C is in light blue, whereas S is in violet. R1, R2, R4, R5, and R6 refer to the positively charged arginines numbered according to their position along the S₄ primary sequence. (C) Macroscopic currents from the KCNQ3 (WT), KCNQ3 R227Q (R1Q), KCNQ3 R230C (R2C), KCNQ3 R230S (R2S), or KCNQ3 R230H (R2H) homomeric channels in response to the indicated voltage protocol. Inset shows an enlarged view of KCNQ3 traces. The arrows on the voltage protocol indicate the time chosen for current analysis, as explained in the text. Current scale, 100pA; time scale, 0.2 seconds. (D) Conductance/voltage curves for KCNQ3 (WT, filled circles), KCNQ3 R227Q (R1Q, empty circles), KCNQ3 R230C (R2C, inverted triangles), KCNQ3 R230S (R2S, triangles), or KCNQ3 R230H (R2H, squares) homomeric channels, as indicated. Continuous lines are Boltzmann fits to the experimental data. Each data point is the mean standard error of 9-21 cells recorded in at least 3 separate experimental sessions.

indicative of channel selectivity for K⁺ ions, were unchanged from the wild type (see Table 3).

To mimic the genetic condition of patients, who carry a single mutant allele, and considering that I_{KM} in adult neurons is mainly formed by tetrameric coassembly of KCNQ2 and KCNQ3 subunits, we transfected CHO cells with *KCNQ2* and *KCNQ3* cDNAs at a 1:1 ratio (to mimic the genetic balance of normal individuals), and *KCNQ2* + *KCNQ3* + mutant *KCNQ3* at a 1:0.5:0.5 ratio (to mimic the genetic balance of affected individuals). Coexpression of KCNQ3 R227Q, R230C, R230H, or R230S subunits with KCNQ2 and KCNQ3 subunits caused a statistically significant hyperpolarization in activation voltage-dependence of about 6mV, without affecting current density or TEA sensitivity when compared to KCNQ2 + KCNQ3 channel controls (see Table 3).

Mechanistic Basis for the GoF by KCNQ3 R227 and R230 Variants

We used a model based on the atomic structure of Kv1.2/2.1 channels to analyze the mechanistic basis for the functional effects observed. In the resting state, the positively charged side chains of R227 (R1) and R230 (R2) in the KCNQ3 VSD establish ionized hydrogen bonds with nearby polar or charged residues: R227 with C136 in S₁, and R230 with E170 and D202 in S₂ and S₃, respectively (Fig 2). These interactions are all lost when the S₄ moves toward the extracellular space during activation²⁴; therefore, the R227Q or the R230C/S/H substitutions are predicted to selectively destabilize the resting (closed) conformation of the VSD, possibly explaining the observed GoF effects. It is noteworthy that R198 in KCNQ2 (R1, corresponding to KCNQ3 R227), in addition to C106 (corresponding to KCNQ3 C136), also establishes a strong hydrogen bond with S110; in KCNQ3, this position is occupied by a nonpolar residue (A140) that is unable to interact with R227 (R1). That the R227 residue in KCNQ3 only establishes a weak hydrogen bond with the nearby C residue, whereas the corresponding R198 residue in KCNQ2 is also engaged in a stronger hydrogen bond with S110 renders the VSD resting state less stable in KCNQ3 when compared to KCNQ2, likely contributing to the lower activation midpoint of the former,¹² and possibly to the more dramatic V_{1/2} hyperpolarizing effect of the KCNQ3 R227Q substitution (Q1) when compared to the R198Q substitution in KCNQ2 (Q1).²⁴

Discussion

Inherited variants in *KCNQ3* are known to be associated with BFNE. Our series describes the novel phenotype in patients with de novo *KCNQ3* missense variants at R227 and R230, characterized by NDD, ASD, and sleep-activated near-continuous multifocal spikes, and increases

TABLE 3. Biophysical and Pharmacological Properties of Channels Carrying *KCNQ3* Variants

	No.	$V_{1/2}$, mV	k, mV/efold	$I_{inst}/I_{steady-state}$	Current Density, pA/pF	E_{K} , mV	Blockade by TEA, %		
							0.3mM	3mM	30mM
KCNQ3	21	-38.4 ± 1.0	7.1 ± 0.4	0.04 ± 0.02	10.6 ± 1.3	-79.0 ± 0.1	6.4 ± 1.8	13.0 ± 3.4	61.7 ± 5.7
KCNQ3 R1Q	9	-112.0 ± 2.4^a	10.8 ± 0.9^a	0.91 ± 0.02^a	89.6 ± 17.5^a	-79.9 ± 0.3	–	–	61.1 ± 6.8
KCNQ3 R2C	12	–	–	1.00 ± 0.01^a	121.0 ± 21.0^a	-79.9 ± 0.3	–	–	58.6 ± 13
KCNQ3 R2S	16	–	–	0.98 ± 0.03^a	89.7 ± 12.2^a	-80.1 ± 0.1	–	–	66.1 ± 6.1
KCNQ3 R2H	12	–	–	0.98 ± 0.02^a	132.2 ± 20.0^a	-79.3 ± 0.4	–	–	70.9 ± 7.3
KCNQ2 + KCNQ3	16	-33.6 ± 1.2	13.6 ± 0.4	0.04 ± 0.02	133.5 ± 19.0	–	15.6 ± 3.1	50.5 ± 3.1	78.8 ± 5.6
KCNQ2 + KCNQ3 + KCNQ3 R1Q	9	-39.5 ± 3.0^b	14.7 ± 0.8	0.04 ± 0.01	101.3 ± 20.2	–	19.3 ± 2.0	44.1 ± 4.3	85.3 ± 2.1
KCNQ2 + KCNQ3 + KCNQ3 R2C	9	-39.9 ± 3.7^b	15.3 ± 0.7	0.10 ± 0.03^b	108.8 ± 16.9	–	14.0 ± 6.2	47.1 ± 9.9	77.0 ± 7.3
KCNQ2 + KCNQ3 + KCNQ3 R2S	14	-39.0 ± 1.5^b	15.0 ± 0.6	0.07 ± 0.02^b	116.7 ± 12.0	–	12.9 ± 2.3	43.6 ± 8.2	80.1 ± 6.5
KCNQ2 + KCNQ3 + KCNQ3 R2H	14	-39.5 ± 1.5^b	14.2 ± 0.4	0.08 ± 0.02^b	123.0 ± 15.5	–	20.8 ± 3.1	47.4 ± 2.5	78.8 ± 3.2

^a $p < 0.05$ versus KCNQ3.
^b $p < 0.05$ versus KCNQ2 + KCNQ3.
TEA = tetraethylammonium.

the number of reported patients with this mutational hotspot to 16. The R230C, R230H, and R230S variants all resulted in strong GoF effects, whereas similar but smaller effects were exhibited by R227Q.

Although formal calculation of genome-wide significance was not possible, given our inability to know the total number of individuals sequenced for NDD, we calculated an upper limit of 47,000. Our collaborative study is highly unlikely to have drawn from such a large population. Supporting this, the largest NDD cohort from which cases have been identified to date, the Deciphering Developmental Disorders Study, was smaller than this limit by an order of magnitude and identified 2 such patients.¹⁰ The similarity of clinical presentation and the complementary functional work we present provide additional support for *KCNQ3* as an NDD gene.

Patients with *KCNQ3* GoF variants at R227 and R230 presented with developmental delay within the first 2 years of life, with more than one-third of the cohort presenting before 12 months. Patients with R230C/H/S variants were usually ambulatory by 2 years of age, but were either nonverbal or had single words only and were cognitively impaired with ASD or autistic features. Patient 7, whose testing revealed mosaicism for R230H, had a relatively milder phenotype, and the mother of Patient 3, with low-level mosaicism for R230H, was unaffected. The NDD of the 2 patients with R227Q was also less severe, consistent with our findings of milder alteration of in vitro functional properties of channels carrying this variant compared to

those carrying R230C/H/S variants. Although these findings are suggestive of a positive correlation between the extent of GoF and severity, current data are insufficient for proper statistical assessment, which will have to wait for larger numbers of patients.

Previous studies sequencing cohorts of patients with DEE, NDD, ID, and cortical visual impairment have identified 1 patient with R227Q, 3 with R230C, and 2 with R230S DNVs in *KCNQ3*.^{8–11,16} Although limited, the clinical features reported in those five patients (Table 4) seem consistent with the ones in our cohort.

Multifocal Status Epilepticus during Sleep

EEG recordings showed sleep-activated spikes in all but 2 patients monitored during sleep. In 6 patients who had EEGs performed between 1.5 and 6.5 years of age, spikes became near-continuous during sleep, raising concerns for epileptic encephalopathy in the clinical setting. Continuous spike and wave during slow wave sleep is an epilepsy syndrome characterized by neurocognitive regression or stagnation associated with near-continuous diffuse spike-waves occurring during sleep, an electrographic pattern referred to as electrical status epilepticus during slow sleep. When we analyzed the EEGs, we found that the spikes were multifocal with a posterior predominance, which suggested the term “multifocal status epilepticus during sleep” (MSES). Some of our patients had language regression, but we do not have longitudinal testing to determine the timing and extent of regression or developmental plateauing or correlate it with the appearance of

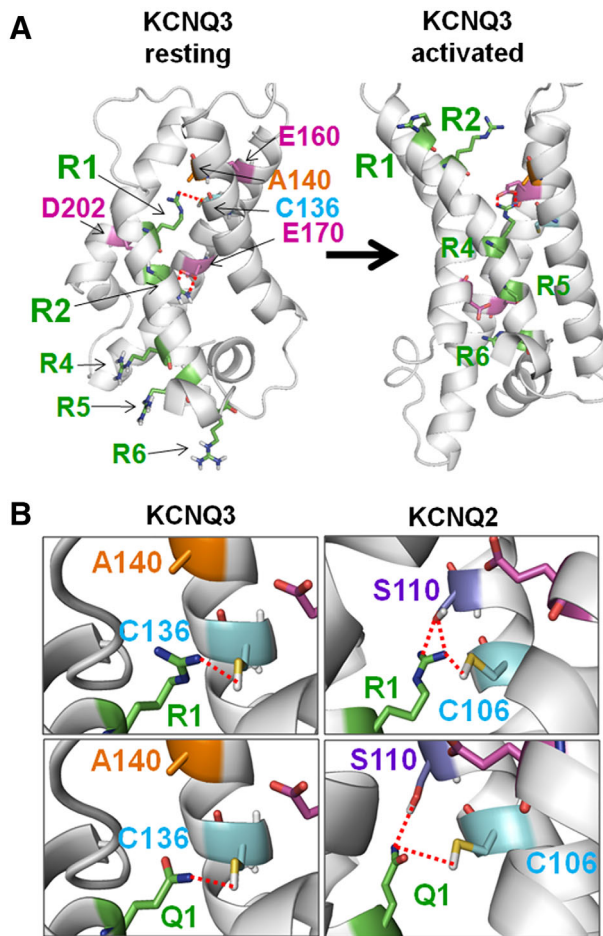


FIGURE 2: Structural modeling of KCNQ3 voltage-sensing domain (VSD) in resting and activated states, and comparison with KCNQ2. (A) Structural model of the resting (left panel) and activated (right panel) gating states of the VSD from a single KCNQ3 subunit, as indicated. Residues relevant to the present study are colored as follows: green for positively charged, pink for negatively charged, orange for nonpolar, and blue and purple for polar (C is in light blue, S is in violet). R1, R2, R4, R5, and R6 refer to the positively charged arginines numbered according to their position along the S₄ primary sequence. **(B)** An enlarged view of the resting state of the VSD of KCNQ3 (top left panel) and KCNQ2 (top right panel). Lower panels highlight the ionic interactions established when the R1 residues are substituted with Q (Q1) in KCNQ3 (left) or KCNQ2 (right) subunits. In all panels, the dashed red lines indicate ionic interactions among residues.

MSES. In most patients in whom MSES was detected, EEG monitoring was prompted by concern for seizures. Although these patients were not diagnosed with seizures, the presence of near-continuous spikes during sleep led to treatment based on the concept that reducing the abundance of epileptiform abnormalities may prevent or reverse developmental stagnation or regression.^{25,26} Our numbers are too small to draw conclusions about electrographic responses to standard therapies, such as diazepam,²⁷ and more recently described treatments, such as amantadine, were not used.²⁸

Two patients in our cohort were diagnosed with generalized tonic-clonic seizures, atonic seizures, and absence seizures, although their events were never captured on EEG. Absence epilepsy/seizures were intriguingly also noted in the limited clinical details for 2 patients with *KCNQ3* variants in previously reported cohorts (see Table 4).^{10,11} However, the full spectrum of epileptic disorders in patients with *KCNQ3* GoF variants awaits further characterization with ictal video-EEG recordings and classification of the events. Our study has the limitations of being retrospective; evaluation (eg, cognitive/behavioral testing, timing, and length of EEG recordings) and treatment (including medication selection and duration of treatment) were determined at the discretion of the treating physicians and did not follow a research protocol.

***KCNQ3* and *KCNQ2* Genotypes and Phenotypes**

Brain *KCNQ2* and *KCNQ3* subunits coassemble as heteromeric channels,²⁹ and inherited LoF missense variants in these genes cause an autosomal dominant phenotype, BFNE.^{30–32} Most de novo *KCNQ2* LoF variants result in a severe DEE with seizure onset in the neonatal period.^{6,15,17,33} However, de novo *KCNQ2* GoF variants R201C and R201H are associated with a distinct neonatal syndrome characterized by nonepileptic myoclonus, pathological breathing, and a suppression-burst EEG pattern in the absence of seizures.¹⁴ We now report that de novo GoF variants at the *KCNQ3* R230 position, homologous to *KCNQ2* R201, cause NDD associated with ASD/autistic features and MSES without neonatal seizures. Whereas the *KCNQ2* R198Q variant has been found recurrently in patients with West syndrome without prior neonatal seizures,²⁴ we found the homologous *KCNQ3* variant, R227Q, in 2 patients with less severe NDD without any history of seizures. These findings further extend the phenotypes associated with *KCNQ2* and *KCNQ3* GoF variants, which have in common the absence of neonatal seizures, the main characteristic of LoF variants (Table 5).

Our understanding of the mechanism by which GoF changes in *KCNQ3* subunits result in the described clinical phenotype with NDD and without neonatal seizures is limited by the lack of in vivo studies. In particular, it is unclear why the LoF condition presents in the neonatal period, whereas the GoF condition results in cognitive and behavioral disturbances that only become apparent later. Interestingly, a parallel but reverse genotype–phenotype correlation has been reported for *SCN2A*-related disorders, where GoF results in early epilepsy and LoF imparts neurodevelopmental disability with autistic features and more variable epilepsy phenotypes with later onset.³⁴ This similarity may not be coincidental, as both channels are localized at the axon initial segment and seizures in early epilepsy caused by *KCNQ3* LoF variants, like

TABLE 4. Previously Published Patients with *KCNQ3* R227 and R230 Variants

Publication /Case ID	Variant	Sex	Neurodevelopment	Other Features	EEG	Seizures	Brain MRI
Rauch et al 2012/TUTLN	c.688C>T, p.R230C	F	Sat at 12 mo, walked at 24 mo; nonverbal at 42 mo; moderate ID; autistic, aggressive, anxious	Strabismus	Multifocal sharp waves, sharp slow waves	No	6-mo MRI: "hypointensity in left ventricle"
Grozeva et al 2015/5410783	c.688C>A, p.R230S ^a	F	Nonsyndromic ID				
Bosch et al 2016/24	c.688C>T, p.R230C	F	ID at 4 yr	Cortical visual impairment		Absence of epilepsy	
DDD 2017/261649	c.688C>A, p.R230S	F	Broad-based gait; delayed speech and language; severe ID; recurrent hand flapping	Strabismus, microcephaly		Absence of seizures	
DDD 2017/272471	c.680G>A, p.R227Q	M	Global developmental delay				

^aInheritance unknown.
 DDD = Deciphering Developmental Disorders Study; EEG = electroencephalogram; F = female; ID = intellectual disability; M = male; MRI = magnetic resonance imaging.

those caused by *SCN2A* GoF variants, are responsive to sodium channel blockers, such as carbamazepine.^{35,36}

The reason for the differences in phenotypes between *KCNQ2* and *KCNQ3* variants at homologous positions is unknown, and fuller investigation of this will likely require in vivo developmental studies. In rodents, the ratio of *KCNQ3* to *KCNQ2* expression is low at birth and increases during postnatal development.³⁷ Similar findings have been shown in the human brain,³⁸ and may explain the earlier

onset and more severe disability of *KCNQ2* GoF pathogenic variants compared to *KCNQ3*.

Whereas the features of neonatal onset *KCNQ2*- and *KCNQ3*-related epilepsy are distinctive,^{35,39} enabling early recognition of the phenotype and genetic testing, global NDD is clinically and genetically heterogeneous. The prevalence of *KCNQ3* R227 and R230 variants in the general population of children with NDDs is unknown, but is likely under-recognized, as neither exome sequencing nor sleep

TABLE 5. Gain-of-Function Variants in the Voltage Sensor Domain S4 Segments of *KCNQ2* and *KCNQ3* Have Diverse Electroclinical Phenotypes

S4 Arginine	<i>KCNQ2</i>		<i>KCNQ3</i>	
	Known Variants	Phenotypes	Known Variants	Phenotypes
R1	R198Q	West syndrome (hypsarrhythmia, infantile spasms, emergence of developmental delay) without preceding neonatal seizures or encephalopathy	R227Q	Neurodevelopmental disability: verbal, with autism spectrum disorder or autistic features and sleep-activated spikes
R2	R201C, R201H	Profound neonatal onset encephalopathy with nonepileptic myoclonus, burst-suppression EEG and apnea, with West syndrome later in infancy	R230C, R230H, R230S	Neurodevelopmental disability: nonverbal, with autism spectrum disorder or autistic features and multifocal status epilepticus during sleep

EEG = electroencephalogram.

EEG is currently routinely included in the evaluation of children with NDD and autism.

A Monogenic Cause of NDD and Autism

Monogenic subtypes of autism are increasingly being identified, particularly when comorbid with ID.^{40,41} Epilepsy, ID, and autism often co-occur and share genetic causes and perhaps underlying mechanisms.⁴² As near-continuous epileptiform activity during sleep may interfere with development, and treatment with benzodiazepines may be successful at abolishing the electrographic pattern, sleep EEG recording for patients with NDD/ID with autism may have clinical utility.

Limitations of this study arise from the rarity of the disorder, and include differences in patient evaluation between sites, and the potential for ascertainment bias, as parents of severely affected children may be more likely to seek clinical genetic evaluation and participate in research. Additional work, including standardized assessment of a larger patient group, will enable further characterization of *KCNQ3* GoF pathogenic variants.

Conclusion

Our findings show that GoF missense variants at R230 and R227 in *KCNQ3* do not cause neonatal epilepsy, and instead result in a novel phenotype characterized by NDD with ASD and MSES. Our work provides another example of the delineation of distinct phenotypes associated with different classes of variants in ion channel genes, expands the phenotypic spectrum associated with pathogenic variants in *KCNQ3*, complements the GoF phenotypes reported for *KCNQ2*, and adds *KCNQ3* to genetic causes of autism.

Acknowledgment

The present work was supported by the Telethon Foundation (GGP15113) and by the Italian Ministry for University and Research (PRIN 2017ALCR7C) to M.T.; the Italian Ministry for University and Research (Project Scientific Independence of Researchers 2014 RBSI1444EM and PRIN 2017YH3SXX) and the University of Naples “Federico II” and Compagnia di San Paolo within the STAR Program “Sostegno Territoriale alle Attività di Ricerca” (project number 6-CSP-UNINA-120) to F.M.; the Italian Ministry of Health Ricerca Finalizzata Giovani Ricercatori 2016 (project GR-2016-02363337) and the Italian Ministry for University and Research (PRIN 2017ALCR7C) to M.V.S.; National Institute of Neurological Disorders and Stroke (R01 NS49119 and U54 NS108874) to E.C.C.; the Jack Pribaz Foundation (E.C.C. and S.W.), the *KCNQ2* Cure Alliance (E.C.C.

and S.W.), and the Miles Family Fund (E.C.C.). The present work was also supported by the University Research Fund—University of Antwerp (FFB180053) and Scientific Research Flanders (1861419N) to S.W. and by the NIH National Institute of Neurological Disorders and Stroke (R01 NS069605) to H.C.M. Genome sequencing for Patient 11 was performed by the SNP&SEQ Technology Platform in Uppsala, Sweden, in collaboration with Lars Feuk. This facility is part of the National Genomics Infrastructure Sweden and Science for Life Technologies. The platform is supported by the Swedish Research Council and the Knut and Alice Wallenberg Foundation. Exome sequencing for Patient 4 was ascertained in the Duke Genome Sequencing Clinic, supported by the Duke University Health System, Durham, NC.

We thank the patients and their families for participation in this research, and the *KCNQ2* Cure Alliance and Jack Pribaz Foundation for collaboration and parent referrals.

Author Contributions

Acquisition and analysis of data: all authors. Study concept and design: T.T.S., E.C.C., M.T., and M.R.C. Drafting the text and preparing the figures: T.T.S., F.M., E.C.C., M.T., and M.R.C.

Potential Conflicts of Interest

Nothing to report.

References

1. Wang HS, Pan Z, Shi W, et al. *KCNQ2* and *KCNQ3* potassium channel subunits: molecular correlates of the M-channel. *Science* 1998; 282:1890–1893.
2. Grinton BE, Heron SE, Pelekanos JT, et al. Familial neonatal seizures in 36 families: clinical and genetic features correlate with outcome. *Epilepsia* 2015;56:1071–1080.
3. Miceli F, Striano P, Soldovieri MV, et al. A novel *KCNQ3* mutation in familial epilepsy with focal seizures and intellectual disability. *Epilepsia* 2015;56:e15–e20.
4. Ambrosino P, Freri E, Castellotti B, et al. Kv7.3 compound heterozygous variants in early onset encephalopathy reveal additive contribution of C-terminal residues to PIP2-dependent K(+) channel gating. *Mol Neurobiol* 2018;55:7009–7024.
5. Orhan G, Bock M, Schepers D, et al. Dominant-negative effects of *KCNQ2* mutations are associated with epileptic encephalopathy. *Ann Neurol* 2014;75:382–394.
6. Weckhuysen S, Mandelstam S, Suls A, et al. *KCNQ2* encephalopathy: emerging phenotype of a neonatal epileptic encephalopathy. *Ann Neurol* 2012;71:15–25.
7. Long SB, Campbell EB, Mackinnon R. Voltage sensor of Kv1.2: structural basis of electromechanical coupling. *Science* 2005;309: 903–908.
8. Rauch A, Wieczorek D, Graf E, et al. Range of genetic mutations associated with severe non-syndromic sporadic intellectual disability: an exome sequencing study. *Lancet* 2012;380:1674–1682.

9. Grozeva D, Carss K, Spasic-Boskovic O, et al. Targeted next-generation sequencing analysis of 1,000 individuals with intellectual disability. *Hum Mutat* 2015;36:1197–1204.
10. Deciphering Developmental Disorders Study. Prevalence and architecture of de novo mutations in developmental disorders. *Nature* 2017;542:433–438.
11. Bosch DG, Boonstra FN, de Leeuw N, et al. Novel genetic causes for cerebral visual impairment. *Eur J Hum Genet* 2016;24:660–665.
12. Miceli F, Soldovieri MV, Ambrosino P, et al. Early-onset epileptic encephalopathy caused by gain-of-function mutations in the voltage sensor of Kv7.2 and Kv7.3 potassium channel subunits. *J Neurosci* 2015;35:3782–3793.
13. Millichap JJ, Miceli F, De Maria M, et al. Infantile spasms and encephalopathy without preceding neonatal seizures caused by KCNQ2 R198Q, a gain-of-function variant. *Epilepsia* 2017;58:e10–e15.
14. Mulkey SB, Ben-Zeev B, Nicolai J, et al. Neonatal nonepileptic myoclonus is a prominent clinical feature of KCNQ2 gain-of-function variants R201C and R201H. *Epilepsia* 2017;58:436–445.
15. Millichap JJ, Park KL, Tsuchida T, et al. KCNQ2 encephalopathy: features, mutational hot spots, and ezogabine treatment of 11 patients. *Neurol Genet* 2016;2:e96.
16. Consortium EK, Project EPG, Allen AS, et al. De novo mutations in epileptic encephalopathies. *Nature* 2013;501:217–221.
17. Miceli F, Soldovieri MV, Ambrosino P, et al. Genotype-phenotype correlations in neonatal epilepsies caused by mutations in the voltage sensor of K(v)7.2 potassium channel subunits. *Proc Natl Acad Sci U S A* 2013;110:4386–4391.
18. Lek M, Karczewski KJ, Minikel EV, et al. Analysis of protein-coding genetic variation in 60,706 humans. *Nature* 2016;536:285–291.
19. Genome Aggregation Database. Available at: <http://gnomad.broadinstitute.org/variant/8-133192492-C-T>. Accessed August 1, 2018.
20. Ng PC, Henikoff S. SIFT: predicting amino acid changes that affect protein function. *Nucleic Acids Res* 2003;31:3812–3814.
21. Adzhubei IA, Schmidt S, Peshkin L, et al. A method and server for predicting damaging missense mutations. *Nat Methods* 2010;7:248–249.
22. Kircher M, Witten DM, Jain P, et al. A general framework for estimating the relative pathogenicity of human genetic variants. *Nat Genet* 2014;46:310–315.
23. Jiang Y, Han Y, Petrovski S, et al. Incorporating functional information in tests of excess de novo mutational load. *Am J Hum Genet* 2015;97:272–283.
24. Gourgy-Hacohen O, Kornilov P, Pittel I, et al. Capturing distinct KCNQ2 channel resting states by metal ion bridges in the voltage-sensor domain. *J Gen Physiol* 2014;144:513–527.
25. Robinson RO, Baird G, Robinson G, et al. Landau-Kleffner syndrome: course and correlates with outcome. *Dev Med Child Neurol* 2001;43:243–247.
26. Scholtes FB, Hendriks MP, Renier WO. Cognitive deterioration and electrical status epilepticus during slow sleep. *Epilepsy Behav* 2005;6:167–173.
27. De Negri M, Baglietto MG, Battaglia FM, et al. Treatment of electrical status epilepticus by short diazepam (DZP) cycles after DZP rectal bolus test. *Brain Dev* 1995;17:330–333.
28. Wilson RB, Eliyan Y, Sankar R, et al. Amantadine: a new treatment for refractory electrical status epilepticus in sleep. *Epilepsy Behav* 2018;84:74–78.
29. Cooper EC, Aldape KD, Abosch A, et al. Colocalization and coassembly of two human brain M-type potassium channel subunits that are mutated in epilepsy. *Proc Natl Acad Sci U S A* 2000;97:4914–4919.
30. Biervert C, Schroeder BC, Kubisch C, et al. A potassium channel mutation in neonatal human epilepsy. *Science* 1998;279:403–406.
31. Charlier C, Singh NA, Ryan SG, et al. A pore mutation in a novel KQT-like potassium channel gene in an idiopathic epilepsy family. *Nat Genet* 1998;18:53–55.
32. Singh NA, Charlier C, Stauffer D, et al. A novel potassium channel gene, KCNQ2, is mutated in an inherited epilepsy of newborns. *Nat Genet* 1998;18:25–29.
33. Weckhuysen S, Ivanovic V, Hendrickx R, et al. Extending the KCNQ2 encephalopathy spectrum: clinical and neuroimaging findings in 17 patients. *Neurology* 2013;81:1697–1703.
34. Sanders SJ, Campbell AJ, Cottrell JR, et al. Progress in understanding and treating SCN2A-mediated disorders. *Trends Neurosci* 2018;41:442–456.
35. Sands TT, Balestri M, Bellini G, et al. Rapid and safe response to low-dose carbamazepine in neonatal epilepsy. *Epilepsia* 2016;57:2019–2030.
36. Wolff M, Johannesen KM, Hedrich UB, et al. Genetic and phenotypic heterogeneity suggest therapeutic implications in SCN2A-related disorders. *Brain* 2017;140:1316–1336.
37. Hadley JK, Passmore GM, Tatulian L, et al. Stoichiometry of expressed KCNQ2/KCNQ3 potassium channels and subunit composition of native ganglionic M channels deduced from block by tetraethylammonium. *J Neurosci* 2003;23:5012–5019.
38. Kanaumi T, Takashima S, Iwasaki H, et al. Developmental changes in KCNQ2 and KCNQ3 expression in human brain: possible contribution to the age-dependent etiology of benign familial neonatal convulsions. *Brain Dev* 2008;30:362–369.
39. Numis AL, Angriman M, Sullivan JE, et al. KCNQ2 encephalopathy: delineation of the electroclinical phenotype and treatment response. *Neurology* 2014;82:368–370.
40. van Bon BW, Coe BP, Bernier R, et al. Disruptive de novo mutations of DYRK1A lead to a syndromic form of autism and ID. *Mol Psychiatry* 2016;21:126–132.
41. Bernier R, Golzio C, Xiong B, et al. Disruptive CHD8 mutations define a subtype of autism early in development. *Cell* 2014;158:263–276.
42. Buckley AW, Holmes GL. Epilepsy and autism. *Cold Spring Harb Perspect Med* 2016;6:a022749.